UNIVERSITÀ
DEGLI STUDI
DI PADOVA

Sede Amministrativa: Università degli Studi di Padova
Dipartimento di Ingegneria Elettrica

SCUOLA DI DOTTORATO IN INGEGNERIA INDUSTRIALE
INDIRIZZO ENERGETICA
CICLO XXIII

CONCEPTUAL DESIGN OF THE POWER SUPPLY SYSTEM FOR THE IN-VESSEL SADDLE COILS FOR MHD CONTROL IN ASDEX UPGRADE

Direttore della scuola: Ch.mo Prof. Paolo Bariani

Coordinatore di indirizzo: Ch.mo Prof. Alberto Mirandola

Supervisore: Ch.mo Prof. Giorgio Rostagni

Tutor: Dott. Ing. Vanni Toigo

Dottorando: Andrea Zamengo

31 Gennaio 2011

Contents

Sommario

Lo sfruttamento di processi di fusione nucleare per la produzione di energia rappresenta un'importante alternativa nel panorama energetico mondiale. I vantaggi di tale fonte energetica sono la piena compatibilità con l'ambiente (non viene prodotto alcun gas serra), la sicurezza degli impianti ed il fatto che le risorse necessarie per sostenere il fabbisogno mondiale di energia possono essere considerate virtualmente inesauribili.
La ricerca sulla fusione termonucleare inizia a metà del secolo scorso, tuttavia, le prestazioni degli esperimenti a confinamento magnetico (la più comune di queste macchine è il Tokamak nei quali il plasma è confinato in una camera a forma toroidale) sebbene abbiano raggiunto traguardi importanti, sono ancora distanti da permettere uno sfruttamento industriale di tale forma di energia.
L'esperimento ITER (International Thermonuclear Experimental Reactor) costituisce il prossimo passo nell'ambito del programma di ricerca internazionale della fusione. Esso opererà in stato quasi stazionario con lo scopo di dimostrare la fattibilità scientifica e tecnologica della fusione termonucleare a scopi energetici. Tuttavia, tale esperimento non può da solo garantire la piena comprensione dei fenomeni fisici che avvengono in un plasma termonucleare e la soluzione dei problemi tecnologici che impediscono il pieno controllo dei fenomeni di fusione.
Nell'ambito del programma di fusione europeo, la macchina ASDEX Upgrade si propone come esperimento satellite per la comprensione dei fenomeni d'instabilità di tipo MHD che impediscono, negli attuali esperimenti, il raggiungimento di scenari operativi avanzati. I risultati del suo programma scientifico avranno un sicuro impatto nel progetto di ITER.
La proposta di modifica di ASDEX Upgrade, frutto della collaborazione di quattro laboratori europei tra cui il Consorzio RFX, è di realizzare un sistema di controllo delle instabilità MHD del plasma basato su un insieme di 24 bobine a sella, installate all'interno della camera da vuoto, in grado di creare campi magnetici radiali che interagiscono direttamente con i campi magnetici prodotti dal plasma.
Il lavoro esposto in questa tesi di dottorato, svolto principalmente presso il Consorzio RFX, si inserisce nell'ambito di tale progetto. In questo lavoro viene presentato lo sviluppo concettuale del sistema di alimentazioni elettriche che andrà ad alimentare le 24 bobine di controllo.
Un esperimento di fusione nucleare è uno scenario atipico per un sistema di alimentazioni elettriche. Oltre alle elevate prestazioni richieste, è necessario considerare le pecularità del carico (solitamente non lineare e parzialmente attivo) e la necessità di garantire l'integrazione del sistema in un contesto caratterizzato dalla presenza di un numero elevato di diagnostiche. Per quest'ultima ragione, lo studio dei disturbi

elettromagnetici (EMI) dovuti alle operazioni di un alimentatore switching rappresenta una tematica che non può essere sottovalutata.

Outline della Tesi

I Capitoli della tesi sono organizzati come segue:
Nel *Capitolo 1* viene presentata la fusione termonucleare nell'ambito del panorama energetico mondiale evidenziandone peculiarità e vantaggi. Viene quindi illustrato il funzionamento delle macchine di tipo Tokamak con particolare attenzione ad ASDEX Upgrade e ITER.
Il *Capitolo 2* illustra in modo sintetico quali sono i principali tipi di instabilità del plasma presenti in macchine di tipo Tokamak e descrive le strategie che attualmente vengono impiegate per mitigare o sopprimere i loro effetti per mezzo di bobine attive. Il Capitolo illustra poi le linee guida utilizzate nel design del sistema di alimentazione per le bobine attive.
Il *Capitolo 3* descrive il nuovo sistema di bobine di controllo proposto per la macchina ASDEX Upgrade. Vengono quindi illustrati i requisiti strettamente connessi alla fisica delle instabilità MHD traducendo questi ultimi in un insieme di specifiche elettriche necessarie per la definizione del progetto dei sistemi di alimentazione.
Il *Capitolo 4* è il cuore della tesi e presenta in maniera esaustiva il progetto concettuale dei sistemi di alimentazione. Lo schema circuitale proposto per le A-Coils è innovativo nell'ambito dei sistemi attualmente impiegati nella macchine da fusione e prevede l'impiego di topologie di tipo multilivello nelle quali la tensione di uscita del sistema è ottenuta combinando l'azione di due o più inverter. L'attività di progettazione si è poi dedicata all'ottimizzazione del sistema complessivo avendo anche come obiettivo la riduzione dei costi e dell'ingombro delle nuove apparecchiature. Il capitolo si conclude con la simulazione numerica degli schemi proposti e l'analisi dei possibili guasti ai quali il sistema può essere soggetto.
Il *Capitolo 5* è dedicato allo studio delle tematiche relative ai disturbi EMI (in particolare al problema del cosiddetto *modo comune*) prodotti dal nuovo sistema di alimentazione. All'interno del capitolo viene analizzato il modo in cui i disturbi vengono generati e viene individuato lo schema ottimale di messa a terra. Viene inoltre proposta una soluzione per il filtraggio del rumore di *modo comune* in grado di mitigare ulteriormente gli effetti dei disturbi EMI. Nell'ultima parte del capitolo viene presentata l'attività sperimentale svolta nel dicembre 2009 nei laboratori IPP di Garching, che ha consentito di verificare in loco l'impatto di un'alimentazione di tipo switching sul normale funzionamento delle diagnostiche di ASDEX Upgrade.

Abstract

The nuclear fusion processes exploitation for energy production represents an important option in the world energetic scenario. The advantages of this energy source are many: full environmental compatibility (there is no production of greenhouse gases), the intrinsic safety of fuson power plants and the fact that the resources needed to support the world energetic demand are potentially unlimited.
The thermonuclear fusion research began around the middle of the last century. The performance of magnetic confinement experiments (the most common of these machines is Tokamak, where the plasma is confined into a toroidal shaped vessel) reached some important achievements, but the industrial exploitation of this energy source is yet far.
ITER experiment (acronym for *International Thermonuclear Experimental Reactor*) constitutes the next step in international fusion research program. It will be a quasi-steady state machine, its main scope will be to prove the scientific and technological feasibility of thermonuclear fusion for energetic purposes. However, this experiment can't ensure alone the full comprehension of the physical phenonomena occurring in the thermonuclear plasma that prevent the full control of fusion processes.
In the framework of European Fusion Program, the ASDEX Upgrade machine intends to be a satellite experiment for the comprehension of MHD plasma instabilities phenomena in tokamak which prevent to achieve advanced operational scenarios in actual experiments. Its scientific results will have a sure impact on ITER project.
The ASDEX Upgrade enhancement proposal (resulting from collaboration of four european laboratories, among which there is Consorzio RFX), is to realize a MHD plasma instabilities control system, based on 24 saddle coils installed into the vacuum vessel, able to produce a radial magnetic fields which directly interacting with the magnetic fields produced by the plasma.
The work exposed in this Ph.D. Thesis (carried out at Consorzio RFX) complies with this enhanchment of the AUG experiment. In the present work it is presented the conceptual design of the power supply system, that will supply the 24 control coils.
A nuclear fusion experiment constitutes an atypical scenario for a power supply system. In addition to the high-level performance requirements, it is necessary to consider the load peculiarities (usually non-linear and partially active) and to guarantee the power supply integration into a system characterized by a number of diagnostics. Therefore, the analysis of electromagnetic interference (EMI) caused by a switching power supply operation can't be undervalued.

Thesis Outline

The thesis chapters are organized as follows:
In the *Chapter 1* there are presented peculiarities and advantages of thermonuclear fusion in the world energetic scenario. Then, it is described the functioning of Tokamak machines, with a particular attention to ASDEX and ITER.
Chapter 2 concisely illustrates the main types of plasma instabilities in Tokamak machines and describes the strategies actually used to mitigate or suppress their effects by means of active coils. The chapter illustrates also the guidelines used for the design of the active coils power supply system.
Chapter 3 describes the new coils system proposed for the ASDEX Upgrade machine. Then, there have been illustrated the requirements that are strictly connected to the MHD instabilities physics and the translation into a series of electrical specifications, which are strictly necessary to define the power supply system design.
Chapter 4 is the heart of this thesis and exhaustively presents the conceptual design of the power supply system. The electrical scheme proposed for the A-coils is innovative in the actually used fusion machines systems and it contemplates the use of multilevel topology, in which the output voltage is obtained combining one or more inverters. Then, the design activity has been dedicated to the whole system optimization, having as additional goal the reduction of system cost and size. The Chapter ends with the numerical simulation of the proposed scheme and with the analysis of the possible electrical faults of the system.
Chapter 5 has been dedicated to the study of problems related with EMI disturbs (in particular to the so called "common mode" problem) produced by the new power supply system. In this Chapter it is analyzed the way in which these disturbs are generated and it has been identified the optimal ground connection. Then, it has been proposed a solution for the filtering of common mode noises in order to mitigate the EMI disturbs effects. In the last part of the chapter, it has been presented the experimental activity of December 2009 in Garching, where it has been able to verify in loco the impact of a switching power supply on the normal diagnostics functioning of ASDEX Upgrade.

Chapter 1

Thermonuclear magnetic controlled fusion

1.1 The Energy problem

Humankind is confronted with a continually rising energy demand: this increase is due both to the world population growth and the increase of emerging economies energy needs. At the end of last century, in 1999, the power consumed in the world was around 12.6 TW, considering the expected world population in 2030, 10 billion people, and the expected per capita power consumption, 3 kW, the energy demand will be 30 TW [1].
The huge future world energy demand will not be satisfy by the currently dominant resource, fossil fuels, and probably the lack of mature alternatives will lead to conflicts (the energy crisis of the 1970's gives a clear example). Another important aspect to be considered is the possible consequences to our environment of the massive use of fossil fuels, and the consequent production of CO_2, which is probably the cause of the so called global warming [2] (in figure 1.1 is showed the acceleration of CO_2 concentration in the atmosphere).

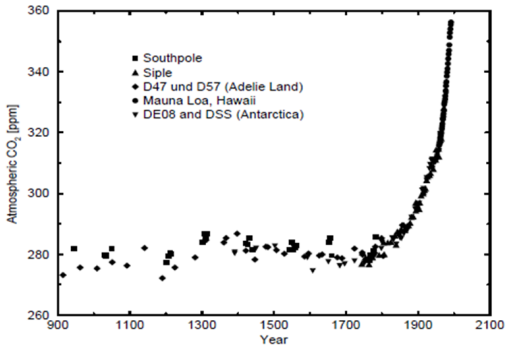

Figure 1.1: Evolution of the CO_2 concentration in the atmosphere (in ppm) during the last 1000 years [1].

Nowadays the world is not yet running short of fossil fuel (coil and oil production peak will be in the future, around the 2030 [3][4]), the abundance of this energy

Renewable	Investment Needed
Photovoltaic panels	about 100 km^2 in middle Europe ($\epsilon = 10\%$)
Windmills	6660 mills of 150 kW
Biogas	$60{\cdot}10^6$ pigs or $800{\cdot}10^6$ chickens
Bioalcohol	6200 km^2 sugar beer
Bio-oil	24000 km^2 of rape-seed
Biomass	30000 km^2 of wood

Table 1.1: Investment needed for 1 GW power plant for different kinds of renewables technologies [1].

source and its low cost represent the most important reason of the slow transition to a clean and renewable energy.
In the near future, when the cost of burning hydrocarbons to produce energy will rise, the alternatives energy sources are three: renewables, nuclear fission and nuclear fusion. The former option has theoretically huge capability (the power delivered to the Earth by the Sun is 174 PW!), but nowadays the available technologies have low power density with respect to fossil fuels which are packed with energy (see Table 1.1); this lead to a lack of competitiveness on the world energy market. Moreover it is necessary to take into account the greater intermittency of renewables: gas-fired or nuclear power plants operate 75 % to 90 % of the time, in contrast all the renewables that use the sun radiation is guaranteed to be unavailable half the time.
It is important to point out that the renewables resources are not useless, the increasing of power capability gives clear benefit to the mankind but on the present world energy scenario they could not considered a real alternative to burning fossil fuel. Among the different approaches to renewable the largest effort to scale up is represented by the Desertec project [5] which goal is to build solar and other renewable power project in Nord Africa and Middle East with a power capability of 500 GW and a predicted cost of 400 billion Euros.
Nuclear fission, after the Three Mille Island accident (March 1979) and the more famous Chernobyl accident (April 1986), stalled. Yet today the concern about climate change and the depletion of fossil fuel have led to a revival of interest in nuclear power generation. Fission energy could represents a long-term energy source, at least when product by means of the new generation reactors[1]. The challenges of nuclear fission are to reduce the risk of proliferation of nuclear weapon technologies and to deal with the highly radioactive waste produced: even if new methods are being developed to store waste in a safe way, the long term radioactivity represents a problem for the future generations.

[1] the lifetime of world uranium resources is about 50 years with present consumption, with breeder technology is possible to stretch world resources by a factor of about 60

1.2 Fusion Reaction

There is another approach to nuclear energy which could provide clean energy with intrinsic safety and abundant fuel resources: Nuclear Fusion. According to Einstein's mass-energy equation in every reaction in which the total mass of the final product is smaller than that of the reacting nuclei there is production of energy:

$$E = mc^2 \tag{1.1}$$

where m is the mass defect of reaction and c is the light speed. Fusion is a common process in nature, it is the mechanism that permit the energy production in the stars, and then their shining.
The fusion reaction can take place if the distance between nuclei is short enough to permit to the short-range attractive nuclear force to overcome the Coulomb repulsion force among them. For this reason it is necessary to give to nuclei enough kinetic energy, for example hydrogen atoms needs 400 keV to exceed the Coulomb wall. Thanks to the quantum tunneling effect, fusion reaction can take place with a reasonable probability at lower kinetic energy.
The possibility of realizing controlled fusion reaction in laboratories has been studied for several decades. The studies started on 1940 as part of the Manhattan project, shortly after World War II there was an international wave of interest in nuclear fusion an many countries set up national fusion programs. Since the research had military significance, most experiments were secret and there was no international collaboration at that time. This changed in 1958 during the *Atoms for Peace* conference in Geneva: many countries including Russia and the US revealed the results of their fusion programmes.
In order to get a controlled fusion reaction it is necessary to confine an high temperature ionized gas (named plasma, which represent the fourth state of matter) and give it the condition for fusion reaction. When a considerable number of particles react together, part of the energy produced are used to heat the gas itself, the remaining energy could be extracted to other purpose.
To be a useful energy source fusion reaction must satisfy several criteria. The most promising candidates for terrestrial reactions are:

$$D + D \rightarrow He^3 + n + 3.3\,MeV \tag{1.2}$$
$$D + D \rightarrow T + H + +4\,MeV \tag{1.3}$$
$$D + T \rightarrow He^4 + n + 17.6\,MeV \tag{1.4}$$
$$D + He^3 \rightarrow He^4 + H^+ + 18.3\,MeV \tag{1.5}$$

where D stands for deuterium (hydrogen isotope composed of one proton and one neutron), T for tritium (hydrogen isotope with a nucleus of two neutrons and one proton). He^4 is an Helium isotope with two neutrons (known as α particle), n indicates a neutron, while H^+ a proton.
The reaction rates is a parameter used to understand the frequency of reaction and it could determines the easiest fusion reaction among the ones listed above, this parameter is defined as the average (done over particles of all the possible velocities) of the product $\sigma\upsilon$ where σ is the particles cross section and υ its velocity. The reaction rate represents the volume crossed by a particles which is proportional to

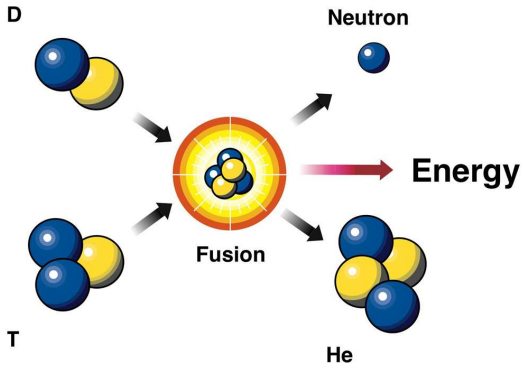

Figure 1.2: D-T Fusion Reaction

the probability of the reaction. Figure 1.3 shows the dependency of reaction rate on the temperature (expressed in keV): D-T reaction is the more probable reaction at low plasma temperature.

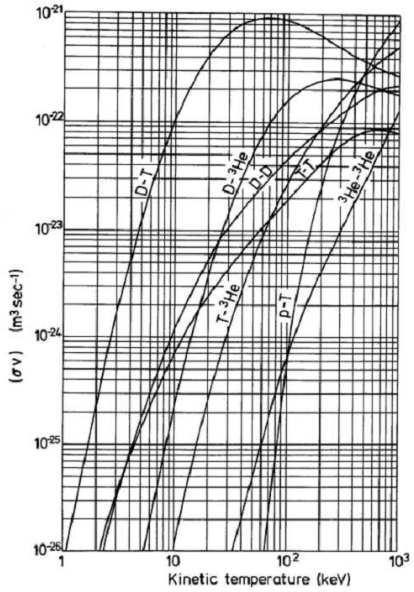

Figure 1.3: Fusion reaction rate $\sigma\nu$ for couples of reactants.

Deuterium is present on Earth and can be easily found in the ocean water: 0.0156% of the all naturally occurring hydrogen in the oceans is Deuterium. To date the most common use of Deuterium on industry is the production of heavy water used as neutron moderator in nuclear fission reactor plants. The other reactant, Tritium, is extremely rare on Earth (it occurs naturally due to cosmic rays interacting with atmospheric and has an half-time of only 12.3 years) and the quantities available in nature are not sufficient for technical applications. It's possible to obtain

considerable amount of tritium by using a reaction including Lithium:

$$Li_3^6 + n_0^1 \rightarrow T_1^3 + He_2^4 + 4.6\,MeV \tag{1.6}$$
$$Li_3^7 + n_0^1 \rightarrow T_1^3 + He_2^4 + n_0^1 - 2.5\,MeV \tag{1.7}$$

The latter reaction is endothermic and generates a neutron that permits the continuation of the breeding reaction. In the future fusion power plants the adoption of a lithium blanket on the vacuum vessel could provide the conditions to produce the needed amount of Tritium for fusion reaction in site.
Nuclear Fusion represents a promising energy resource for future centuries: the fusion fuel supplies are almost inexhaustible and in comparison to fission there are no long-term radioactive wastes to be managed. Moreover there is no production of greenhouses gases, since the main natural product of the fusion reaction is helium, which is harmless and does not contribute to global warming.
It is necessary to undeline that energy production by means of fusion reaction could be a real alternative to other energy resources if it could be produced easily, reliably and with a competitive prize.

1.2.1 The burning criteria

The total power per unit in a D-T plasma reaction is:

$$P_{TH} = n_D n_T \langle \sigma\nu \rangle \varepsilon \tag{1.8}$$

where n_D and n_T are the densities of deuterium and tritium, $\langle \sigma\nu \rangle$ is the reaction rate cited above and ε is the energy released for each reaction. Equation 1.8 is maximized by $n_D = n_T = n/2$ (where n is the plasma density):

$$P_{TH} = \frac{1}{4} n^2 \langle \sigma\nu \rangle \varepsilon \tag{1.9}$$

With the same procedure the power given by α particles heating could be derived:

$$P_\alpha = \frac{1}{4} n^2 \langle \sigma\nu \rangle \varepsilon_\alpha \tag{1.10}$$

Since the energy contained in the plasma is not perfectly confined on it (among the energy loss processes: bremsstrahlung emission, power losses due to collisional and turbulent transport phenomena) for the balance of a fusion reaction to be positive the wasted energy has to be replaced.
A simple relation that describes the energy losses in a fusion plasma due to mechanism different from bremsstrahlung is $P_L = 3nT/\tau_e$ where confinement time τ_e is introduced and $3nT$ is the energy per unit volume of plasma. Using the above relations the self sustainement condition for a D-T reaction could be written as:

$$P_\alpha > P_L \tag{1.11}$$

$$\frac{1}{4} n^2 \langle \sigma\nu \rangle \varepsilon_\alpha > \frac{3nT}{\tau_e} \tag{1.12}$$

Equation 1.12 provides the condition for which the D-T plasma is entirely heated by the kinetic energy of alpha particles and no external heating is required for the reaction. The ignition condition could be rewritten as:

$$n\tau_e > \frac{12}{\langle\sigma\nu\rangle} \cdot \frac{T}{\varepsilon_\alpha} \tag{1.13}$$

Considering that the right hand side function has a minimum at 30 keV, and the linear dependence of $\langle\sigma\nu\rangle$ over temperature the requirement for ignition at this temperature is:

$$nT\tau_e > 3 \times 10^{21} m^{-3} keV s \tag{1.14}$$

The equation 1.14 is the classical form of the so-called Lawson criterion for plasma ignition [6]. For temperature of 20 keV and electron density of $10^{20} m^{-3}$, parameters achievable on laboratory experiments the energy confinement time τ_e has to be greater than 1s.
To approach ignition condition two different confinement methods have been studied: magnetic and intertial confinement. The former uses strong magnetic field to confine the plasma which can be sustained for long times, the latter maximizes the density of D-T fusion reaction to reach or exceed the Lawson criterion by the implosion of small fuel pellet.
This thesis is focused on the magnetic confinement which is usually considered more promising for energy production. In figure 1.4 is showed the triple product in fusion device experiments based on magnetic confinement since the beginning of fusion research, it could be noted the dramatic improvement of this parameter and that it is now close to reactor conditions.

1.3 Tokamak

Magnetic confinement represents the most studied approach to obtain the fusion condition on earth. Among the different magnetic configurations the most promising device, named Tokamak [2], confines the thermonuclear plasma in a torus shape vacuum vessel (pressure of the background gas typically not exceeding 10^{-7} mbar). The current generation of modern, large tokamaks was designed during the 1970s. The biggest operating tokamak is the Joint European Torus (JET), located near Oxford in England, which was put into operation in 1983. Other large tokamaks are located in Germany, France, Japan and the US. In the operating devices, fusion plasmas of hundreds of millions of degrees Celsius are routinely generated and maintained for several minutes.
The principal magnetic field on Tokamak is the toroidal one, but it couldn't guarantee alone the stability to the plasma configuration (in which the plasma pressure is balanced by the magnetic forces), thus a poloidal field must be added, in a Tokamak this field is produced by the current flowing in the plasma in the toroidal direction. The sum of the toroidal magnetic field B_ϕ and the poloidal magnetic field B_ϑ produces a magnetic field with helical field lines around the torus as shown in Figure 1.5.

[2] the name derived from the russian form *toroidal'naya kamera s aksial'nym magnitnym polem* which means 'toroidal chamber with an axial magnetic field'

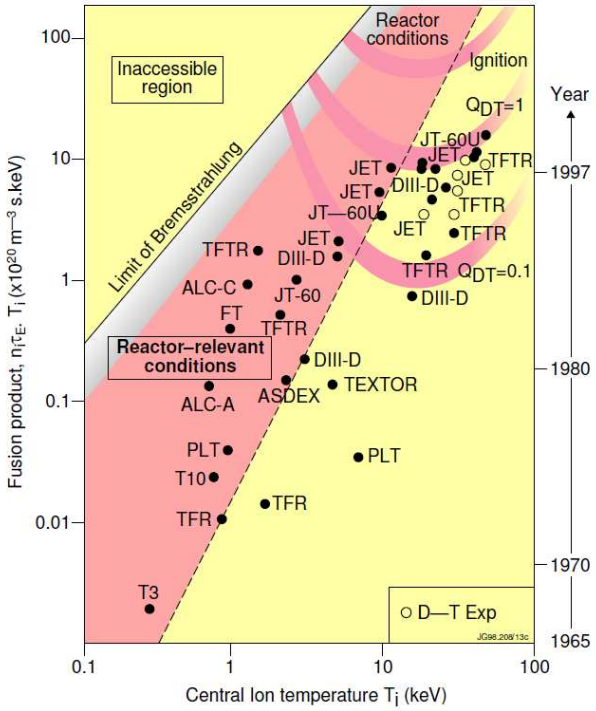

Figure 1.4: The triple product in fusion devices experiments, as a function of the central ion temperature.

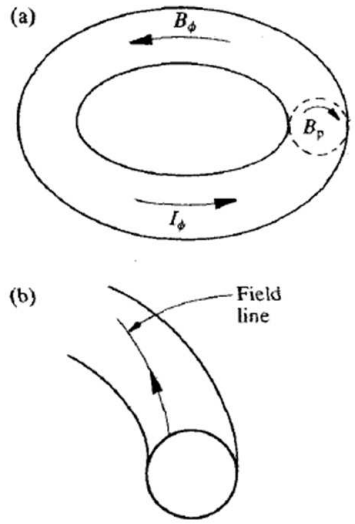

Figure 1.5: Magnetic Fields of a Tokamak machine

The plasma reactivity depends on particle density and temperature, it is useful to define the plasma pressure as:

$$p_{plasma} = n \cdot k_B \cdot T \tag{1.15}$$

where k_B is the Boltzmann constant and n is the plasma density. The pressure which can be confined is determined by the plasma stability and increases with the strength of the magnetic field. The ratio of the plasma pressure to the magnetic pressure (defined as $B^2/2\mu_0$) is a dimensionless number know in fusion science as plasma beta:

$$\beta = \frac{p_{plasma}}{p_{mag}} = \frac{n \cdot k_B \cdot T}{B^2/2\mu_0} \tag{1.16}$$

This parameter is a widely used figure of merit for magnetic confinement and is directly connected to plasma stability: on tokamak machines there is a limit of the value β can have before instabilities occurs. In order to obtain high β and therefore high plasma performance a strong toroidal magnetic field is necessary.
Technological factors limit the achievable magnitude of magnetic fields on fusion machines: copper coils operations are limited by the Joule heating losses, hence superconducting coils are envisaged (even if the cryogenic requirements to maintain coils temperature below the characteristic temperature have a dramatic impact on the cost of fusion machines). Unfortunately the superconductive coil cease to superconduct above a critical magnetic field, and this represent another limitation.
For given plasma pressure and toroidal magnetic field the plasma stability increases with the toroidal plasma current (which produce the poloidal field necessary to the stable magnetic configuration). In present tokamaks the plasma current is in the range of Megamps, but 20-30 MA are foreseen in the future reactors.
The plasma current is driven into the plasma chamber by a toroidal electric field induced by a flux change through the torus, this flux change is induced by a poloidal magnetic system. Poloidal coils are also used to control the plasma shape and position. The magnetic system of a tokamak are shown in figure 1.6.

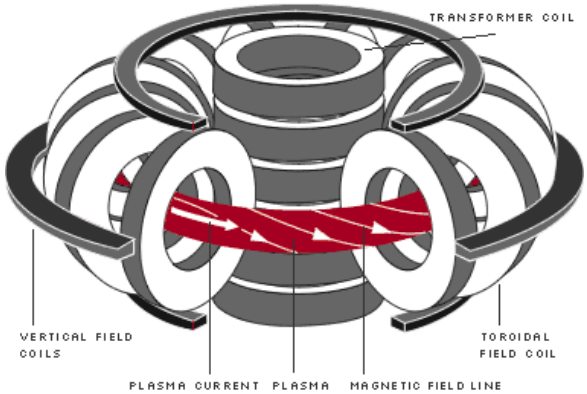

Figure 1.6: Magnet system of a Tokamak machine

To reach burning conditions is necessary to increase the temperature of the plasma to tens of keV or more. Since plasma is a conductor the current which flows through it produces heating by Joule effect, the effectiveness of this kind of heating (known

Weight	W	800 tons
Major plasma radius	R_0	$1.65m$
Minor plasma radiuos	a	$0.5m$
Half plasma height	b	$0.8m$
Plasma elongation	$s = b/a$	1.6
Plasma aspect ratio	$A = R_0/a$	3.3
Plasma Volume	V	14 m^3
Plasma current	I_P	< 1.4 MA
Discharge time	t_{pulse}	< 10 s
Plasma temperature	T_p	$< 150 \cdot 10^6$ degrees
Plasma density		$< 2 \cdot 10^{20}$
Energy Confinement time	τ_e	< 0.2 s
Toroidal magnet field	B_T	4 T
OH flux swing	Φ	$9.5Vs$
Neutral Particle heating	P_{NBI}	20 MW
Ion Cyclotron heating	P_{ICRH}	6 MW
Electron Cyclotron heating	P_{ECRH}	4 MW

Table 1.2: Essential parameters of ASDEX Upgrade.

as ohmic-heating) is limited by the plasma resistance which decreases with temperature. In Tokamak this represents a strong limit: additional heating system have to be used.
The limited capability of poloidal magnet system in terms of available flux swing limits the inductive current drive and therefore the possibility to sustain steady state operations. The Neutral Beam Injector system, which is the most used heating device in Tokamaks, involves the introduction of high-energy neutral particles into the torus, the high kinetic energy of neutrals is then transfered to the plasma particles. This process increase the temperature of the plasma, the delivered momentum is also used to drive the plasma current.
The additional heating techniques used in tokamaks include also electromagnetic waves in which the plasma is heated by the means of suitable resonances between plasma particles and radio-frequency fields, various techniques exist including electron cyclotron resonance heating (ECRH) and ion cyclotron resonance heating (ICRH).

1.3.1 ASDEX Upgrade

The ASDEX Upgrade tokamak, in operation at Max-Planck-Institut fur Plasmaphysik (IPP) in Garching, is a medium size device commissioned during 1991 [8][9]. Its name is an acronym that stands for **A**xial **S**ymmetric **D**ivertor **EX**periment, it suggests the main characteristic of this device: the poloidal divertor which permits to study advanced plasma scenario (the H-Mode), energy transfer through the plasma boundary to the material structure, impurity control for reactor-like conditions and ash removal. The main parameters of the ASDEX Upgrade tokamak are reported in Table 1.2.

The magnet system of ASDEX Upgrade consists of the Toroidal Field magnets (TF) and Poloidal Field magnets (PF). The TF system is composed of 16 D-Shaped water cooled copper coils, in which every coil is composed of two pancakes with 12 windings each. All the coils are connected in series and driven by a power supply to produce the nominal 4 T toroidal field. The PF system is composed by three groups of coils: ohmic heating coils (OH) for breakdown and plasma current control, V coils for horizontal equilibrium and plasma shaping and Control Coils for vertical plasma position control.

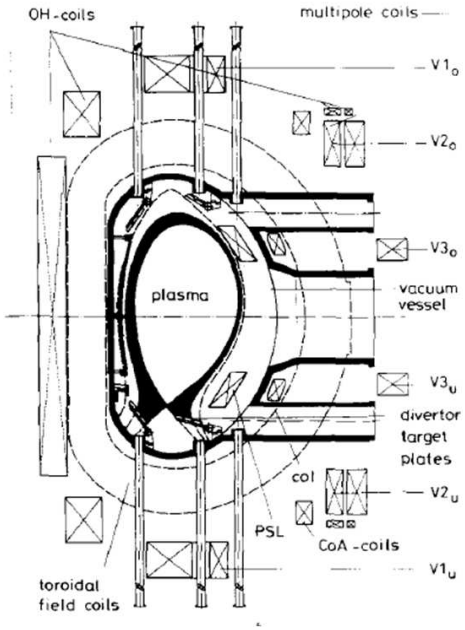

Figure 1.7: ASDEX Upgrade cross section [8].

The elongated plasma of ASDEX Upgrade is unstable respect the vertical displacement, for this reason a Passive Stabilization Loop (hereafter PSL) has been provided. Its main role is to reduce the instabilities grow rate from microseconds to tens of milliseconds timescale. This allows the control of plasma vertical position by the means of active coils with reasonable power consumption.
The flexible heating systems consist of the neutral beam heating (NBI) with powers up to 20 MW, the ion cyclotron resonance system (ICRH) and electron cyclotron system which allows electron heating (ECRH) and current drive (ECCD).

1.3.2 ITER

The International Thermonuclear Experimental Reactor (ITER) [10][11][12] represents the next step of the fusion international program. The project was originated at a summit meeting between Reagan and Gorbachev in 1985 in Geneva. The joint statement of US-Soviet summit on fusion research is as follows.

> *The two leaders emphasized the potential importance of the work aimed at utilizing controlled thermonuclear fusion for peaceful purposes and, in*

> *this connection, advocated the widest practicable development of international cooperation in obtaining this source of energy, which is essentially inexhaustible, for the benefit of all mankind.*

The ITER Agreement was officially signed at the Elysée Palace in Paris on 21 November 2006 by Ministers from the seven ITER Members. The fusion reactor will be constructed in Europe, at Cadarache in the south of France.
The main objective of ITER is to demonstrate controlled ignition and extended burn and to achieve stationary conditions using non-inductive current drive methods. This D-T fusion reactor has been designed to produce 500 MW of output power with a power gain of ten in respect of the input power provided by the additional heating systems. The pulse length will be 3600 s. The main design parameters of ITER are listed on table 1.3, the cut-away view of the ITER tokamak is showed on figure 1.8.

Plasma major radius	$6.2\,m$
Plasma horizontal minor radius	$2.0\,m$
Plasma volume	$840\,m^3$
Plasma current	$15\,MA$
Toroidal magnetic field	$5.3\,T$
Fusion power	$500\,MW$
Power amplification	> 10

Table 1.3: ITER main parameters

ITER will be about ten times larger in plasma volume than JET, its construction started in 2008 while the first plasma shot is expected in 2018. ITER's operational phase is expected to last for 20 years. During the first period of operation in pure Hydrogen the machine will remain accessible for repairs. After the second phase, characterized by operation in Deuterium with a small amount of Tritium, the machine will become activated by neutron absorption to such an extent that human access to the machine will be precluded: maintenance of in-vessel components will then have to be carried out remotely. On the final stage frequent operation with an equal mixture of Deuterium and Tritium, at full fusion power will be carried out.
Consequently ITER, an experiment with the same size as a power plant, will provide an essential bridge from previous physics experiments to commercial power plant. The new device will be called Demonstration Power Plant (DEMO) [13], it will be able to produce 2.3 GW of thermal output power, the same scale of a modern electric power plant. Scope of this device is to demostrate that Fusion could be an attractive and advanced energy source for the future society and energy market.

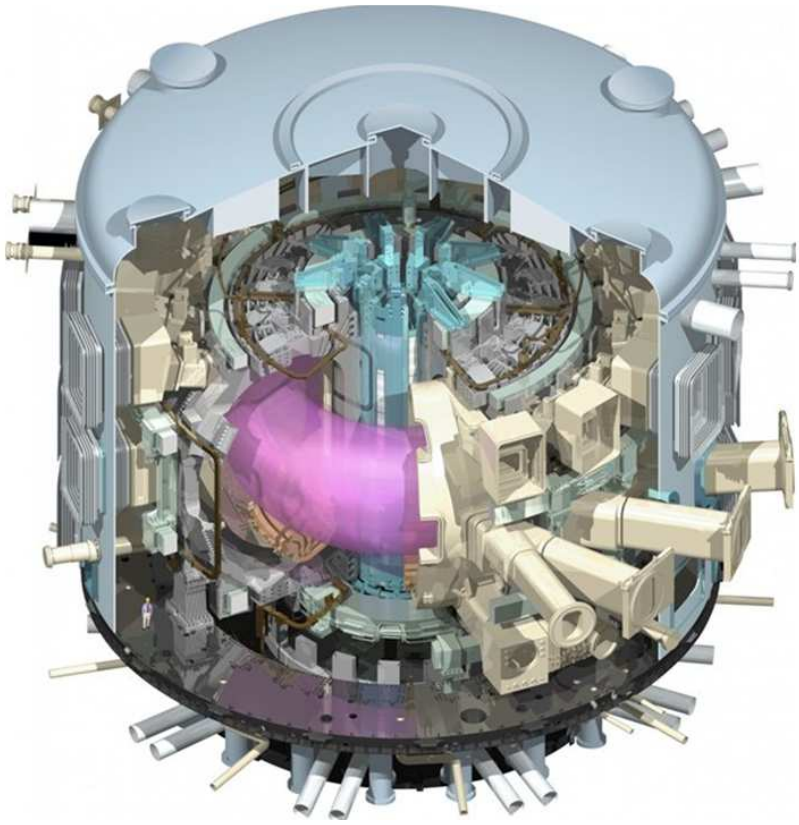

Figure 1.8: A cut-away view of the ITER tokamak [10]

Chapter 2

Plasma instabilities control by means of active coils in Tokamaks

2.1 Overview on MHD instabilities on fusion devices

One of the most important aspects of fusion science is the plasma stability.
Magnetohydrodynamic (MHD) instabilities limit sensitively the accessible operation areas of Tokamak, and in particular the confined plasma pressure. The next step devices and in particular the future reactors, which need to be compact and cost-effective, require plasma operation at high β. The use of active control system for MHD instabilities control seems to be mandatory to reach advanced plasma scenario.
This chapter gives a brief introduction to the different types of MHD plasma instabilities on Tokamaks, with a particular emphasis on the instabilities which control is the object of the AUG enhancement, giving also a description of the different methods to control them.
The description of active control of MHD plasma instabilities is focused on the use of active coil which perturb the plasma edge by means of radial field.

2.1.1 Neoclassical Tearing Mode

Neoclassical Tearing Modes (NTMs) are resistive tearing mode islands that are sustained by a helically perturbed bootstrap current [14]. This type of instability became unstable at high plasma pressure because the flattening of the pressure profile in the island interior causes a sufficiently large helical defect current which enhances the perturbation field and island width. The NTMs degrade both plasma energy and angular momentum and can lead to disruption in advanced plasma scenario.
The stabilisation of NTMs has been successfully demonstrated in different Tokamak including AUG. Different strategies for avoid deleterious NTMs exist. Among the different strategies: the use of electron cyclotron current drive (ECCD) to replace the defect current inside the islands. The same approach can be performed through optimization of the current and pressure profiles, using Neutral Beam Injection

(NBI). At high beta and low plasma rotation large peripheral NTMs might lock to stationary error fields (mode locking), in this case the fast grow rate could cause a disruption. In case of mode locking the presence of a rotating error field with sufficient amplitude can induces a NTM rotation leading to a reduction of its growth rate. This reduced growth rate gives the plasma controller time to react and avoid a pending disruption by proper action. The rotation of the NTM can be induced by means of set of saddle coils with a sinusoidal reference and proper phase shift.

2.1.2 Resistive Wall Mode

Resistive Wall Mode (RWM) is an ideal external kink mode whose growth rate is influenced by the presence of a conducting wall with finite resistivity surrounding the plasma.
The control of RWM in tokamak is achieved by means of passive and active control techniques. Passive control of RWM is based on the relation between the grow rate of RWM instabilities and the properties of the conductive wall surrounding the plasma: the grow rate of instabilities is on the time scale of magnetic field diffusion through the resistive wall.
Active control is based on the magnetic perturbation of the plasma by means of saddle coils. Various control schemes using helical perturbation fields have been employed in reversed field pinches[1] (RFP), EXTRAP T2R and RFX [15], and in the DIII-D tokamak. All these experiments use external coils that produce a helical magnetic field to counteract the field perturbation produced by the RWM, or to induce mode rotation which generally has a stabilizing effect. Active RWM stabilization in tokamaks for performance enhancement is a relatively new field: various control schemes have been proposed and tested, mostly in RFP experiments; there is still a need for evaluating RWM control methods in tokamaks in view of their possible application for ITER.

2.1.3 ELM

Among the various type of plasma confinement in tokamak, the High-confinement mode (H-mode) discovered on the ASDEX machine in the eighties enables improvement of confinement times with respect to other modes: the H-mode is still today the reference scenario for the next step machine ITER.
As drawback the H-mode plasmas are usually characterized unstable modes: the Edge-Localized Modes (ELMs) [16] that release plasma particles and energy from inside the plasma into the scrape-off-layer[2] (SOL) in short bursts. Since the phenomenon is fast ($t < 1ms$), the high power load on targets during an ELM poses a threat to the reliable quasi-steady state operation of a tokamak.
ELMs most obvious signature is a short (ms) spike in H^{α} emission from the plasma boundary, as shown by the data from an H-mode discharge in JET (figure 2.1).

[1] The reversed field pinch is an axisymmetric toroidal system similar to a tokamak. The name of the configuration derives from the fact that the toroidal magnet field in the outer region is reversed with respect to its direction in the axis.

[2] The outer layer of a magnetically confined plasma, where the field lines come in contact with a material surface (such as a divertor or limiter)

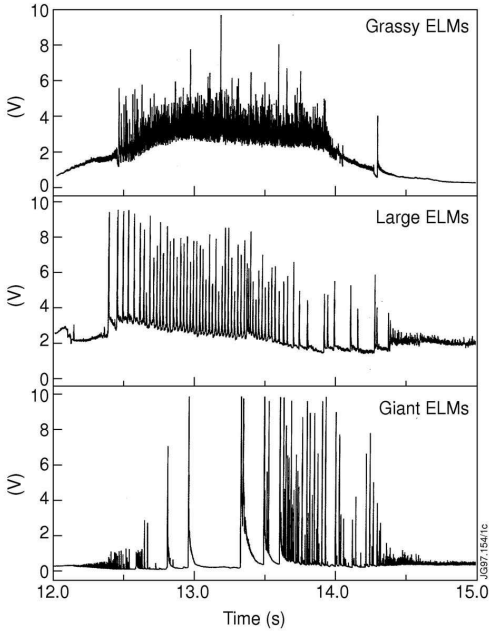

Figure 2.1: ELMs observation in the plasma edge as repetitive peaks e.g. in H^{α} light intensity [17].

The precise mechanism of the ELM instability and heat losses and the extrapolation to a reactor are still unknown, however, it is expected that the heat load in the divertor of ITER can be near the ablation limit for graphite or the melting limit for tungsten.
Various stationary H-mode regimes with small, tolerable ELMs or complete absence of ELMs (Quiescent H-mode) have been identified in various tokamaks including ASDEX Upgrade. These small or no ELM regimes occur in certain parameter regimes and it is not clear whether they can be reproduced in ITER or a reactor.
A few years ago it has been discovered at the DIII-D tokamak that a non-axisymmetric magnetic perturbation field can lead to stationary H-mode discharges without ELMs [18]. A set of in-vessel saddle coils (I-coils) has been used to produce a magnetic perturbation which has sidebands resonant with the magnetic field in the H-mode pedestal region. This condition is termed a *Resonant Magnetic Perturbation* (RMP). With DC operation and coil current above a threshold, type I ELMs either disappear altogether or give way to benign grassy MHD activity.

2.2 Power supply system for plasma instabilities control with active coils

As showed in the previous paragraphs the use of active coils that perturb the radial field of plasma can help the control of various types of MHD instabilities. The field shape required for the control depends on the type of instability. It could be resonant for the control of RWM and NTM, stationary for the control of ELM or

it could have a random-like shape for the feedback control of RWM.
The power supplies that feed the control coils have to be designed to perform the various control action with a reasonable error. In the following are reported the guidelines for the design of the power supply system.

2.2.1 Requirements definition

The first step of the design is to define the set of physical requirements for the control of MHD plasma instabilities. On this design stage it is important to have in mind that a system approach must be adopted since the effectiveness of the coils on the instabilities control depends on many factors.
On the first phase of the system design the mechanical studies give important information; among these: the coil Ampere-turns which is directly connected with the voltage an current requirements of the power supply, the coil position with respect to the vacuum vessel and in some cases the mutual coupling among coils.
Directly connected with mechanical design of the coils is the power supply load characterization. Usually the load, composed of the coil itself, the plasma and passive structures surrounding the coils, is not linear and its parameters depend on the frequency (due to the skin effect and eddy losses on the passive structure nearby the coil). Moreover the mutual coupling between coils and plasma could implies a bidirectional power flow which can be dangerous in case of sudden disruption of the plasma. An accurate electromagnetic characterization of the load is difficult; usually a large margin has to be adopted with respect to the nominal value given by the analyses.
Once defined the load characteristics and the physical requirements in terms of field shape and magnitude it is necessary to translate them into a set of power supply requirements.
Apart from current, voltage and frequency the power supply requirement definition needs a series of additional information as bandwidth, response delay, ripple of the output current and quality of the output waveforms.
One of the most important requirement for feedback control of MHD instabilities is the delay time in the PS response.

2.2.2 Selection of the power supply type

After having studied the overall system optimization and clearly understood the requirements, the PS design is addressed at identifying the suitable architecture to guarantee the required performance on the single coils but also to optimize the global features in terms of modularity level, size, cost, impact on grid. The first choice is related to the PS type.

Linear amplifiers

This PS type represents a highly desirable solution for MHD control applications; in fact, it allows the widest bandwidth of the output waveforms and best dynamic performance. Moreover it does not produce the electrical noise typical of the switching converters. They are based on power Mosfets and in general, the highest power applications do not exceed some tens of kW due to the limits in the semiconductor power losses. Unfortunately, the power level

for plasma instabilities control is generally too high to allow adopting this type of amplifier.
An example of use of linear amplifiers on MHD instabilities control system is the experiment EXTRAP T2R. In this experiment the set of coils for RWM control are driven by broadband linear audio amplifiers with a bandwidth of $f_{amp} = 25 kHz$. The maximum coil current is around 20 A per turn producing a maximum radial field of the order of 3 mT at the coil center, which is a few percent of the equilibrium poloidal field [19].

Line commutated converters

In the basic configurations this PS type is composed of two quadrant amplifiers supplying unidirectional current. Four quadrant operation is achieved with bridges connected in antiparallel and suitably controlled in particular around the current inversion region; this is the only configuration allowing energy recovery to the grid but in times not less than some ms. This family of converters is widely used in fusion experiments to feed the main magnets due to the requirements of very high power and relatively slow dynamic behaviour; for the same reasons, their use is rather limited for MHD modes control.

Switching converters

This PS type is the most widely utilized type of PS for MHD control; a broad variety of topologies exists, but Voltage Source Converters composed of input rectifier, capacitive dc link and inverter are usually the best choice.
Besides the better dynamic behaviour with respect to line commutated converters, the switching ones allow decoupling the load from the grid. In this way, the input rectifier can be unidirectional and rated just for the load losses, while the fast bidirectional energy exchange with the load is handled by the capacitive dc link.
The cost is probably the major drawback: switching converters are always considered more expensive than line commutated converters but the comparison should be carefully made, case by case, taking into account many aspects, including size considerations. In fact, the basic structure above described can allow providing a common input rectifier and dc link for many inverters.

2.2.3 Outline of control techniques

The control is a key part of the design; here just some main concepts are recalled. First of all, it is important to have in mind that these PSs are equipped with their own control, nested within a higher level control system, which calculates the reference waveforms (either current, voltage or open loop reference waveforms) in order to perform the desired magnetic configuration.
An optimal control technique for power supply dedicated to the plasma MHD instabilities control does not exist. The best solution is represented by the compromise between different requirements:
In the scenario of feedback control of plasma instabilities the delay of PS response is the driving requirement for the power supply design: the promptness will be preferred to the accuracy of the response. For this reason open loop (direct gate control) operations are preferred to the feedback current or voltage control.

On the contrary when a preprogrammed magnetic field shape is used to control the plasma (mode rotation, stationary magnetic field) the response accuracy is more important than system promptness. On this operational scenario is important to keep the current ripple (for dc current) and Total Harmonic distortion (for ac current) at acceptable level to avoid excessive distortion of produced magnetic field.
On the following will be described the two approaches for the power supply control: current or voltage control.

Current control

Two basic approaches are commented here for those aspects mainly affecting the most important requirements for the applications: the control based on Pulse Width Modulation (PWM) [20] and the hysteresis control.
The PWM modulation technique is a widely used technique for controlling power converter. In the simplest PWM technique the converter output has two output states; the output voltage (or current) is controlled by switching at a constant frequency and adjusting the on duration of the switch. The average value of voltage (and current) fed to the load proportional to the switch duty cycle δ defined as the ratio of the on duration to the switching time period. With PWM control the power converter switches work at fixed frequency that allows a deterministic calculation of the losses. This control requires the presence of a regulator; feedforward compensation of dc-link voltage variations can be provided. The PWM modulator introduces a delay, which also depends on the hardware implementation, but can not be less than a switching period. However, the response speed is mainly affected by the regulator, which operation is affected by the load and by the mutual coupling.
The hysteresis modulation is a feedback current control method where the converter current tracks the reference within a hysteresis band (figure 2.2 illustrates the operation principle of hysteresis current control).

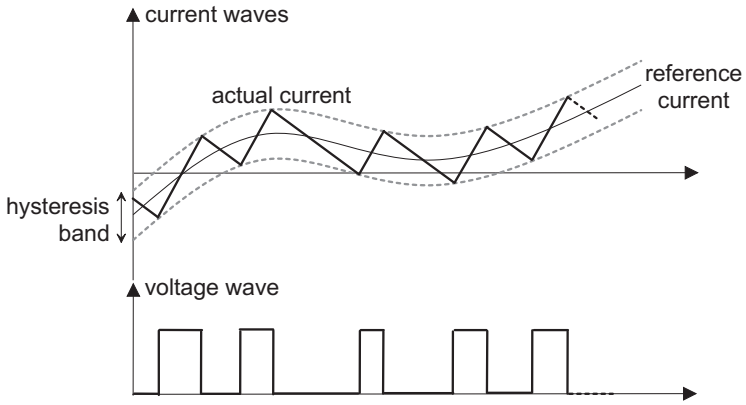

Figure 2.2: Operation principle of hysteresis current control.

Hysteresis control permits faster operations; it is also completely independent from the loads since the current profiles depend only on the reference signal and the hysteresis band. The main drawback of this modulation technique is the variable switching frequency which can't be easily predicted and can imply excessive power dissipation on converter due to switching commutations. Therefore converters sys-

tems based on hysteresis need an active control of the switching frequency to maintain the switches within their operational limits: the cost of this additional control is the reduction of converter speed and accuracy.

Voltage control

Voltage control could be based on closed or open loop. Feedback control of the voltage is not usually implemented; the overall performance achievable in terms of accuracy is comparable with the operation in open loop with feedforward compensation, which has the advantage of higher speed.
In PS units with bridges in series, hysteresis control of the total voltage can be utilized. A good example of this control approach is that implemented in the JET Enhanced Radial Field Amplifier [21].

Chapter 3

The enhancement of ASDEX Upgrade Tokamak

3.1 The enhancement proposal

In 2007 it was proposed an enhancement of the ASDEX Upgrade tokamak consisting in a set of saddle coils and AC power supplies, which allow magnetic field perturbations to be produced with different configurations suitable for suppression of Edge LocalisedModes (ELMs), rotating error fields for disruption avoidance and studies of the effect of mode rotation variations on the plasma [22]. In combination with a conducting wall, to be added at a later stage of the proposal, resistive wall modes will be stabilized with active feedback control.
The system of 24 saddle coils will be mounted inside the vacuum vessel, close to the plasma surface, they are arranged in three groups of eight toroidally distributed coils. The groups of coils are placed at different poloidal positions on the low field side of the torus in order to allow flexibility to adjust the toroidal and poloidal mode spectra.
The AUG enhancement could represent an important step toward the comprehension of MHD instabilities phenomena in advanced plasma scenarios and will help the design of future fusion devices.

3.1.1 Objectives of the proposal

On a short term time scale the proposed enhancement of AUG could have a significant impact on the ITER design: one of the main design uncertainties of the new device is related to the avoidance of ELMs, prior to the final design of the ITER machine it will be necessary to decide if an in-vessel coil system is mandatory for the suppression of this type of plasma instability. On a longer term the AUG team proposal could also enhances the knowledge of advanced scenarios both for ITER and DEMO where high β induces MHD instabilities and in some cases plasma disruption.
ITER is designed to achieve Q=10 in the H-mode which is usually accompanied by the occurrence of ELMs. The large peak of heat flux (the expected ELMs in each discharge are $\geq$ 1000, with an energy range of 5-30 MJ) likely to cause material erosion and ablation especially on the divertor surface: standard H-mode operation

at low to moderate density is likely to be unacceptable [23]. On the foreseen plasma scenarios of ITER there are to date only two possibilities to avoid ELMs: *Quiescent H-mode* which requires the injection of neutral particles in opposite direction to plasma toroidal current and the application of static error fields, the latter possibility has been demonstrated recently in the DIII-D tokamak [24].
To date there is not complete comprehension of the physical reason for ELM suppression by helical fields and the extrapolability to ITER is unknown. ASDEX Upgrade, which operates in H-mode and produces advanced β scenario has an excellent set of diagnostic to study the effect of field perturbation, its medium size allows also a fast implementation of hardware extension: for these reasons the proposed enhancement of the machine (in particular step 1 and step 2, see 3.1.3) represent a clear answer to the ITER design needs.
To study the ELM suppression with stationary fields is not the only objective of the machine enhancement proposal. Two important type of instabilities and its suppression techniques will be: Neoclassical Tearing Modes and RWM.
At high plasma pressure Neoclassical Tearing Modes (NTM) can become unstable. When this kind of MHD modes interact in the tokamak with non-axisymmetric error field the resulting electromagnetic torque tends to slow down the differential rotation between the mode and external field (*mode locking*), as a result tearing modes can present low or zero rotation, in some cases this could leads to subsequent disruption of the plasma current. In ASDEX Upgrade the proposed set of coils will be used to apply differential rotation of different modes, as a result the grow rate of unstable modes can be reduced. In ASDEX Upgrade the production of rotating error field could be done in conjunction with other disruption mitigation techniques of AUG: ECCD [25], gas puffing and/or injection of cryogenic pellets.
The proposed enhancement of AUG include, in the latter stage, the installation of conductive wall which reduce the growth rate of Resistive Wall Modes. The set of MHD control coils, the 24 independent AC power supplies and suitable sensor and external control system will be used to control the RWM with a feedback control.

3.1.2 The new set of in-vessel control coils

The new set of active coils system designed for AUG consists of 24 saddle coils, which produce a non-axisymmetric, mainly radial, magnetic field (the design of the new magnet system is widely described on [22][26][27][28]). The system consists of three different sets of eight toroidally distributed coils, each coil is mounted inside the vacuum vessel. The poloidal position of the coils is sketched in figure 3.1. One set of coils is located at the outer midplane, around the vacuum A ports of ASDEX Upgrade, and is therefore subsequently dubbed A-coils. Two sets, marked as 'B_L' and 'B_U', are mounted below and above, in front of the lower and upper passive stabilising conductor, respectively. The radial position is chosen as to avoid unnecessary restrictions to the plasma shaping capabilities of AUG. In figure 3.1 is reported the 3D and the poloidal position of the new set of MHD control coils.
Each of the 24 in-vessel coils consists of a copper conductor with internal cooling channel. The 'A' and 'B_L' coils have six windings in two layers, the B_U coils, mounted on the surface of the upper passive stabilizing loop (PSL), have five windings in one layer.

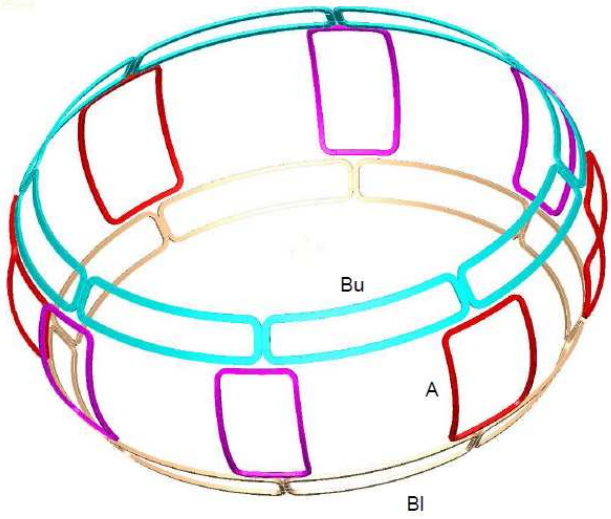

(a) 3D view

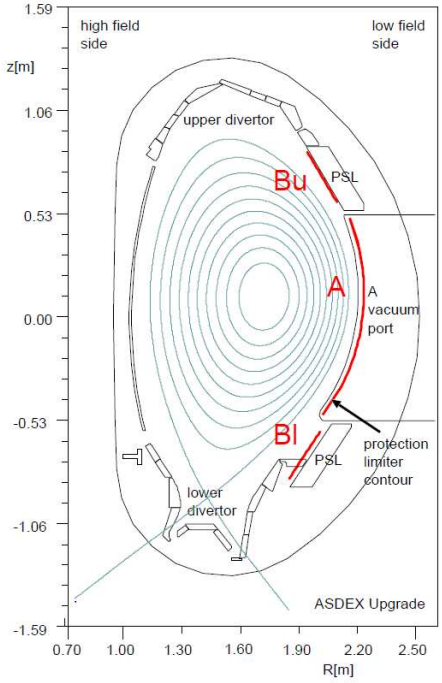

(b) AUG poloidal cross section showing the position of the MHD control coils

Figure 3.1: MHD control coils of ASDEX Upgrade (taken from [22]).

The coil housing and feeds are designed for 3.5 kV isolation voltage and will be operated at 2.5 kV or below. For a pulse duration of 10 seconds, the coils can be safely operated with a maximum DC or r.m.s. current of 1.5 kA . The targeted maximum operation frequency is f = 3 kHz for the A coils.

3.1.3 Stepwise implementation of the proposed enhancements

The structure of the proposed enhancement suggests a division into separate stages. These stages build on previous stages and can be implemented simultaneously or sequentially. Experimental possibilities are enhanced with each step.

1. In a first stage the 16 B_U and B_L active in-vessel coils with power supply feedthroughs are installed in ASDEX Upgrade. The coils will be operated with an existing DC power supply to produce Resonant Magnetic Perturbations (RMP) at the plasma edge.

2. Addition of 8 midplane "A" coils, for a total of 24 coils for larger configurational flexibility.

3. Installation of 12 fast AC power supplies, which can be configured for even n or odd n perturbations (toroidally opposite coils connected in series or anti-series, respectively). This allows to study the interaction of rotating error fields with NTMs and to implement disruption avoidance schemes. The additional power supplies also provide more flexibility to produce RMP fields for ELM control, with the special feature that the toroidal phase can be varied quasi-continuously between the three toroidal sets of coils.

4. Installation of the conducting shell. The passive shell and the active coils are designed from the beginning to be mechanically compatible. With 12 power supplies, either n = 1 or n = 2 RWMs can be controlled. The coils are designed to be capable of AC operation up to frequencies up to 3 kHz, sufficient to stabilise the RWM with the proposed wall.

5. Completion of the power supply system with another 12 AC power supplies, providing now full voltage capability and free choice of individual coil currents for each coil. In individual mode control, mixtures of odd and even n modes can be controlled simultaneously. There is the new possibility of controlling the magnetic flux individually at each coil with its own sensor (*intelligent shell* control [29]).

3.2 Specification for the AC power supply system

3.2.1 General requirements

As a general requirement, it is highly desirable the contemporary control of dc and ac operation during the pulse, the control reference signals in many operational scenarios will not be pre-programmed and the power supply will have to cope with any reference waveforms shapes (within the system capability).
A modular solution was considered as a first approach due to the advantages in

terms of optimization of the design, operation, spares etc. Actually, being the requirements for A and B coils significantly different, the selection of a modular design would have led to a not acceptable cost increase. As a consequence, the agreed approach was to perform dedicated design for the PS of the A and B coils, but trying to push as much as possible the modularity level.
The maximum pulse length of AUG tokamak is 10 s; but at lower plasma currents and smaller effort in plasma shaping theoretically up to 20 s could be reached. The duty cycle assumed for the power supply design is 10 s over 10 min at full current. The new power supply system will be source of ElectroMagnetic Interferences (EMI) since it will be based on switching converter (the detail of the design will be reported on Chapter 4). For EMI there is not a specific quantitative requirement, but the indication to reduce as much as possible this type of noise, which can disturb very much the diagnostic apparatus of the plasma placed all around the torus. On Chapter 5 are reported all the consideration related with the EMI issues due to the new power supply system.

3.2.2 Performance required for the different control actions

ELM suppression

Experiments for ELM suppression by resonant magnetic perturbation require a static (time independent) error field with toroidal mode numbers n = 2, n = 3 or n = 4 toroidal symmetry, and sufficient field amplitude as to induce ergodisation of the magnetic field at the edge pedestal in high-confinement mode (H-mode) plasmas. At this purpose a continuous current of at least 1.0 kA has to be supplied both to the A and B coils. It is extremely important that the power supply system is able to apply the required action in the minimum time in case of perturbation of the plasma stability. The power supply will therefore be able to initiate, perform and complete the transition from any initial output voltage level to the required output voltage level in less than 100 μs from the issuing of the relevant command, including therefore the transition from the full negative to the full positive voltage or viceversa. The delay is defined as the time between the request and the effective response of the power supply (the time when the output voltage reaches the desired value), in figure 3.2 the meaning of the delay time definitions is shown.

RWM stabilization

The feedback system for resistive wall mode (RWM) stabilization will use the complete coil set as actuators, including the B-coils and the faster A-coils. The response of the feedback loop, including actuators, must be fast enough to warrant sufficient phase margin for stability [30]. At present stage the feedback loop for RWM control is not fully specified and therefore no particular requirements have been given for the power supply for this operational scenario.
The RWM will be controlled on the initial experiment with rotating fields which can induce mode rotation. In terms of power supply requirements, this operational scenario requires an ac current of 440 A at 500 Hz.

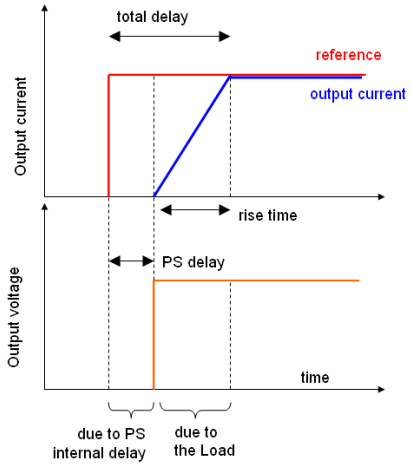

Figure 3.2: Delay Time definitions for the MHD power supply.

NTM rotation

The most demanding performance requested to the new control system is to prevent a disruption by locking an existing tearing mode to a rotating error field. In ASDEX Upgrade, this implies a perturbation field of of B = 3 mT amplitude, rotating with up to 3 kHz frequency. The production of fast rotating error fields will be achieved by dedicated coils, the "A" coils. In terms of power supply requirements the ac current in the coil shall has peak amplitude of 1 kA at 3 kHz.
This application does not call for specific requirements for the B-coils proposed in stage 1; however, mode rotation control experiments can be done with the B-coils too, though in a reduced parameter space.

3.2.3 Reference waveforms for the PS design

The voltage reference from the external controller may vary in an unpredictable way, in relation to the evolution of plasma instabilities during the pulse. Therefore, the power supplies may be requested to supply current and voltage waveforms of any shape that they can be capable to reproduce within the limits imposed by voltage and current ratings, switching frequency and load parameters.
However, the definition of a set of reference waveforms have been specified to be used as a reference to design and test the A and B-Coil power supplies. Three reference scenarios have been defined for the new power supply systems (the amplitude and frequency of the reference signals depends on the type of power supply, see Table 3.5):

1. Step current request, instantaneous rise time.
2. Sinusoidal current request.
3. Slow ramp-up and ramp down, frequency: 20 Hz.

An additional reference waveform will be used to check the power supply system performance on the expected RWM scenario with closed loop feedback control. For

this scenario the control of the instabilities requires a non-preprogrammed waveform whose reference shapes look like pink noise (the model used to generate this waveform is a white noise generator followed by a low pass filter).

4. RWM scenario, random current reference.

3.2.4 Load parameters

Table 3.1 reports the parameters of the A and B-coils, feedthrough and cable evaluated with FEM analyses (carried out by the ASDEX Upgrade Team) for three different scenarios: DC, AC(1 kHz), AC(3 kHz). It can be noted the higher equivalent resistance (due to parasitic currents induced in nearby passive conductive structures) of B-coils at high frequency due to the different implementation of the coil screen and the proximity with the PSL. Another important aspect to be considered is the low inductance of the coils, comparable with the characteristics of the power cable.
To perform the design of the power supply system the data reported in Table 3.1 have been used considering the two operational scenarios (DC and AC) separately. This procedure has simplified the power supply design studies and has clarified the definition of the requirements in terms of voltage and current.

		DC	$AC_{1\,kHz}$	$AC_{3\,kHz}$
A-Coil	R $[m\Omega]$	15	-	50
	L $[\mu H]$	30	-	30
B_U-Coils	R $[m\Omega]$	5.2	53.0	180
	L $[\mu H]$	31	23	15
B_L-Coils	R $[m\Omega]$	4.9	120.0	253
	L $[\mu H]$	44	29	15
Feedthrough	R $[m\Omega]$	0.4	1.7	3.4
	L $[\mu H]$	1.6	1.4	1.0
Cable	R $[m\Omega]$	14	30	57
	L $[\mu H]$	14	11	8.1

Table 3.1: Load parameters for the A and B-coils, feedthrough and cable evaluated for three different scenarios: DC, AC(1 kHz), AC(3 kHz)

3.2.5 Voltage and Current rating of the Power Supply

DC scenario

Both set of coils need a dc current of 1 kA in order to mitigate or suppress the ELM by stationary error fields(see 3.2.2 for details). Table 3.2 reports the resistance of the whole load (coils + cable + feedthrough, derived from Table 3.1) for the A, B_L and B_U coils and the voltage needed to feed the DC current.
One of the main requirements of the new MHD control system is to catch as fast as possible the MHD instabilities (the power level required for their control rises with

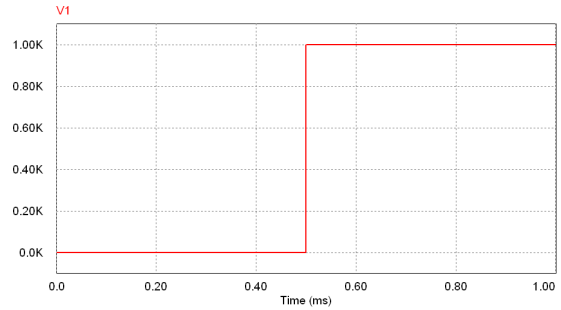

(a) Step current request, instantaneous rise time.

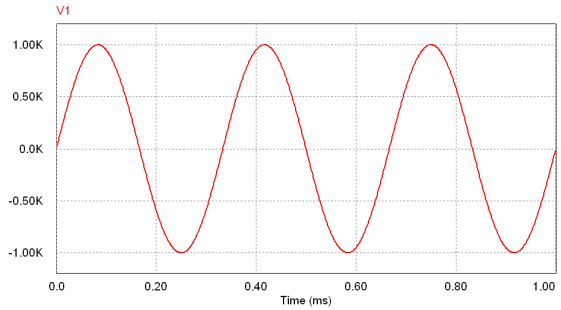

(b) Sinusoidal current request.

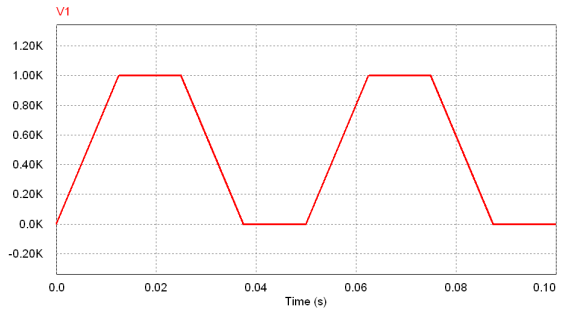

(c) Slow ramp-up and ramp down,frequency: 20 Hz.

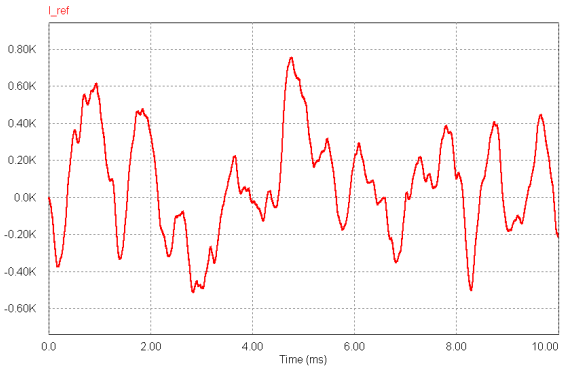

(d) Slow ramp-up and ramp down,frequency: 20 Hz.

Figure 3.3: Reference waveforms for the PS design

	DC resistance	DC Voltage drop
A-Coils	29.4 $m\Omega$	29.4 V
B_U-coils	19.6 $m\Omega$	19.6 V
B_U-coils	19.3 $m\Omega$	19.3 V

Table 3.2: Resistance and voltage drop of PS loads

the time response of the PS): in addition to the requirements in terms of dc voltage given above a constrain on the maximum rise time for a step current request will be added. On this conceptual design it has been assumed as requirements a maximum rise time of 100 μs for the A-Coils and 200 μs for the B-Coils when an instantaneous current step with magnitude 1 kA is requested by the external controller.
Considering a continuos feeding voltage V_{out} and using the classical equation of current rise for a RL circuit, the needed voltage to satisfy the requirement given above is:

$$V_{out} \geq \frac{I_{ref} \cdot R_{dc}}{1 - e^{-t_{rise}/\tau}} \tag{3.1}$$

The summary of parameters and required voltage is reported on Table 3.3.

	$\tau\ [ms]$	$I_{ref}\ [kA]$	$t_{rise}\ [\mu s]$	$V_{out}\ [V]$
A-Coils	1.55	1.0	100	470
B_U-coils	2.38	1.0	200	243
B_U-coils	3.09	1.0	200	308

Table 3.3: Rise time voltage requirements for the three power supply systems.

Another requirement for dc operation is the maximum ripple allowed at the nominal dc output current: the values selected are $\pm$ 1 % for the A-Coils PS and $\pm$ 2 % for the B-Coils PS.

AC Scenario

The AC requirements for A and B coils are quite different: while the requirement for the A-Coils is to follow a sinusoidal current reference with magnitude 1 kA and frequency 3 kHz the B-coils corner frequency (1.2 kHz) excludes operation at 3 kHz. The needed field produced by B-Coils to control RWM instabilities requires 1 mT (which mean a peak current of 440 A) with a frequency of 500 Hz, on this conceptual design it has been decided to increase the frequency capability of the B-Coils PS to 1 kHz in order to give more flexibility to future scientific programs of AUG.
The minimum voltage needed for AC operation is given by equation 3.2:

$$V_{ac\,peak} = I_{ac\,peak} \cdot \sqrt{R_{ac}^2 + (2\pi \cdot f \cdot L_{ac})^2} \tag{3.2}$$

The summary of parameters and required voltage for AC scenario is reported on Table 3.4.
In addition to the output voltage requirements for the AC operation it is necessary to

	f [kHz]	$I_{peak}\,[kA]$	$Z_{coil}\,[\Omega]$	$V_{ac\,peak}\,[V]$
A-Coils	3	1.0	0.745	745
B_U-coils	1	0.44	0.139	139
B_U-coils	1	0.44	0.199	199

Table 3.4: Voltage requirements for the three power supply systems.

define the maximum Total Harmonic Distortion (THD) allowed in case of sinusoidal reference waveform. THD is defined as the ratio of the powers of all the undesired harmonic components to the power of the fundamental frequency (equation 3.3).

$$THD = \frac{P_2 + P_3 + \ldots + P_\infty}{P_1} = \frac{P_{signal} - P_1}{P_1} \tag{3.3}$$

The THD could be defined using also the current signal spectrum. Its definition is equivalent to the one given in 3.3.

$$THD = \frac{I_2^2 + I_3^2 + \ldots + I_\infty^2}{I_1^2} \tag{3.4}$$

Maximum allowed THD for the A-Coils and B-Coils PS is 2% at the maximum operational frequency and maximum current amplitude in ac operation (considering the load parameters reported in Table 3.1).

3.2.6 Summary of the main specification data for the PS

To date the design of the A-Coils is not yet frozen, as a result uncertainty is still present with respect to load parameters. The values reported on Table 3.1 represent the present assumption for the coils parameters. A wide margin has been adopted in order to cope with the possible increase of the inductance (which implies an higher voltage to drive the oscillating current reference) and the increase of the resistance (which rises the power losses).
The proposed rating for the power supply systems which summurize all the considerations made in this chapter are reported in Table 3.5.

		A-Coils PS	B-Coils PS
	Number of Units	8	16
AC	Current magnitude	1 kA	440 A
	Maximum frequency	3 kHz	1 kHz
	THD	$\leq 2\%$	$\leq 2\%$
DC	Current magnitude	1 kA	1 kA
	Current ripple	$\leq \pm 1\%$	$\leq \pm 2\%$
	Output Voltage	$\pm 1\,kV$	$\pm 300\,V$

Table 3.5: Power Supply system requirements.

Chapter 4

Power Supply Conceptual Design

This chapter is the core of this thesis and includes all the analysys and the consideration that lead to the definition of the structure of both the A-Coils and B-Coils power supply systems.
The first part of the chapter is dedicated to the explanation of the general design criteria which include the selection of the modulation strategy and the power semiconductor devices used in the power supply system. Then the A-Coils and B-Coils power supply designs are reported in detail followed by computer simulation of current and voltage profiles in normal and fault scenarios.

4.1 General Criteria

The overall power supply system has to be able to feed 24 different coils (8 A-coils and 16 B-coils) running independent of each other. The following assumptions have been used as design guide lines:

- Each power supply system has to follow in real time any possible reference given by the central control system. The major impact of this requirements on the design is the necessity to size the systems in order to guarantee the maximum performance for any reference waveform for the entire pulse lenght (10 seconds).
- The bidirectional power flow calls for a four quadrants topology.
- The necessity of high bandwidth and system promptness needs a power supply topology based on fully controllable devices.
- Switch-mode converter represents the obvious choice due to the power and frequency level involved of the MHD instabilities control. The design will be based on Voltage Source Inverters (VSI)[1] where a dc voltage source is used

[1]The other type of inverters, used only for very high power application are the current source inverters (CSI) where the dc input for the inverter is a dc current source

to feed the H-bridge inverter. The VSI is composed of ac/dc input stage, dc link capacitors and H-bridge inverter, the latter device will be based on hard-switching techniques. Figure 4.1 shows the block diagram of VSI.

- The design will be performed using the load parameters reported in 3.2.4 and both dc and ac scenario will be evaluated. The mutual coupling among coils will be neglected.

- Goal of the design is to minimize the system cost and size and improve its reliability, standard solutions and implementations are preferred where applicable.

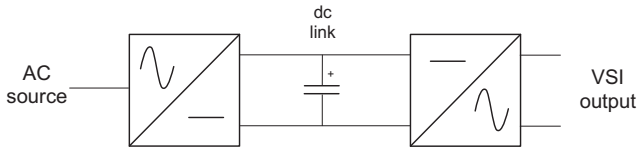

Figure 4.1: Voltage Source Converter block diagram.

The design process which includes selection of the topology, the semiconductor rating, switches modulation law selection etc. has been derived from an iterative process aimed at reaching a satisfactory compromise among performance, availability, cost and size; the results of this process is summarized in the following.
The possibility to adopt a full modular solution was considered first because of the advantages in terms of design and test economy, availability, spares, etc, but the overall cost was too high due to the significant differences between the A and B power supply requirements (see Table 3.5). A customized design was therefore followed for A and B PS trying however to push as much as possible the modularity level by identifying a basic module and relevant control which could be suitable for both.

4.1.1 Modulation strategy selection

Two important aspects need to be considered for the selection of the VSI modulation strategy: the evaluation of switch losses and the impact of the modulation on the conducted noise.
Two large families of modulation techniques can be applied to VSI: the first one includes all the modulation laws in which the switches operate at fixed frequency, the most used technique is the PWM where the control signal, $v_{control}$ is compared with a periodic triangular waveform which frequency is kept constant. The second category includes all the techniques in which the switching frequency can vary during the inverter operation (this family includes for example the hysteresis current control where the power supply system tries to maintain the current within a tolerance band, see figure 2.2).
The high performances required to the power supply system (in terms of switching frequency) call for the adoption of Unipolar Voltage switching technique in which the power supply system can generate output voltage equal to zero: this technique has the advantage of an effectively doubling of the switching frequency and the

disadvantage of the generation of the so called *common mode voltage* on the output or the input side of the inverter (it depends on the position of the grounding point of the power supply). The common-mode voltage implies the injection of common mode current on the ground circuit, it produces disturbance to the electronic devices placed nearest to the common-mode current path (which is closed by the ground conductor). Chapter 5 is dedicated to the analyses of the effect of this type of noises in the new power supply system.
Being the conducted noise a direct consequence of the swing of common-mode voltage in case of Unipolar PWM the fixed frequency implies a noise power spectrum composed of discrete harmonics. Proper filtering techniques could be used to mitigate the effect of conducted noise on diagnostic signals.
In the other scenario, the usage of non-fixed frequency modulation technique features the injection of common mode current with a non periodic repetition, as result noise spectrum is distributed on a wider range of frequencies leading to lower peak spectral density of the noise power. The mitigation *a posteriori* of the noise effects on diagnostic signals is not possible with filtering techniques.
From the point of view of losses calculation the unpredictable switching behaviour of the non-fixed frequency technique does not permit the evaluation *a priori* of the losses on the inverter, to limit semiconductors junction temperature it is necessary to control properly the inverter modulation (this can be done by the control of the hysteresis band, as reported on [31], [32]). On the contrary, the adoption of PWM modulation strategy permits to evaluate *a priori* the worst scenario from the inverter losses point of view.
In this conceptual design the possibility of a deterministic calculation of the losses was preferred and led to assume fix switching frequency. In any case the two modulation strategy can be applied to any H-Bridge inverter ([33] illustrates the multilevel modulation techniques for hysteresis current controlled inverter). The present choice does not exclude possible future revision of the modulation strategies.

4.1.2 Selection of power semiconductor device for A and B-Coil PS

Nowadays exist a wide portfolio of power semiconductors which can sustain safely the power rating required by the A-Coil and the B-Coil power supply. While the low-voltage ($\leq$ 600 V) sector is dominated by the MOSFET, the range 800 V - 3.3 kV belongs to the Insulated Gate Bipolar Transistor (IGBT) [35], which has also penetrated into the 4.5 and 6.5 kV classes, the traditional domain of Integrated Gate Commutated Thyristor (IGCT) [34]. In the particular field of voltage source inverters, the region below 10 MVA is rather covered by IGBTs while above 10 MVA by IGCTs [36].
The rated output voltage, the needed switching frequency and the output current of A and B-Coil inverters calls for adopting IGBT as switching device for both power supply systems. A solution based on IGCT is anyway possible but it implies higher commutation losses which could be reduced by means of additional paasive circuit (snubber). In the following is reported a brief comparison of IGCT and IGBT focused on the power level required by the A-Coil and B-Coil power supply.
In Table 4.1 are reported the main characteristics of two semiconductors with similar

	IGCT	IGBT	
Manufacturer	ABB	Infineon	
Device	5SHY 35L4510	FZ1800R12	
Collector-emitter voltage	2800	1200	V
DC-collector current	1700	1800	A
Pepetitive peak collector current	32	3.6	kA
Forward voltage$_{@1kA}$	1.72	1.83	V
Lead resistance	325	70	$\mu\Omega$
Turn-on energy loss per pulse	134	213	mJ
Turn-off energy loss per pulse	1960	273	mJ
Turn-on delay time	3.5	0.61	μs
Turn-off deleay time	7	1.18	μs
Thermal resistance R_{JH}	11.5	17	K/KW

Table 4.1: Comparison of commercial IGCT (ABB - 5SHY35L4510) and IGBT (Infineon - FZ1800R12) devices with similar current rating characteristics. The turn-on and turn-off energy has been scaled to 1kA-1kV operating condition in the hypothesis of linear scaling

current rating, both suitable for the A-Coil and B-Coil power supply systems.
In Figure 4.2 it is showed the maximum operating switching frequency for a single H-bridge implemented with IGCT and IGBT whose parameters are reported in Table 4.1. The analysis has been performed considering:

- PWM modulation
- Maximum power losses scenario
- Temperature swing 85°C ($T_{jmax} = 125°C, T_{amb} = 40°C$)
- Ideal power transmission from heatsink to ambient ($R_{thHA} = 0$)
- Continuous current on an inductive load
- 1kV dc-link voltage
- Snubberless implementation

The maximum operating frequency of inverter has been calculated considering the thermal properties of the components (in terms of thermal resistance) and the allowed power loss in the semiconductor junction. Fixed the load current (and therefore the conduction losses) the switching frequency is derived by the commutation losses value. In section 4.2.4 is reported the analysis done for the A-Coil PS inverter. The results show that the IGBT inverter allows a larger switching frequency with respect to the IGCT inverter (this is mainly due to the high turn-off losses of the latter). Another aspect to be considered (as reported in Table 4.1) is the high turn on and turn off delay of the IGCT which seem to be too high for an application where it's required a fast response to a control request.
All the analyses described in this conceptual design study have been performed assuming IGBT technology and in particular the Infineon FZ1800R12 device, whose parameters (see Table 4.1) seem adequate to satisfy the system requirements both for A-Coils and B-Coils power supplies.
Even if the IGBT is a good candidate for application to operate at high voltage

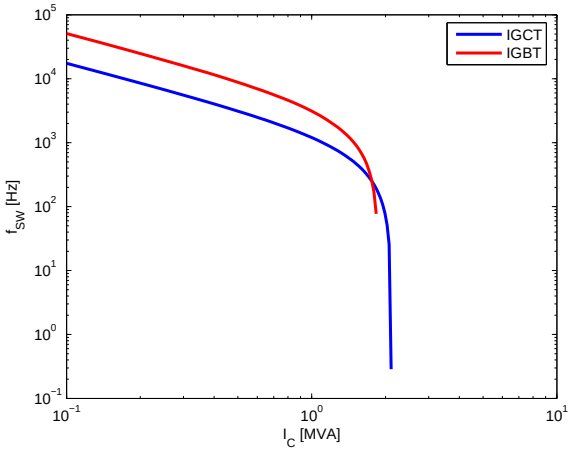

Figure 4.2: Comparison of inverter performance based on IGCT (ABB - 5SHY35L4510) and IGBT (Infineon - FZ1800R12).

and high frequency, its particular semiconductor structure implies a relatively high current tail[2] at turn-off which limits the operations of the device. This conceptual design foreseen a limitation of the minimum turn-on and turn-off time of the switches in order to avoid the tail current problems.

4.2 A-Coils Power Supply Design

This paragraph describes the relevant design criteria followed to identify the structure of the A-coils power supply.

4.2.1 Output Section design

The high bandwidth required for the A-Coils PS, 3 kHz, could be satisfied only if the frequency of the output voltage is above 15 kHz (this value is derived from a thumb rule of PWM converter design where the switching frequency should be at least five times the maximum frequency of the voltage reference). In addition to this requirement it is necessary to fed in dc scenario a continuous current of 1 kA. A technical solution based on a single hard-switched H-bridge was judged not viable because in the worst case scenario for the power losses (dc current on an inductive load) the wasted power on switching modules could be excessive and can't be sustained safely, at high switching frequency, by the available commercial components. Goal of the design is to minimize the power supply switching frequency assuring at the same time the voltage, current and frequency requirements. Series connection of VIS can improves load frequency and distribute the losses among different power modules.

[2]The tail current of IGBTs are caused by stored excess carriers in the wide and lightly doped N-base layer during its forward conduction. The width of this layer determines the voltage blocking ability of the device; however this layer adds significant resistance during forward conduction that results in stored excess carriers. These carriers produce a collector tail current during its turn OFF transient [37][38].

The SOA (safe operating area) combined with the long-term stability against cosmic radiation help to define the IGBT voltage rating: for improved reliability and to avoid false triggering due to cosmic radiation the maximum allowed voltage applied to the IGBTs is generally derated by approximately 40 % from the maximum device voltage. In order to use 1200 V IGBTs, a well rugged and widely available semiconductor family, the voltage requirements for A-Coils calls for at least two bridges in series:

$$N_{level} > \frac{V_{OUT}}{1200\,V \cdot (1-\epsilon)} = \frac{1000\,V}{720\,V} = 1.39 \tag{4.1}$$

The current rating IGBT devices has been selected considering that the maximum dc current on the control coils is 1500 A (see 3.1.2): this values can be easily achieved by a single component (the commercial 1.2 kV IGBTs support up to 3.6 kA) and therefore no parallel connection of multiple switches is needed. The current rating selected for the inverter switches is 1.8 kA which allows a good design margin with a reasonable cost (which increase with switch current rating).
In conclusion the A-Coils power supply output section will be composed of two inverter in series, whose switches are rated for 1.2 kV, 1.8 kA.

4.2.2 Multilevel Inverter Topology Selection

Multilevel voltage-source inverter technology has emerged recently as a very important alternative in the area of high-power medium-voltage energy control [39] [40],[41]. Nowadays, there exist three commercial topologies of multilevel voltage-source inverters: Neutral Point Clamped (NPC), Cascade H-Bridge (known as Cascade Multilevel (CM) converter) and flying capacitors. The technologies taken in consideration for the A-Coil Power Supply design were NPC and Cascade Multilevel.

NPC

Neutral Point Clamped topology has been proposed by Nabae in 1981 [42]. This converter was based on a modification of the classic H-Bridge adding two semiconductors and two clamping diodes per phase. This solution due to the reduced harmonic content of its output voltage has become an established technology in power electronic inverters.
Many schemes and modulation techniques have been presented in the past (NPC is the dominant technology on motor drive application).Most f the applications of NPC are in the field of three-phase systems, relative small number of applications involving NPC are applied to the single-phase converter. Among the latter group of applications a single-phase NPC with a 5-level modulation technique presented in [43] and [44] has been selected as candidate topology for the A-Coils power supply: its electrical scheme is showed in figure 4.3.
Each leg of the single phase NPC inverter is modulated with a modulation technique similar to the Unipolar PWM. A particular refinement, well described in [44] it is necessary to preserve the peculiarities of the NPC topology. The control circuit is the same for each inverter leg with a difference between the phase carriers (shifted by $\pi/2$); the control scheme is showed in figure 4.3.

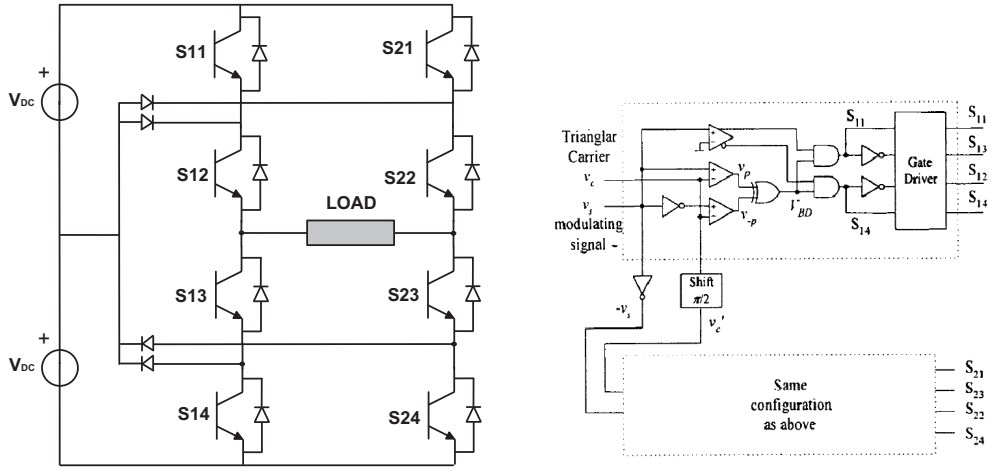

(a) Switches Topology

(b) Control Scheme, taken from [44]

Figure 4.3: Single phase 5-levels NPC converter

Cascade Multilevel

A Cascade Multilevel (CM) single-phase converter structure is obtained by series connecting some H-bridge modules, each one supplied by an insulated dc voltage source. The resulting phase voltage is synthesized by the addition of the voltages generated by the different cells. Using a three-levels modulation for each inverter (which implies three output voltage levels: $v_{dc}, 0, -v_{dc}$) the number of output levels is given by:

$$N_{level} = 2 \cdot N_{inv} + 1 \tag{4.2}$$

Where N_{inv} is the number of power modules.
Based on such a solution, several applications have been proposed, the main advantages are the reduced voltage stress of switches due to the series connection, the reduced dv/dt due to the lower voltage swing of each power module, the use of off-the-shelf semiconductors for medium-voltage applications, the high modular implementation and the high quality of the voltage and current waveforms. The main drawback of this technology is the need of large number of separated dc voltage sources. In many applications the dc link voltage is obtained by:

- single or three phase rectifiers, each ac-source is fed by a dedicated transformer secondary [45].
- Isolated dc source, for example photovoltaic panels [46] or isolated dc/dc converter [47].
- In some applications that don't need the injection of power into the load (like power quality devices) the dc voltage can be fed by a floating capacitor. [48]

The circuit scheme for a five-levels inverter based on Cascade topology is depicted in figure 4.4.
A large number of control strategies have been proposed for CM converter; the high number of power electronic devices and therefore the switching redundancies

permit high level of complexity of the control, which can be used to improve some features of the converters: reduction of the switching frequency, minimization of the common-mode voltage, balance of the dc-link voltages etc. Among the various PWM modulation techniques the Phase Shifted Carrier PWM (PSCPWM) represents a standard for several reasons: it offers an evenly power distribution among power modules and permits an easy implementation for topologies composed of large number of inverter. With this type of modulation, each power module (internally modulated with a three level modulation technique) shares the same modulation signals while the carriers between the bridge inverters are phase shifted by π/N (where N is the number of full bridge inverters in a multilevel phase leg). The electric and control scheme for a 5-levels CM inverter, composed of two H-bridges, are depicted in figure 4.4.

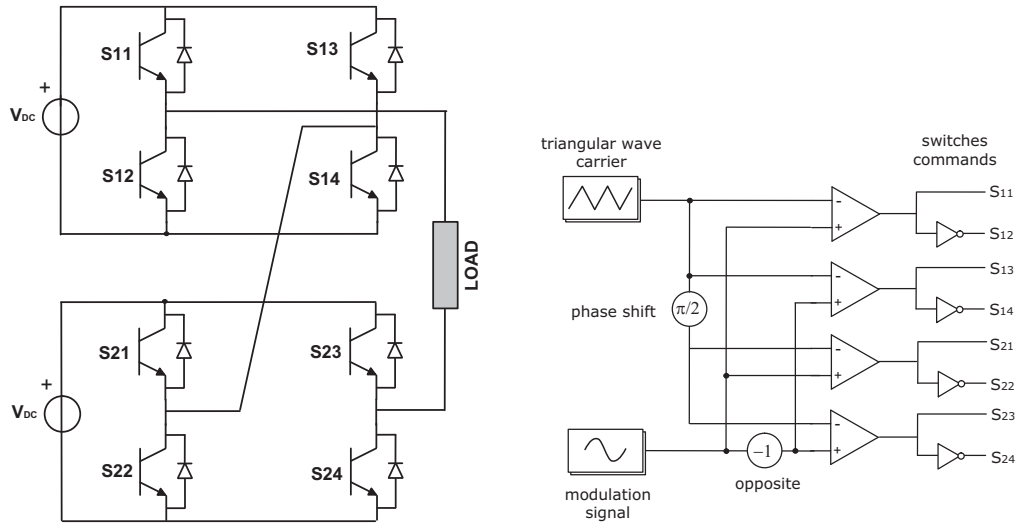

(a) Switches Topology (b) Control Scheme

Figure 4.4: Single phase 5-levels Cascade converter

NPC and Cascade performance comparison

During the conceptual design studies of the AUG new set of power supply the NPC topology has been taken in consideration due to its advantage with respect to the cascade topology:

- The dc-link system could be unified for all the A-coils Power Supplies
- The zero-voltage state is generated through the clamp diodes, as result no common mode voltage is generated[3].

The analyses described below show the disadvantages of NPC solution with respect to the Cascade one, in particular for the dc scenario (1kA on the load). The general assumptions, used in the analyses are the following:

[3]The definition of common-mode voltage for power supply is given in Chapter 5.

- the load parameters (reported in Table 3.1) are considered frequency independent during the VSC operation.
- The maximum output voltage for A-Coils PS is 1 kV.
- The switching frequency is 6 kHz (the switching frequency selection is reported in 4.2.4).

Prior to the topologies comparison the current ripple for a 5-level inverter will be derived.
It is well known that a Unipolar Voltage Source Converter drives a continuous current on an inductive load by applying a squarewave voltage which width depends on the voltage level to be applied. For a five levels inverter if the needed voltage to drive the load current ($V_{dc} = R_{dc} \cdot I_{dc}$) is lower than $V_{dc\,out}/2$ the converter generate a sequence of voltage pulses with amplitude $V_{dc\,out}/2$ followed by zero-vector state where the current flows through the inverter freewheeling diodes (the voltage and current shapes for this particular scenario is showed in figure 4.5).

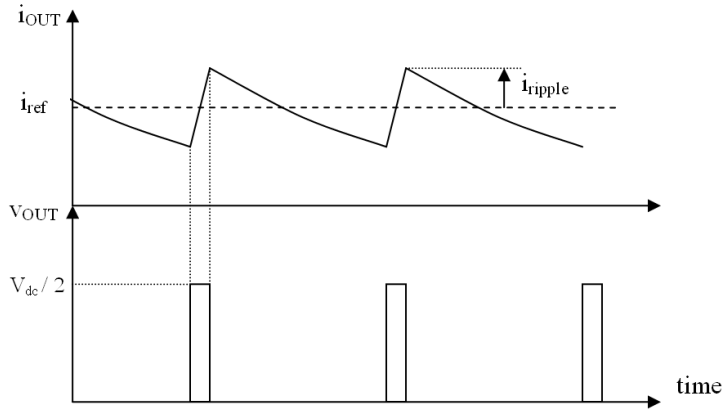

Figure 4.5: 5-levels VSC voltage and current shapes for a continuous current on inductive load.

The voltage pulse width t_{pulse} depends on V_{dc}, the inverter maximum output voltage $V_{dc\,out}$ and the frequency of the PWM carrie signal f_{sw}:

$$t_{pulse} = \frac{R_{dc} \cdot I_{dc}}{2 \cdot f_{sw} \cdot V_{dc\,link}} \tag{4.3}$$

Using the parameters of A-Coils PS the needed width of output pulses in order to drive 1 kA on load current is 2.36 μs and the current ripple, defined as the semi difference of the total current swing around the reference is given by the following equation:

$$i_{ripple} = \frac{V_{dc\,out} - 2V_{dc}}{2R_{dc}} \frac{1 - e^{-t_{pulse}/\tau}}{1 + e^{-t_{pulse}/\tau}} \tag{4.4}$$

where series RL time constant is defined as: $\tau = L/R$. Previous equation gives a total ripple of 12.7 A. This value, independent by the inverter topology, represents the minimum current ripple performance of 5-levels inverter on the A-Coils PS load

for the given dc link voltage and carrier switching frequency.
The two inverter topologies, NPC and Cascade, taken in consideration for the A-Coils PS, generate the output voltage pulses sequence in two different ways. In figure 4.6 are showed the three switches configurations of a NPC converter needed to generate $V_{DC}/2$ (two different configurations to connect the load to the upper or lower dc source) and the zero voltage state where the current flows through the clamp diodes of NPC.
In the first inverter configuration the active switches are S_{11}, S_{12} and S_{23} and the upper dc source is connected to the load. In the second configuration the active switches are S_{12}, S_{23} and S_{24} and the active dc source is the lower one. The last configuration shows the zero-voltage state where the output current flows through S_{12} and S_{23} and the clamps diodes. The current profiles of 5-levels NPC converter feeding a continuous current on an inductive load are showed in figure 4.7.
The analysis of current profiles suggests considering two important aspects:

- The dc sources are connected to the load by switching ON alternatively S_{11} and S_{24} for a small period (given by equation 4.3).
- The output continuous current flows through the middle switches S_{12} and S_{23} for the entire PWM period.

As reported above to avoid problems with the IGBTs tail current it is necessary to maintain the switch turned on for a minimum period (in the order of $5\mu s$). Being the pulse width needed to drive 1 kA lower than this minimum turn-on time the current profile of an NPC converter in the dc scenario presents an unstable behaviour. In figure 4.8 are showed two simulated current profiles for a 5-levels current controlled NPC converter. The regulation is done with a simple P controller, the current reference is kept constant.
In the first simulation it can be noted that the output waveform is not periodic; some *holes* are present in the normal sequence of pulses. This is due to the minimum pulse width of the output pulses which implies a duty cycle greater than the one derived on equation 4.3, as a result the control needs to compensate this excess of effective output voltage by suppressing some output pulse. It can also be noted a drift of current envelop due to the excess of output voltage.
In the second simulation, which is characterized by an higher proportional gain of the regulator, the output voltage is composed of a series of positive and negative voltage pulses with a resulting higher ripple. In figure 4.9 it is represented the result of a parametric simulation used to evaluated the average current ripple as function of the proportional gain of the regulator for a 5-levels NPC converter: it could be noted the transition (when the gain reach $K_P = 10^{-3}$) between the two current behavior showed in figure 4.8.
The second aspect to be considered is the conduction losses of the middle switches S_{12} and S_{23} which sustain a continuos current for the entire PWM period; the simple formula to estimate these losses is the following:

$$P_{loss} = V_T \cdot I_{dc} + R_{cc} \cdot I_{dc}^2 \tag{4.5}$$

Using the IGBT parameters reported in Table 4.1 the total losses for the 1kA dc scenario are 1.87 kW for each switch, this values is below the limit of 2.5 kW which

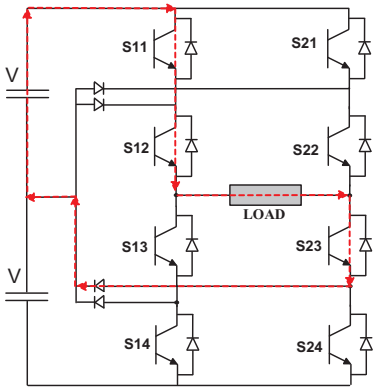

(a) $v_{LOAD} = v_{DC}$, upper dc source connected to the load. Current flows through S_{11}, S_{12} and S_{23} IGBTs

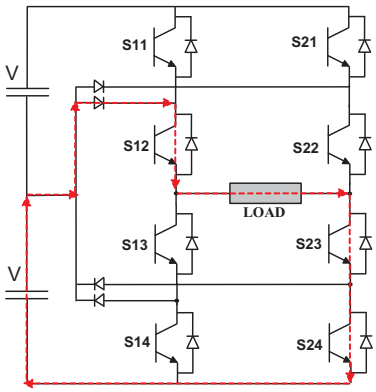

(b) $v_{LOAD} = v_{DC}$, lower dc source connected to the load. Current flows through S_{12}, S_{23} and S_{24} IGBTs

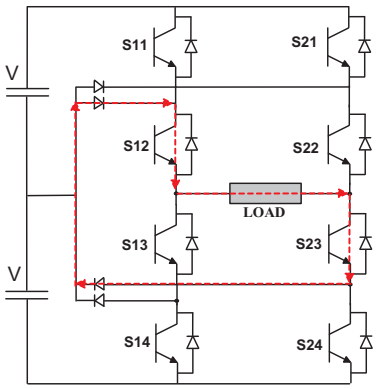

(c) $v_{LOAD} = 0\,V$. Current flows through S_{12}, S_{23} and two clamp diodes

Figure 4.6: 5-levels NPC inverter switches configuration to generate v_{DC} and $0\,V$ on an inductive output

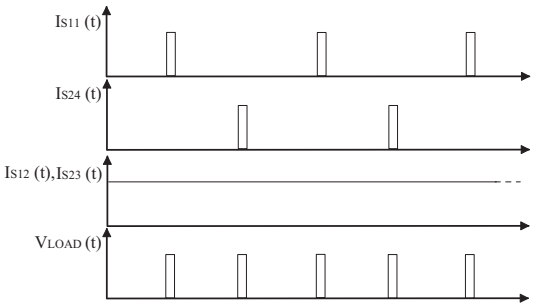

Figure 4.7: Current profile for NPC inverter feeding a dc current on the load. The switches name are referred to Figure 4.6

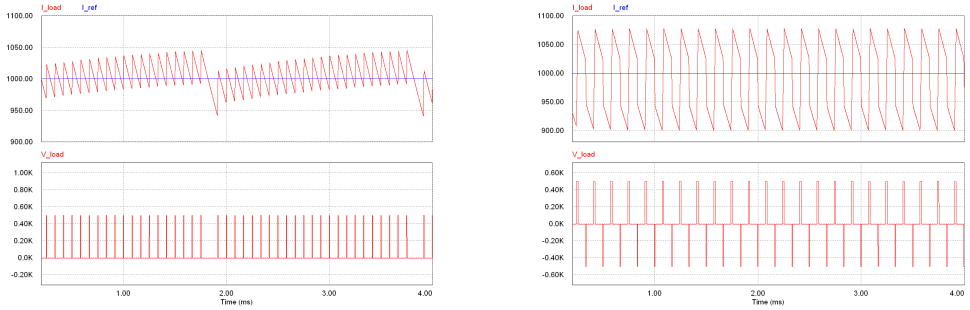

(a) $K_P = 0.5 \cdot 10^{-3}$ (b) $K_P = 1.5 \cdot 10^{-3}$

Figure 4.8: Simulations of an A-Coil power supply based on 5-levels NPC feeding 1 kA current on the load.

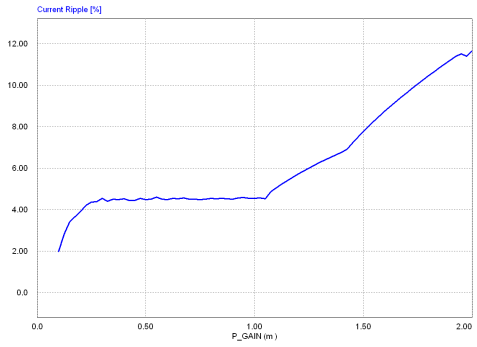

Figure 4.9: Relative current ripple as function of K_P gain of A-Coils PS for the dc scenario using a 5-levels NPC topology.

guarantee a safe operation of IGBT (see 4.2.4). Nevertheless it is necessary to point out that in this scenario there is no equilibrium in the losses of the eight IGBTs that compose the NPC inverter.
The behaviour of a multilevel inverter based on Cascade topology feeding a continuous current on an inductive load is slightly different with respect to the NPC inverter. The modulation strategy is the Phase Shifted Carrier PWM (PSCPWM); each output voltage pulse is generated alternatively by one bridge while the other gives zero-voltage, for this reason is sufficient to study a single H-bridge to define the minimum pulse width achievable and therefore the current ripple.
In a simple three-levels PWM modulation technique the switches in the two legs of the full bridge inverter are not switched simultaneously. Each inverter leg are controlled separately by comparing the triangular carrier $v_{carrier}$ with the modulation index v_m and its opposite v_{-m} the resulting output voltage is then obtained by the voltage difference between the mid potential of the two legs: theoretically, the pulse width of 3-levels converter can be as short as needed.
A possible constraint can be the inverter control implementation: in case it will be based on digital controllers, the IGBT firing command can't be generated in any arbitrary moment but need to be placed in a quantized time scale. This limitation could limit the minimum pulse width, the use of fast DSP is mandatory to guarantee the maximum performance in terms of current ripple.
The Cascade topology has been selected as the reference solution for the A-coils Power Supply due to the better performance in terms of ripple and the better power losses distribution among switches in the dc scenario.

4.2.3 A-Coils Power Supply Schematics

Figure 4.10 shows the block diagram of one A-Coil power supply system. The schematic is composed of two identical power modules each composed by an input section, a dc-link capacitor and one H-bridge inverter. Each power supply is feed by a galvanic insulated ac-source (i.e. one transformer secondary).

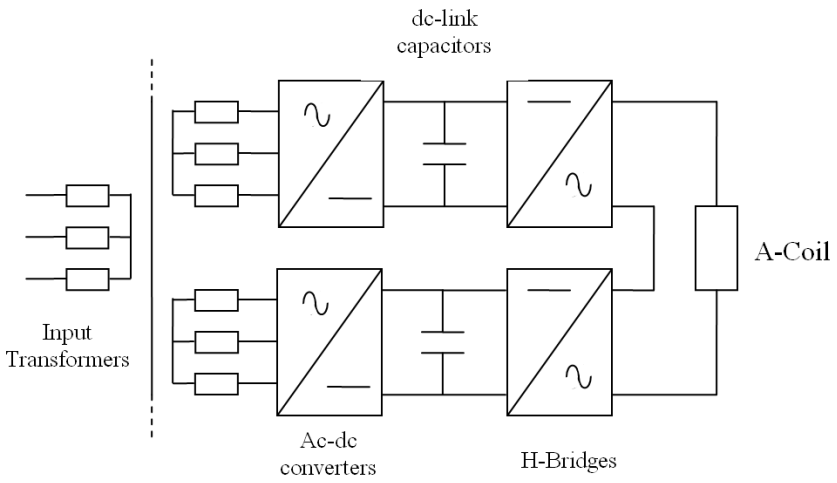

Figure 4.10: A-Coils Power Supply Block Diagram

4.2.4 Inverter Design

DC link Voltage

The DC link voltage sizing is directly related to the voltage requirements of the inverter output. For a five levels cascade inverter the voltage applied is:

$$V_{out} = \delta \cdot (V_{dc-link} - 4 \cdot V_T) \tag{4.6}$$

Where V_T is the saturation voltage of IGBT during conduction ($1.83\,V$ at the nominal dc current) and δ is the inverter duty cycle. Being the latter parameter limited ($\delta_{max} = 0.97$) the previous equation gives the minimum dc-link voltage:

$$V_{dc\,link\,min} = \frac{(V_{out} + 4 \cdot V_T)}{\delta_{max}} = 1038\,V \tag{4.7}$$

Operating Switching Frequency

Once defined the topology of the A-Coils Power Supply it is necessary to define the maximum operating frequency of the inverter switches. Prior to the considerations concerning the inverters operation it is necessary to define the maximum losses allowed for the expected operational conditions of the A-Coils power supply. The cooling system adopted for the power supply system foresees natural or forced air cooling, this choice is due to the low duty cycle of the power supply system 10 s over 10 minutes: the temperature rise could be considered adiabatic during the operational phase while during the machine off phase the heat could be dissipated by the heat exchange with ambient temperature.
In this analysis the following assumption have been taken:

- Constant ambient temperature during the pulse ($T_{AMB} = 40°C$)
- Constant power dissipation on IGBT module during the pulse (worst case scenario).
- Time constant of IGBTs thermal impedance has been neglected, this assumption implies instantaneous temperature rise at pulse starting.
- Heat transfer from the heatsink to the ambient has been negleted during pulses, (adiabatic temperature rise has been considered).
- The residual temperature rise between different pulses has been neglected.

These assumptions represent a worst case scenario; the real temperature rise of IGBT junction are lower than the value calculated hereafter (on section 4.6.5 will be presented the temperature profile simulated). In Figure 4.11 it is depicted the temperature rise during a pulse and the equivalent thermal model used for the analyses.

The temperature profile showed in figure 4.11 can be described by the following equation:

$$T_{Junction}(t) = T_{amb} + P_{module} \cdot (\frac{t}{C_{hs}} + R_{jh}) \tag{4.8}$$

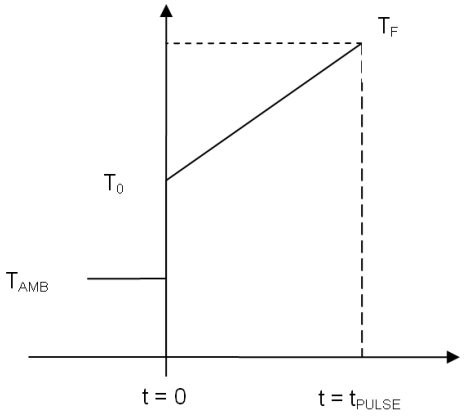

(a) IGBT junction temperature profile in the worst case scenario.

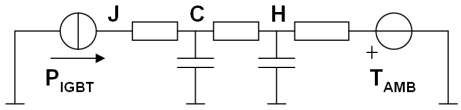

(b) Thermal model IGBT to calculate the temperature profile.

Figure 4.11: IGBT junction temperature analysis.

Where P is the power dissipated by the IGBT, R_{jh} is the thermal resistance between junction and heatsink, C_{hs} is the heat capacity of the heatsink. From the equation 4.8 the maximum power on IGBT junction is:

$$P_{max} = \frac{T_{jmax} - T_{amb}}{t_{pulse}/C_{hs} + R_{TH}} \tag{4.9}$$

The following assumptions can be taken:

- Aluminium Heatsink. Mass: 1 Kg, heat capacity: 897 J/K.
- Pulse duration (t_{pulse}): 10 seconds
- Rth Junction-heatsink = 0.017 K/W (from component data-sheet).

Due to the growing usage of IGBT on automotive and traction application there is a great interest in the lifetime prediction of power modules. An estimation of this lifetime (defined as the number of power cycles to failure) requires a relationship between the number of load cycles versus the temperature conditions (i.e. maximum heat sink temperature and maximum junction temperature) [50]. An important study of the power cycling lifetime of standard base plate modules was conducted during the LESIT-project. Using modules from different suppliers, a comprehensive data base was collected [51], In figure 4.12 are reported the results of the study.
The maximum temperature swing depends on the ambient temperature, the average temperature profile and the expected number of power cycles (defined as the alternating change of high and zero power consumption). As reported in [51] the number of cycles to failure for an IGBT power module can be expressed in a compact form:

$$N_f = A \cdot \Delta T_j^{\gamma} \cdot e^{\frac{E_a}{k_B \cdot T_m}} \tag{4.10}$$

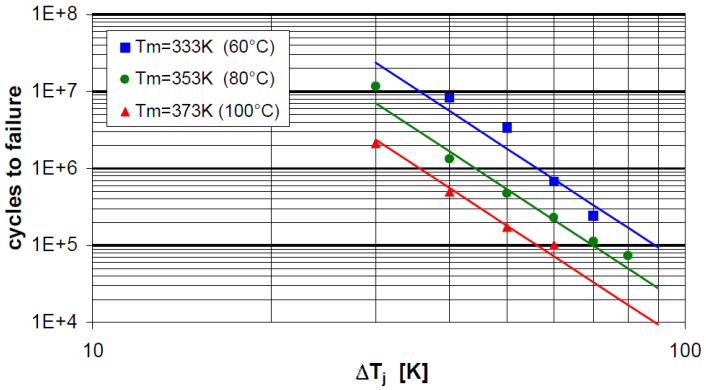

Figure 4.12: IGBTs lifetime as function of junction temperature swing (LESIT project results [51]).

Where $A = 640$, $R = 8.314 J/molK$, $\alpha = -5$, $Q = 7.8 \cdot 10^4 J/mol$ and T_m is the average of temperature swings profile (defined as $T_{jmin} + \Delta T_j/2$). For the A-Coils PS the system lifetime will be 100000 pulses (5000 pulses/year, 10 years times a safe factor of 2) and an average temperature of 80°C (ambient temperature of 40°C and maximum junction temperature of 120°C) the maximum temperature swing have to be less than 70 °C. Using equation 4.9 the maximum power on IGBT can be estimated:

$$P_{max} = \frac{\Delta T_j}{t_{pulse}/C + R_{th}} = 2480W \tag{4.11}$$

Considering the selected inverter topology, an Unipolar PWM modulation and hard-switching technique the worst case scenario for the power losses is represented by the dc scenario. Considering the inductive load as a current source, the current is forced to flow through a couple of IGBTs (which connect the dc-link to the load) and through the opposite freewheeling diodes. In figure 4.13 it is showed the current profiles for a single H-Bridge feeding a low inductance load (the phase shift of the two inverter composing the A-Coils power supply allows to consider the two bridge independent from the losses point of view).

The power dissipation of each IGBT module (switches and freewheeling diode) is the sum of four contributions, condution losses on IGBT and Diode, commutation losses in the IGBT and the reverse recovery losses on Diode:

$$P_{loss} = P_{cond\,IGBT} + P_{comm\,IGBT} + P_{cond\,Diode} + P_{recovery} \tag{4.12}$$

The current profiles depicted in figure 4.13 show that in the switches S_1 and S_4 only the IGBT is conducting (the current flows from the positive pole of dc-link to the load) while in the switches S_2 and S_3 only the freewheeling diode is conducting. To evaluated the most stressed power module it is possible to consider separately the two groups of switches.
In switches S_1 and S_4 the wasted power of IGBTs is the sum of two contributions: conduction losses and switching losses due to the current commutations. A

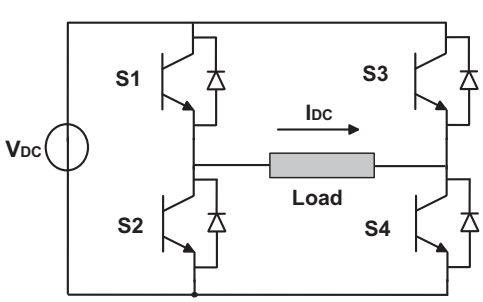

(a) Single phase H-bridge showing the labels of four IGBTs

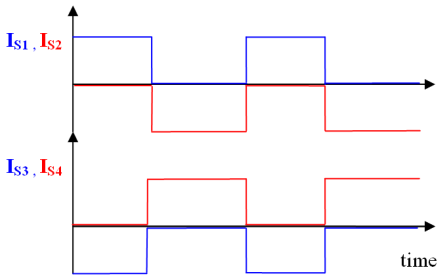

(b) Current profiles in the four IGBTs considering and inductive load fed with a low duty cycle

Figure 4.13: Current profiles on H-bridge switches. Continuos current on an inductive load.

simplified relation can be used:

$$P_{cond\,IGBT} = \delta \cdot (V_T + r_{cc} \cdot I_{dc}) \cdot I_{dc} \tag{4.13}$$

$$P_{comm\,IGBT} = f_{sw} \cdot (E_{on} + E_{off}) \cdot \frac{V_{dc} \cdot I_{dc}}{V_{ref} \cdot I_{ref}} \tag{4.14}$$

where r_{cc} is the differential resistance between IGBTs output terminals, E_{on} and E_{off} are the energy dissipated during a single commutation (calculated at V_{ref} and I_{ref}), V_T is the IGBT voltage drop during conduction, I_{dc} is the load current and δ is the duty cycle which can be considered equal to 0.5 due to the very low duty cycle (see equation 4.3). As showed on equation 4.14 the conduction losses depend on the load current and therefore it is not possible to reduce them. The only degree of freedom to reduce the total wasted power is to adjust switching frequency (the minimum dc-link voltage depends on required output voltage, its minimum value is given by Eq. 4.6).

$$f_{sw} < \frac{P_{comm}}{E_{on} + E_{off}} = \frac{P_{max} - P_{cond}}{E_{on} + E_{off}} \cdot \frac{V_{ref} \cdot I_{ref}}{V_{dc} \cdot I_{dc}} \tag{4.15}$$

Using the IGBT parameters reported in Table 4.1, the equations 4.9 and 4.14 gives a maximum frequency of 6.18 kHz. The same equation gives an additional information: the limit of the product $V_{dc\,link} \cdot f_{sw}$, if the dc link voltage can be decrease an improvment of switching frequency (and therefore the increase quality of the output waveforms) is possible.
The same procedure adopted for the IGBT could be followed for the evaluation of losses of freewheeling diodes (switches S_2 and S_3). Due to the low recovery losses the maximum operating frequency for the diodes is 22 kHz, well above the value calculated for the IGBTs.
On the basis of the previous considerations the selected frequency for this power supply is 6 kHz, with a resulting load virtual frequency of 24 kHz (4 times the switching frequency due to the 3-levels modulation and the modulation technique adopted), eight times the needed bandwidth: the selected circuit topology and the selected components guarantee, in first approximation, a feasible solution for the A-Coils PS.

4.2.5 DC-link section design

The power peaks required from the load in fast transient conditions are handled by the capacitor bank as the ac-dc converter is not able to make a significant contribution in the short time intervals. Moreover, in case of simple two quadrant topology, it can not transfer power from the load to the power grid.
The capacitor bank rating will be therefore derived on the basis of the energy exchanged in fast transient conditions and the accepted dc link voltage drop. The voltage drops on the connections of the dc-link to the inverter bridge are neglected in the calculations. Considering the following assumption:

- Load inductance of A-Coils PS in dc scenario (Coil + Cable + FT) is 45.6 μH.
- Maximum load current is 1 kA.

Maximum magnetic energy stored in the load inductance at its maximum current is given by:

$$W_{load} = \frac{1}{2} \cdot L_{load} \cdot I_{max}^2 = \frac{1}{2} \cdot 45.6\,\mu H \cdot 1\,kA^2 = 22.8\,J \tag{4.16}$$

To rate the capacitor bank, it cab be assumed that, in short time scale, all the magnetic energy is given to the load by the energy stored in the dc link capacitors. The voltage excursion of this component can be derived from the energy balance:

$$W_{load} = W_{C\,max} - W_{C\,min} = \frac{1}{2} \cdot \left(U_{C\,max}^2 - U_{C\,min}^2\right) \tag{4.17}$$

The maximum voltage $U_{C\,max}$ is $1038V$ (two $519V$ dc-link in series) while minimum voltage $U_{C\,min}$ hasn't been specified yet. It is reasonable to fix its value to 5% of the maximum value, the dc-link capacitance is given by the following relation:

$$C_{min} = \frac{2 \cdot W_{coil}}{U_{max}^2 - U_{min}^2} = \frac{2 \cdot 22.8\,J}{1038^2 \cdot (1 - 0.95^2)} = 434\,\mu F \tag{4.18}$$

The total energy stored by dc-link capacitors is:

$$W_{dc\,link} = \frac{1}{2} \cdot C_{min} \cdot U_{dc-link}^2 = \frac{1}{2} \cdot 434\,\mu F \cdot 1038\,V^2 = 234\,J \tag{4.19}$$

distributed evenly between the two power modules. Due to the equivalent series connection each capacitor of the A-Coils PS module should be rated for at least 868 μF.
Due to the particular multilevel topology of the A-Coil PS the different combinantions of active switches in the H-bridges can cause energy exchange between the two dc-link with consequent unbalance between the dc link voltages and a non negligible ripple (the latter depends on many factors, among them: the source input frequency, inverter output frequency, dc-link capacitance, rectifier topology). To reduce the effect of this voltage unbalance two different strategies could be used: feed-forward compensation of the dc-link voltage [49] or a simple over sizing of dc-link capacitance (respect the value derived in the fast transient condition, equation 4.18) can be effective since it reduce dc link voltage ripple.

The proposed capacitor rating is 10 mF (well above the value derived from 4.18), the dc-link voltage ripple in different operational scenario will be quantified by means of numerical simulation described in section 4.6.1 of this design.
The total energy stored by dc-link capacitors is:

$$W_{dc\,link} = C_{dc\,link} \cdot U^2_{dc\,link} \;=\; 10\,mF \cdot 519\,V^2 = 2.7\,kJ \tag{4.20}$$

This high energy value calls for the insertion of a breeder resistor used to discharge the component when the ac-source is switched off. Its power rating and sizing will be discussed on 4.2.6.

4.2.6 AC/DC section design

Description of the topology

An important aspect of the PS design is whether the dc-link voltage needs to be regulated in real time or not. When the PSs are required to supply a dc current, the possibility of reducing the dc link voltage allows reducing the ripple of the output current and inverter losses and this is an important benefit. Nevertheless, in this condition the control system request of fast reaction to a growing plasma instability could not be satisfied because the input ac/dc rectifier takes at least some ms to re-charge the dc link and the available output voltage could be not enough to assure the required current variation. Thus it was chosen to always maintain the dc link at the nominal value, leaving to the inverter the regulation of output current. This assumption allows simplifying the input scheme: a diode rectifier instead of thyristor rectifiers can be chosen; this input scheme can be selected also because the expected range of variation of the ac input voltage is not too high and because the rectifier power rating is quite limited.
A power resistor is inserted between the ac source and the diode rectifier at the system turn-on in order to reduce the in-rush current. Once reached a voltage key point (95%) of the final dc-link voltage each resistor is bypassed by a mechanical switch. The charging resistance has to be selected in order to minimize the power dissipation (which is directly related to the component cost and size) and maintain the charging time within a reasonable value. A possible implementation with standard commercial component use Fairifld RFX600 which can sustain adiabatically 1.5 kJ, a forward voltage of 800 V and dielectric strenght of 3 kV. The resistance value (which can be in the 1.3 to 2 kΩ range) can be selected imposing the maximum charging time equal to 1 s:

$$R_{charge} < \frac{t_{charge}}{5 \cdot C_{module}} = \frac{1s}{5 \cdot 10\,mF} = 40\,\Omega \tag{4.21}$$

The electrical scheme of ac-dc converter of A-Coils PS power module is depcted in Figure 4.14, the pre-charge circuit is composed of three bypass switches (dubbed Sw in the scheme).

Power rating of the ac/dc converter

In the A-coils PS system the fast power transients to and from the load are supplied by the capacitor bank, while the converter system has just to pre-charge the capac-

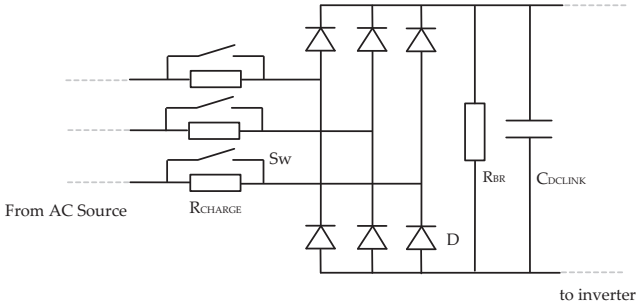

Figure 4.14: A-Coils power supply ac/dc section electric scheme

itor bank and to compensate the losses. It is therefore necessary to estimate the losses in the different operating conditions to identify the worst case to be assumed as reference for the power rating of the ac/dc conversion section.
The main sources of losses are:

- the load
- the conduction and commutation losses of the inverters
- connecting cables.
- auxiliaries (control modules, protection devices, etc)

The losses in the load and in the inverter constitute the main contribution; they have been evaluated and the results are listed below. The contribution of the other components will be taken into account approximately as 10% of the total losses.
The load losses depend on the current flowing and on the equivalent resistance of the load itself (this parameter take account of the resistivity of the various conductors and the eddy current losses in high frequency operations and the skin effects). In Table 4.2 are reported the equivalent resistance of the load components considering the dc scenario and the ac scenario.

	ac scenario	dc scenario
A-Coil	50 $m\Omega$	15 $m\Omega$
Cable	57 $m\Omega$	14 $m\Omega$
Feedthrough	3.4 $m\Omega$	0.4 $m\Omega$
Total	110.4 $m\Omega$	29.4 $m\Omega$

Table 4.2: A-Coils power supply resistive load for different scenarios.

The total losses for two different scenario depend on resistances reported in Table 4.2 and the amplitude of current reference (1 kA in dc and 707 A_{rms} in ac):

$$P_{Acoil\,dc} = R_{Acoil\,dc} \cdot I_{dc}^2 = 29.4kW \tag{4.22}$$

$$P_{Acoil\,ac} = \cdot R_{Acoil\,ac} \cdot I_{rms\,ac}^2 = 55.2kW \tag{4.23}$$

The worst case for the A-coil PS load dissipation is represented by the high frequency operation.

The inverter losses for the two operational scenarios have been calculated by a computer simulation model implemented using PSIM, Matlab and Simulink.

Scenario	f_{sw}	device	conduction	commutation	total
AC	6 kHz	IGBT	270 W	910 W	1180 W
		Diode	196 W	389 W	585 W
DC	6 kHz	IGBT	933 W	1616 W	2549 W
		Diode	673 W	603 W	1276 W

Table 4.3: Simulation results for A-Coils PS switches losses considering an ac ($1\,kA_{peak}/3\,kHz$) and dc ($1\,kA$) current on the load.

In Table 4.3 are reported the simulation results (in steady state condition) for the ac scenario (sinusoidal current reference with $I_{peak} = 1kA$ and $f = 3kHz$) for the losses in each switch (each composed by IGBT and its freewheeling diode). Considering that the power losses are distribuited evenly between the two A-Coils PS inverter and between eight switches, the total wasted power for this scenario is given by:

$$P_{A-coil\,inverters\,ac} = N_{inv} \cdot (4 \cdot P_{IGBT} + 4 \cdot P_{fw\,diode}) = 14.1\,kW \tag{4.24}$$

In Table 4.3 are also reported the simulation results (in steady state condition) for the dc scenario (continuous current reference with $I_{dc} = 1kA$) for the losses in the switches. In this scenario the current flows through a pair of IGBT and a pair of freewheeling diodes, the total wasted power is given by:

$$P_{A-coil\,inverters\,dc} = N_{inv} \cdot (2 \cdot P_{IGBT} + 2 \cdot P_{fw\,diode}) = 15.3\,kW \tag{4.25}$$

The worst case scenario is represented by the ac operation where a large amount of power has to be delivered to the load (mainly wasted by eddy currents). In Table 4.4 are summarized the simulation results of power losses:

Scenario	Load Losses	Inverter Losses	Total Losses	efficency
AC	55.2 kW	14.1 kW	69.3 kW	0.80
DC	29.4 kW	15.3 kW	44.7 kW	0.66

Table 4.4: Power losses for A-Coils PS considering the load and inverter losses

The nominal power of the ac/dc conversion section is equal to the total power dissipation in the load and inverter plus additional 10 % to take into account the other possible losses; the final value assumed is about $69.3\,kW \cdot 1.1 = 76.3\,kW$.
The power rating of each rectifier should be fixed to 38.2 kW (each A-Coil is connected to a pair of basic power supply units). The duty cycle is the same than the AUG machine: 10 second every 10 minutes.
Each A-coil power supply inverter module is fed by a dc capacitor bank charged at 519 V. The maximum power is required to the ac/dc converter when the maximum active power is requested by the load, assuming this condition and neglecting the voltage drop of dc-link voltage the maximum dc output current can be derived:

$$I_{rect\,dc} = \frac{P_{total}}{V_{dc-link}} = \frac{38.2\,kW}{519\,V} = 73.6\,A \tag{4.26}$$

4.3 B-Coils Power Supply Design

Respect the A-Coils power supply system the requirements for the B-Coil PS are less demanding in terms of harmonic response (see 3.5), as consequence the constrain that have led to the choice of two bridges in series can be relaxed and a solution with a single H-Bridge can be adopted. One of the two identical modules of the A-Coils PS, with the same dc-link capacitor rated for 519 V, was assumed for the B-coils PS design. Its capability to fulfill the requirements of the B-Coils PS was verified with numerical simulations. They showed very good performance in terms of ripple, bandwidth and Total Harmonic Distortion (THD) (see section 4.6).

4.3.1 B-Coils Power Supply Schematics

In figure 4.15 is showed the block diagram of one B-Coils power supply system. The schematic is identical to an half of the A-Coils power supply block diagram where two different power modules (composed by an ac/dc converter, a capacitor bank and one inverter) are connected in series.

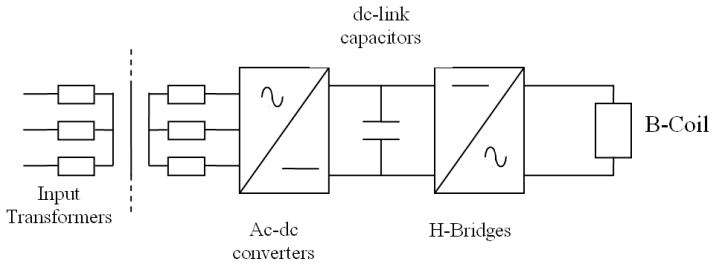

Figure 4.15: B-Coils Power Supply Block Diagram

4.3.2 Inverter Design

The B-Coils PS can be based on single H-bridge inverter topology. As for the A-Coils PS the modulation technique will be based on PWM with fixed frequency carrier, to increase the virtual frequency applied to the load the modulation law selected for the B-Coils PS is a 3-levels PWM. This solution permits the usage of the same control module of the A-Coils PS (in which the 5-levels was achieved by two 3-levels controller with shifted carrier frequency) pushing for the modularity of the overall system.
As for the A-Coils PS the multiple levels technique has the drawback of common mode current injected into the circuit.

DC link voltage

The voltage requirement for the B-Coils is 300 V as reported in Table 3.5, in order to obtain significant margin, which permits a wider operational capability of the B-Coils system, the proposed output voltage for B-Coils PS is 500 V, the same of single A-Coils PS module.
The main advantage of this decision is the improvement of the system modularity,

each power module of the new power supply system is the same. The only different between the two sets of power supply is the power connection and the control which is clearly different for the A-Coils and the B-Coils PS. As for the A-Coils PS module the dc-link voltage is 519 V which takes account of the voltage drop due to the saturation voltage of IGBTs and the limits on the maximum duty cycle of the inverter ($\delta_{max} = 0.97$).

Operating switching frequency

The worst case scenario for the losses in the inverter is represented by a continuous current on the load (with the assumption of fixed switching frequency of PWM carrier). The power module of the B-Coils power supply system has the same dc-link voltage of the A-Coils PS system; the considerations regarding the maximum switching frequency are therefore the same reported on paragraph 4.2.4. To perform the calculations related to this conceptual design the same value of 6 kHz used for the A-Coils power supply has been selected for the B-Coils power supply system.

4.3.3 DC-link section design

The design of the dc link section of B-Coil PS module follows the same procedure adopted for the A-Coils PS system. Using the same procedure adopted on section 4.2.5 and considering the B_L coils that have larger inductance in dc, the maximum magnetic energy stored on B-Coils PS load is:

$$W_{load} = \frac{1}{2} \cdot L_{load} \cdot I_{max}^2 = \frac{1}{2} \cdot 59.6\,\mu H \cdot 1kA^2 = 29.8J \tag{4.27}$$

In short time scale all the magnetic energy is given to the load by the energy stored in the dc link capacitors. The voltage excursion of this component can be derived from its energy balance considering the maximum dc link voltage ($U_{max} = 519\,V$) and its voltage drop (5%):

$$C_{min} = \frac{\cdot W_{coil}}{U_{C\,max}^2 - U_{C\,min}^2} = \frac{2 \cdot 29.8\,J}{519^2 - 493^2} = 2.2\,mF \tag{4.28}$$

The total energy stored by dc-link capacitors is 296 J. The proposed capacitor rating for the B-Coils PS is 10 mF, the same of the A-Coils PS and higher with respect to the value reported above.

4.3.4 Ac-dc section design

The design of the rectifier section for this system can be the same of the A-Coils PS system: 3-phase input section, diode rectifier with additional filter (choke) if needed. The following analyses regarding the power rating of a single B-Coil power supply module share the same type of consideration done in the design of the A-Coil Power supply system 4.2. Total losses in the two different cases are reported in Table 4.5:
The worst case for the load dissipation is represented by the dc operation of B_L-coils.
The losses evaluation of the inverter follows the same procedure adopted for the

Scenario	Coil	R_{LOAD} [$m\Omega$]	I_{peak} [kA]	Load Power [kW]
DC	B_U	19.3	1.00	19.3
	B_L	19.6	1.00	19.6
AC	B_U	151.7	0.44	14.7
	B_L	84.7	0.44	8.2

Table 4.5: Power dissipation in the load for the B-Coils power supply system.

A-Coils power supply design. Although the frequency and the amplitude of the sinusoidal waveform is different (1 kHz and 440 A) the losses estimation for the A-Coil inverter (see Table 4.4) can be assumed as a worst case scenario for the B-Coils PS system. Being the power dissipation distributed evenly on four switches the total power dissipation of the B-Coils PS H-bridge inverter is 7.06 kW.
On dc scenario the estimation of inverter losses is identical to analyses made for the same scenario of A-Coil power supply (same load current, same switching frequency and same dc-link voltage of single power module) the data are the same reported in Table 4.4, in dc operation there are two active IGBT and two active Diode for each bridge: total power on single bridge is 7.65 kW.
Using the data reported above in Table 4.6 the total power dissipation of B_L and B_H-coils power supply systems can be calculated.W orst case for power dissipation of one B-Coil power supply is represented by the scenario where the maximum wasted power is 29.9 kW.

Scenario	B_U	B_L
DC	29.9 kW	27.2 kW
AC	22.0 kW	15.0 kW

Table 4.6: Active power required to the ac/dc converter of one B-Coils power supply module.

The rating power for the ac/dc conversion section is equal to the total power dissipation in the load and inverter plus additional 10 % to take into account the other losses; the final value assumed is $29.95\,kW \cdot 1.1 = 32.9\,kW$.
The power rating of each rectifier has been fixed to 33 kW (each B-Coil PS is connected to a single power supply module), the duty cycle is the same than the ASDEX Upgrade one: 10 second every 10 minutes.
Each B-coil will be fed by dc-link charged at 519 V. The maximum power is required to the ac/dc converter in case of maximum power dissipation of the power module, neglecting the voltage drop of the dc link, the maximum dc output current of ac/dc converter could be derived:

$$I_{rect\,dc} = \frac{P_{total}}{V_{dc\,link}} = \frac{33\,kW}{519\,V} = 63.5\,A \tag{4.29}$$

4.4 Overall Power Supply System Scheme

4.4.1 Basic Power Module Design

In the following paragraphs are summarized the main power supply parameters for the A-Coils and B-Coils systems. Goal of the design is to extrapolate a set of value which permits to fulfill the electrical requirements for both the power supply with a single power supply module composed of an input, an ac-dc rectifier and a inverter section.
The overall power supply system could be based on a common power supply module, identical for the A-Coils and B-coils system. This power module is clearly identical to on B-Coils Power supply system (depicted in figure 4.15), the power supply module will be composed of:

- Input section which provides the ac supply voltage.
- Pre-charge circuit of the dc-link capacitor bank.
- Rectifier section, based on diode bridge, which provides the dc voltage to the converter section.
- DC-Link section.
- Inverter section.

In Table 4.7 are reported the parameters evaluated in the previous paragraphs for the A-Coils and B-Coils power supply. In the third column is reported the proposed rating for the common power module.

	A-Coil PS	B-Coil PS	Power Module
Number of bridges	2	1	1
Output current	1 kA	1kA	1kA
Output voltage	1 kV	500 V	500 V
IGBT voltage rating	1.2 kV	1.2 kV	1.2 kV
IGBT current rating	1.8 kA	1.8 kA	1.8 kA
Total Dc-link Voltage	1039 V	519 V	519 V
Dc-link Capacitance	868 μF	2.2 mF	10 mF
Maximum Load losses	69.3 kW	33 kW	50 kW
Rectifier Current	73.6 A	63.6 A	96.3 A

Table 4.7: A-Coil and B-Coil power supply system main parameters.

In order to push for modularity the power rating of the ac-dc conversion section of the three different systems could be fixed at the same value. This choice simplify the design of the input transformer, no particular customizations are needed for the two types of power supply. It has been proposes as nominal power rating of each power module a value of 50 kW which gives a significant margin for the A-Coils and B-Coils operation (+ 44.3% and + 51.5%).
The maximum active power of the overall system is 1.6 MW (50 kW times 32 secondaries) with a duty cycle of 10 s over 10 minutes.

To save space and to reduce the system cost it is proposed to supply all the power modules of the A-Coils PS, BL-Coils PS and BU-Coils PS system with a 3-phase insulation transformer with single primary windings and separate secondary windings. Each secondary feeds single power module which input section is composed by a full rectifier followed by a dc-link capacitor.
Being the A-Coils power supply composed by two power module in series, during normal operation the power modules can be subjected to different potential to ground (the grounding point of the power supply system will be located in the ac side of the power supply, therefore the dc link capacitors are floating with respect to ground, see 5.4.2 for details). Voltage swing between transformer secondaries, shield (if present), nucleus and primary windings has to be taken in account for two reasons: it is necessary to assure a proper galvanic insulation between parts at different potential and the parasitic capacitances of the transformer have to be minimized in order to avoid current path with low impedance for the conducted noise.
The place reserved for the transformer is indoor nearby the torus hall of AUG experiment, in compliance with safety regulations it is proposed the dry-type cast resin insulated technology (on [52][53] are reported some applications of this type of technology on power supplies operating on fusion devices).
There are two 10.5 kV power grids able to feed the request power for the new power supply system: the local power grid of AUG and the grid powered by the AUG flywheel generator[4]. The latter option and its parameter will be used as reference for this design, its main characteristic are a controlled voltage (no voltage drop during AUG pulses) and a variable frequency due to the slowing down of the flywheels rotation.
In the following is reported the sizing in terms of secondary voltage and current of the transformer. The secondary phase-to-phase voltage is given by the needed dc link voltage per module (519 V) plus the voltage drop of the full bridge rectifier in full load condition.

$$V_{AC\,nom} = \frac{V_{dc\,link}}{3/\pi} + 2 \cdot V_f = \frac{519\,V}{0.955} + 2 \cdot 2\,V = 547\,V \tag{4.30}$$

Where V_f is the rectifier diode voltage drop. The rms voltage of the secondary is:

$$V_{AC\,rms} = \frac{V_{AC\,nom}}{\sqrt{2}} = 386V \tag{4.31}$$

To evaluate the maximum dc current fed by the input rectifier (considered as a 6-pulse rectifier) it is necessary to take account of the nominal power of each power supply system (50 kW) and the nominal dc link voltage:

$$I_S = 0.816 \cdot I_D = 0.816 \cdot \frac{P_{NOM}}{V_{dc\,link\,nom}} \;=\; 78.6\,A \tag{4.32}$$

[4]The flywheel generator power supply grid of AUG consists of three pulsed distribution systems each supplied by a dedicated flywheel generator: EZ2 (1.45 GJ/167 MVA) which solely feeds the toroidal field coils, EZ3 (500 MJ/144 MVA) and EZ4 (650 MJ/220 MVA). For quasi-stationary advanced tokamak experiments with extended flat-top phase, the power systems of EZ3 and EZ4 are connected in parallel [54]

Rated Power	1.68 kVA
Input Voltage	10.5 kV
Input Frequency	80-110 Hz
Secondary Windings	32
Nominal voltage of each secondary	386 V_{RMS}
Nominal current of each secondary	78.6 A_{RMS}
Nominal power of each secondary	52.5 kVA
Secondary Type	3-ph
Type	Cast resin
Installation	Indoor

Table 4.8: Input Transformer Main Parameters

Rated power of each secondary is:

$$P_{sec} = \sqrt{3} \cdot V_{ACrms} \cdot I_S = 52.55kVA \tag{4.33}$$

Total power of the transformer will be:

$$P_{trafo} = N_{SEC} \cdot P_{sec} = 1.68kVA \tag{4.34}$$

The design of the transformer is based on the assumption of using the flywheel generator power grid which has the voltage controlled to 10.5 kV and a variable operating frequency from 110 Hz to 80 Hz (it varies during the AUG pulse). As possible option to spread the possible operational scenario of power supply system can be a tap changer in the primary windings of the transformer. No real-time compensation is needed during the AUG pulses. The main transformer parameters are reported in Table 4.8.
The sizing of the ac/dc converter is related to the maximum current on diode bridge rectifier which is 96.3 A (equation 4.32). A wide range of commercial components could satisfy the requirements in terms of current and voltage applied, the device selected for the new power supply system is Powersem PSD 192, which has a maximum current of 248 A. In order to verify the maximum diodes junction temperature the losses in the rectifier has been evaluated:

$$P_{rectifier} \;=\; 6 \cdot \left(V_T \cdot I_{avg} + r_T \cdot I_{rms}^2\right) \;=\; 194\,W \tag{4.35}$$

Where $I_{avg} = I_{DC}/3$ and $I_{rms} = I_{DC}\sqrt{3}$. The maximum temperature rise of the diodes junction from the heatsink can be calculated as:

$$\Delta_{T\,junction} = P_{rectifier} \cdot (R_{th\,JC} + R_{th\,CH}) \;=\; 19.4\,K \tag{4.36}$$

Where $R_{th\,JC}$ and $R_{th\,CH}$ are the thermal resistance between junction, case and heatsink. The maximum temperature of junction, in steady state, is 59.4° C (the ambient temperature is 40° C) well below the device operational limit.
The DC-Link section is based on a single capacitor bank for each power module; voltage rating should be higher enough to sustain the no-load voltage of the transformer secondary windings. Capacitance value selected for the power module is

10 mF in order to reduce the voltage ripple of different operational scenarios.
An additional inductance can be inserted between the diode rectifier and the dc link capacitor, its function is reducing the ripple of the input dc current. For this power supply design it has been decided to avoid the insertion of additional inductance in order to improve the system promptness.

4.4.2 Overall Power Supply Scheme

As remarked in the previous paragraph the overall power supply system can be based on a common power supply section, the total number of module will be 32 units:

- 16 power modules to feed the 8 A-Coils
- 8 power modules to feed the 8 BU-Coils
- 8 power modules to feed the 8 BL-Coils

Figure 4.16 shows the cheapest solution with a single transformer composed of single primary and multiple (32) secondary windings. To improve the system availability, but with impact on cost and size, two or three independent transformers could be provided. The final choice of the number of input transformers remains to the supplier.

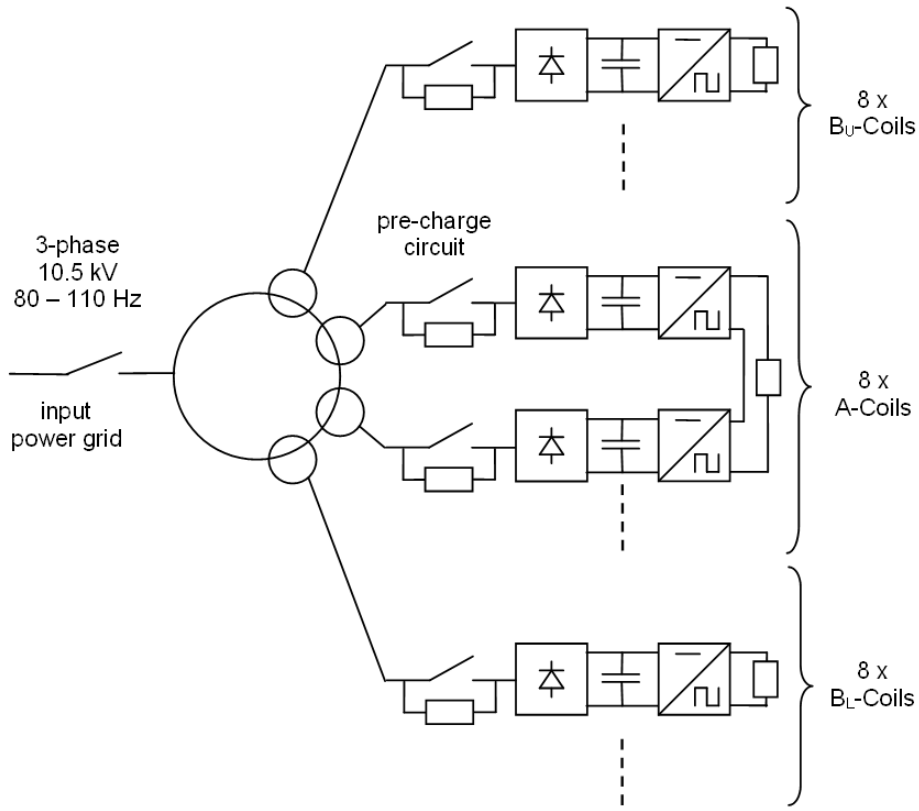

Figure 4.16: Overall Power Supply Schematic

4.5 Outline Design of the control section

The internal control of A-Coils and B-Coils PS shall include a current and voltage loop. In this section will be described the regulation and modulation scheme proposed for the A and B-Coils power supplies used then in the numerical simulations. The preferred modulation scheme for each H-bridge inverter composing A-Coils and B-Coils PS is based on PWM with Unipolar Voltage Switching. With this type of modulation the switches in the two legs of the full bridge rectifier (dubbed A and B) are not switched simultaneously: the two legs are controlled separately by comparing the triangular waveform $v_{carrier}$ with $v_{control}$ and $-v_{control}$ (see figure 4.17). The mid potentials of each leg are connected alternately to the two input dc bus, the load voltage is then obtained by the difference of this two potentials. In total there are four switches configurations which generate three states for the output voltage: $V_{dc\,link}$, $-V_{dc\,link}$ and 0 V (the latter through the upper or lower pair of switches).

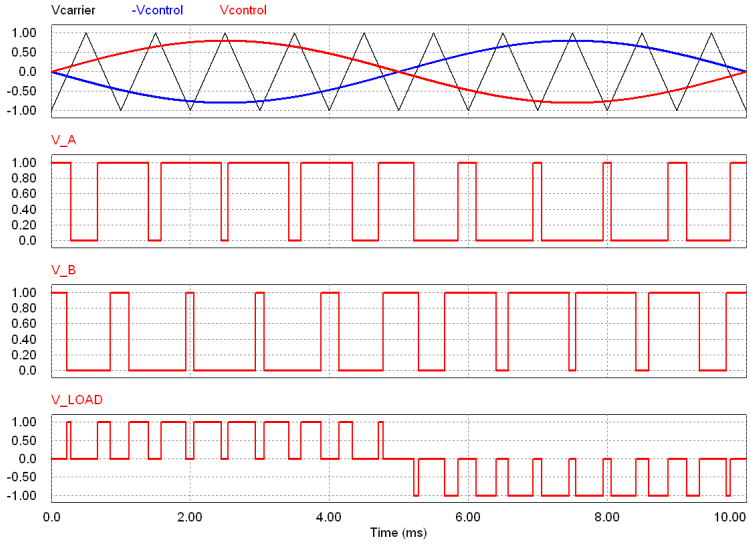

Figure 4.17: PWM with unipolar voltage swing, control signals.

Different kinds of non-linearities are present during inverter operations:

- *IGBT tail current.* To avoid problems with the IGBTs tail current a special constrain of the minimum turn-on time of the switches has been added (its logic scheme is reported in figure 4.24).
- *Blanking time.* Each commutation on two switches in a phase leg is divided on two steps: when the conducting device is turned off the semiconductor need time to recover before it can block voltage, the turn-on of the other device delayed by a blanking time t_Δ. During that interval the potential of the mid point of the leg depends on the direction of the load current (which flows through one of the freewheeling diodes), this effect causes an additional distortion of the voltage output profile. The logic scheme for the blacking time is reported in figure 4.24)

- *Forward voltage.* Voltage drop on switches during conduction causes an additional non linearity (see equation 4.6). In the A and B-Coils PS this effect can be neglected since the forward voltage is lower than 1 % of the total output voltage.

4.5.1 Current Control

The first scheme presented is the block diagram of control loop based on fixed-frequency control for B-Coils PS, showed in figure 4.18.

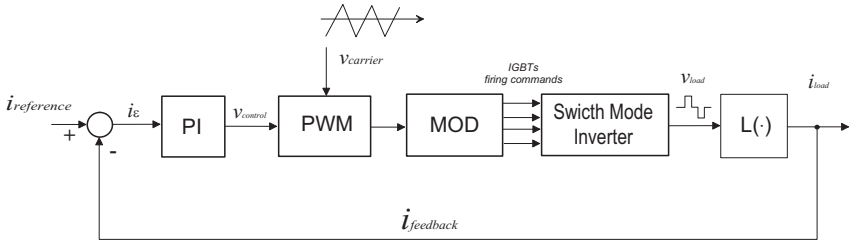

Figure 4.18: Current control block diagram for B-Coils PS.

The error signal i_ϵ between the reference and the actual current is fed through a proportional integral (PI) controller: ($v_{control} = K_P \cdot i_\epsilon + K_I \cdot \int i_\epsilon$). The output signal of the regulator is processed by a modulator circuit that produce the firings command for the inverter IGBTs.
The control circuit of A-Coils PS is based on the B-Coils PS one. A PSCPWM modulation techniques has been adopted (see 4.2.2): two 3-levels inverters are connected to obtain a 5-levels output voltage. The two inverter (in figure 4.19 the inverters are dubbed U and L) are controlled separately with the same control signal $v_{control}$, the only difference is the phase shift between the two carriers. The turn-on and blanking time controls are added also in the modulation circuit of A-Coils PS.

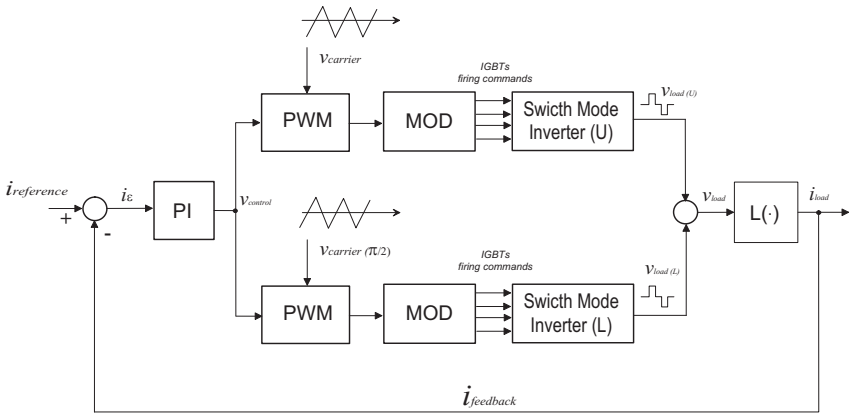

Figure 4.19: Current control block diagram for A-Coils PS.

To perform the simulations a set of PI gains K_P and K_I both for A-Coils and B-Coils PS has been selected. Since the frequency response of both set of coils has not be yet defined an heuristic approach has been preferred to the classic linear one

based on the analyses of control loop transfer functions. This kind of approach has been preferred also because the nonlinearities described above and the small duty cycle on dc operations could have a non negligible effect when the output voltage pulses width is comparable with the blanking time and the minimum turn-on time of the switches.
The approach used to select the PI controller gains is based on a series of parametric simulations. The goal of the analysis is minimizing the power of current error signal with regards to the reference waveforms described on 3.2.3.

$$\min_{(K_P,K_I)} \int i_\epsilon^2(t)dt = \int (i_{ref}(t) - i_{feedback}(t, K_P, K_I))^2 dt \tag{4.37}$$

In figure 4.20 is reported the parametric simulation results for the K_P gain on dc and ac scenario considering fixed the integral gain ($K_I = 0.5$).
The selected pair for the A-Coils PS regulator gains used for the simulations (section 4.6) was $K_P = 1.8 \cdot 10^{-3}$, $K_I = 0.5$ for all the operational scenarios (ac and dc operations can be performed during the same shot, see the general requirements described on 3.2.1) .
The same procedure has been adopted for the B-Coils PS, in this case the PI gains selected for the simulations was $K_P = 2.5 \cdot 10^{-3}$, $K_I = 0.5$.

4.5.2 Voltage Control

The Power supply systems could be also voltage controlled. In the particular field of power supply for MHD plasma instabilities control the most important features is the system promptness then the accuracy of output voltage. Usually the adoption of open loop control with feedforward compensation of inverter non-linearities is preferred, this allows faster operation with the drawback of reduced accuracy.
The block diagrams of voltage control circuits for A-Coils and B-Coils PS is showed on figure 4.21

4.6 Simulation of the system performance in normal operating conditions

The operation of the A-Coil and B-Coil Power Supply schemes was reproduced by means of numerical simulations in order to verify that the conceptual design worked out is capable to fulfill the requirements.
The following simulations are performed selecting a current loop to verify the system operation with a current request from the central control system.

4.6.1 A-coils power supply simulations

The Model

Figure 4.22 shows the PSIM[55] schematic of the A-Coils Power Supply system, this model is composed by four sections:

Power section two identical IGBT H-bridge inverter are connected in series. Each inverter is feed by an ac source electrically insulated to the other, a full bridge

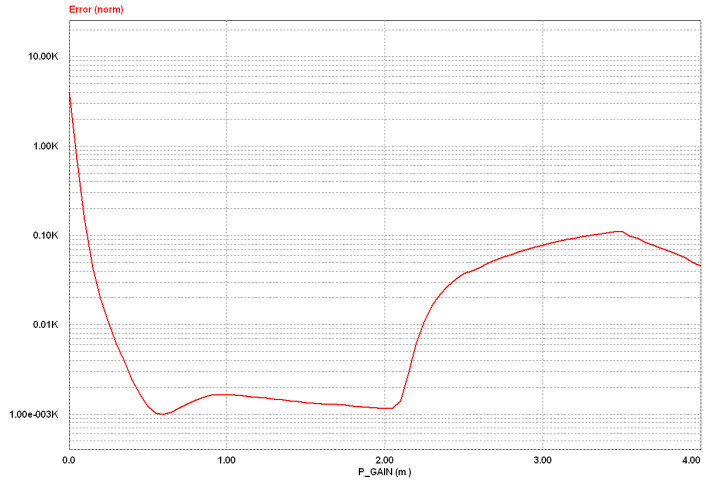

(a) Normalized current error for dc scenario

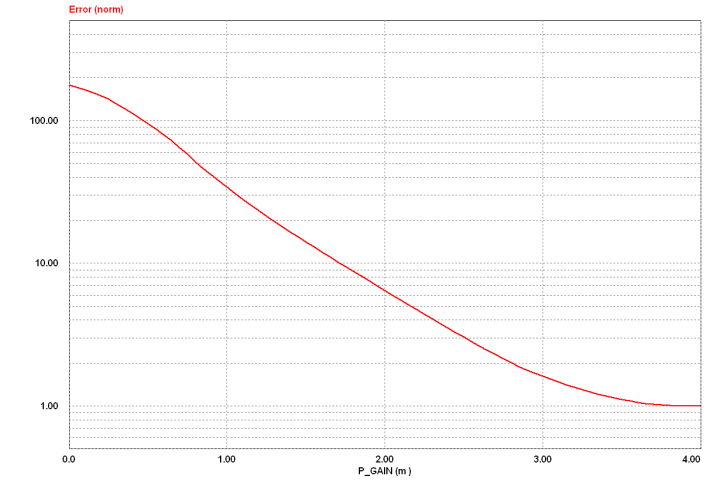

(b) Normalized current error for ac scenario

Figure 4.20: Parametric simulations results for the K_P gain tuning for the A-Coils PS. The error signal is normalized to its minimum value.

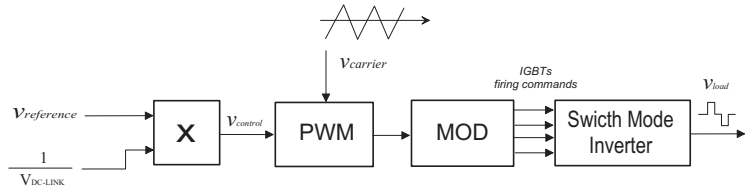

(a) B-Coils PS

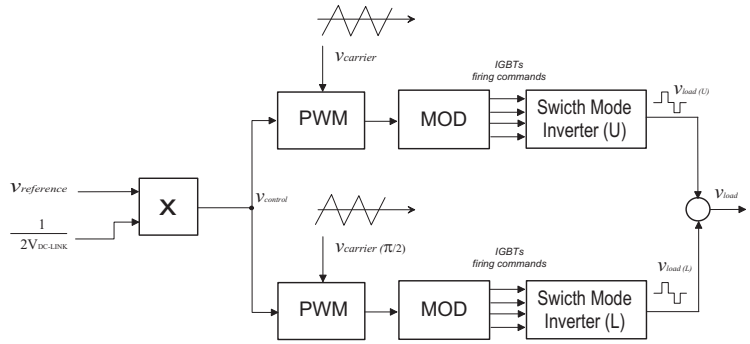

(b) A-Coils PS

Figure 4.21: Voltage control block diagrams.

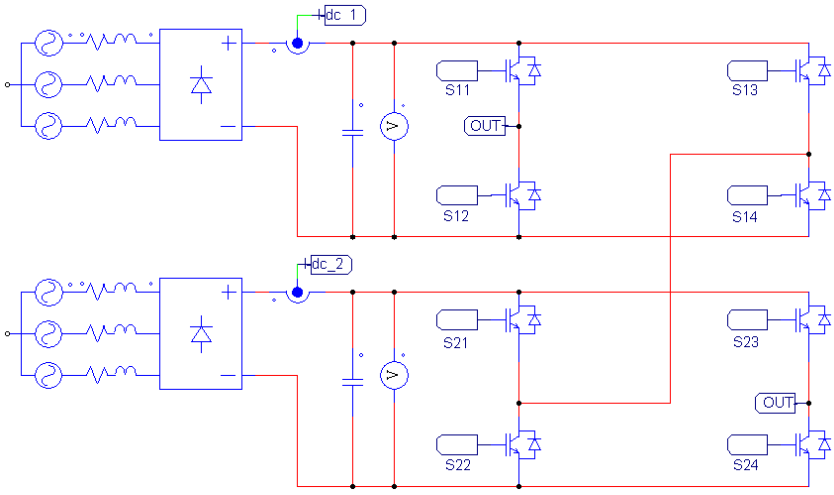

Figure 4.22: PSIM schematics of A-Coils PS power section.

rectifier and dc-link capacitor bank (the in-rush current are limited by the ac power cable inductances).

Load section in the PSIM model power cable, feedthrough and coils have been considered as a single load. Resistance and inductance is referred to the ac and dc columns reported in Table 3.1 and are not dependent on frequency. The load is grounded by a couple of resistors which has no effect in the dynamic response of the system (resistors value is above the maximum impedance of the load, discussion related to the selection of ground point and its sizing si reported on 5.4.2).

Regulator section in the numerical simulations the control foreseen a current regulation in close loop with a simple PI controller. Figure 4.23 shows the PSIM model of the regulator used in the simulations. A low pass filter has been used to process the feedback signal, a limiter has been used to keep the modulation index within its proper range. It can be noted that the regulator doesn't include on these simulation a compensation of the dc-link voltage (a simple model for dc-link compensation is illustrated on [49]), the feedback signal is sampled with a 1 MHz frequency and processed with a low pass filter.

Modulator section this section is composed of two identical modules which implement Unipolar (3-level) modulation (the scheme of single modulator is showed in figure 4.24), the only difference between two modulators is the phase of the carrier which is shifted of $\pi/2$. The modulation includes two additional features: a logic circuit forces the minimum turn on time of each IGBT to 5 μs, another block is used avoid a *shoot through* on inverter legs which implies dc-link capacitance short circuit: the switches turn-on in the same leg is delayed by a pre-selected dead time (1 μs in these simulation).

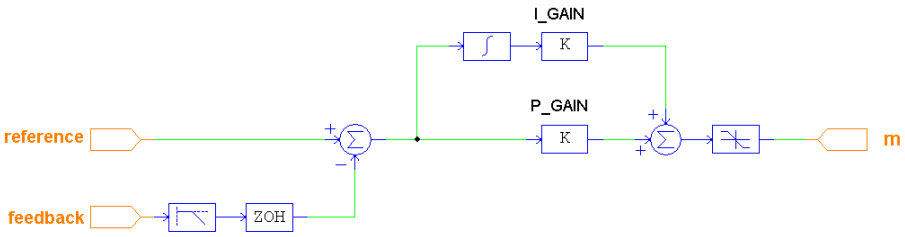

Figure 4.23: Regulator PSIM model used for the A-Coils PS Simulations

DC Scenario

The model previously described has been used to verify the operation of the system when reproducing a step request of 1kA, with total load inductance and resistance relative to dc operation of the coils. Since we were not interested in thermal analyses, it was not necessary to reproduce the full length of the pulse.
Total ripple respect the average value of the load current is 15.8 A ($\pm 1,58\%$), with an equivalent frequency of 24 kHz, which is four times the frequency of the PWM

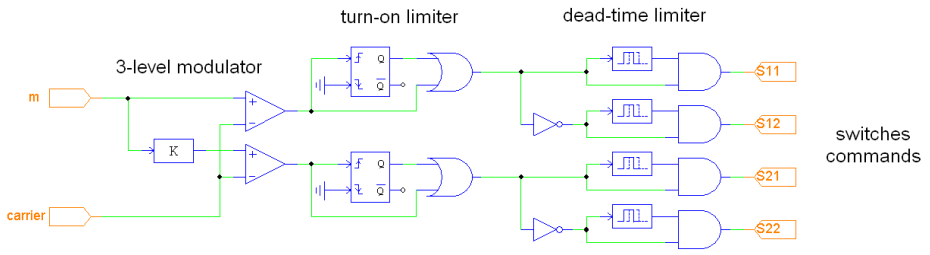

Figure 4.24: Modulator PSIM model used for the A-Coils PS Simulations

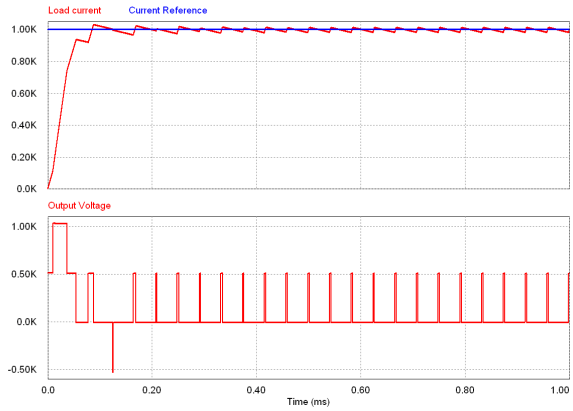

(a) Current rise phase

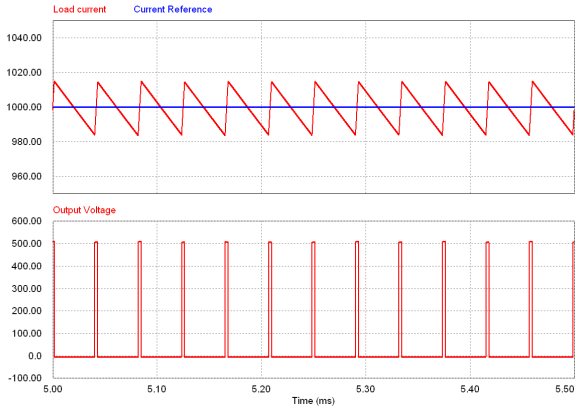

(b) Current ripple

Figure 4.25: A-Coils PS output profiles for the dc current scenario

carrier. The dc-link voltage variation is quite limited (as showed in figure 4.26), it could be noted the phase displacement of the rectifier current peaks (12-pulses operation) and the 600 Hz ripple of dc-link voltage.

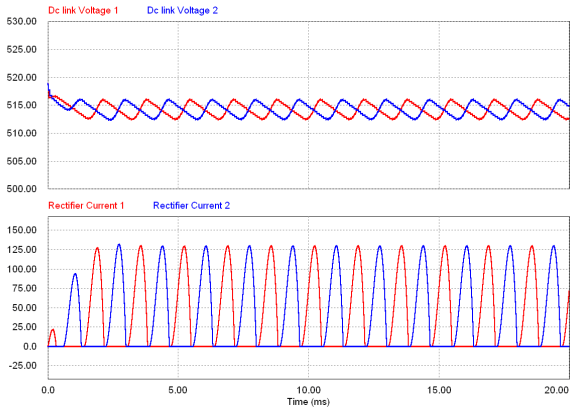

Figure 4.26: A-Coils PS dc-link voltage and current profiles for the dc current scenario

AC scenario

Figure 4.27 shows the load current and voltage in case of a 3 kHz sinusoidal current reference which represents the higher frequency requested to the A-coils power supply. In the same figure is reported the Fast Fourier Transform of current signal, used to evaluate the harmonic distortion of the load current.

Slow Current Ramp-up

Figure 4.28 shows the current waveform in case of slow ramp up request with a current magnitude at flat-top of 1 kA and a repetitve frequency of 20 Hz. Current ripple during the flat top is the same of dc current request (Figure 4.25).

RWM scenario

In the RWM scenario the current shape needed to control the instabilities will look like noise (white or pinkish), although there is no special requirements for this kind of reference waveform can be useful to verify the behaviour of the power supply in this scenario.
In order to mimic the current reference request a pink noise generator has been used (Figure 4.29): it is composed of a white noise generator followed by a filter (2-order with cut frequency equal to 3kHz) and a saturation block which limits the maximum current amplitude to $\pm$1kA). The simulated load current for A-Coil PS which reference signals is the pink-noise described above is showed in figure 4.30.
In figure 4.31 are reported two different dc-links voltage profiles of the A-Coils PS operating with a pink-noise shape reference. It could be noted that the dc-link

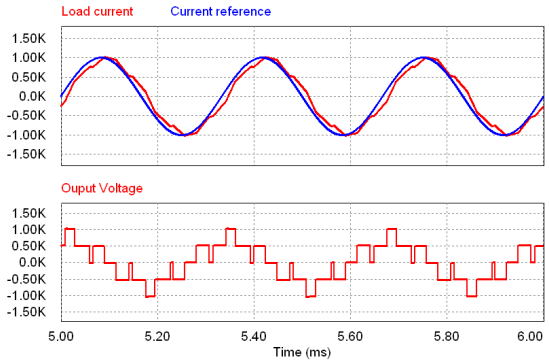

(a) Time domain

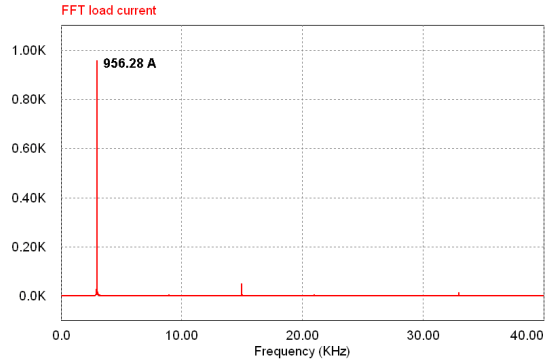

(b) Current signals FFT

Figure 4.27: A-Coils PS output profiles for the ac current scenario (1kA/3kHz)

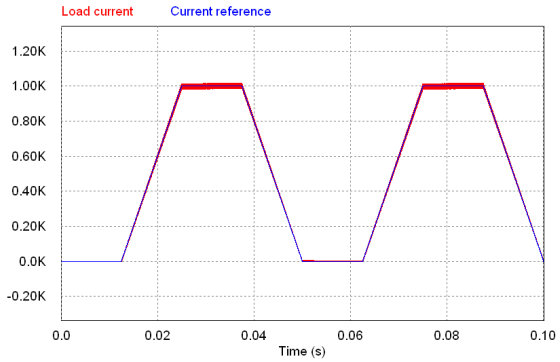

Figure 4.28: A-Coils PS. Slow current reference ramp-up: 1kA during flat top, frequency 20 Hz

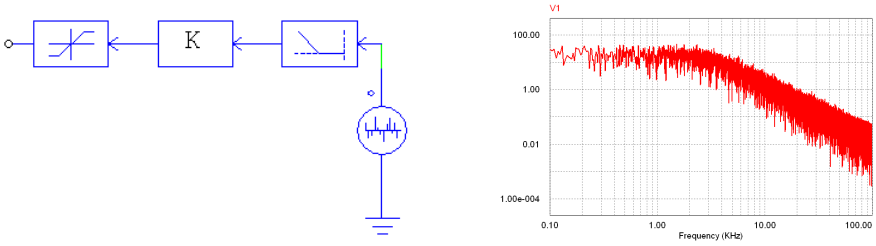

(a) Model Implementation (b) Output Spectrum

Figure 4.29: Pink Noise Source

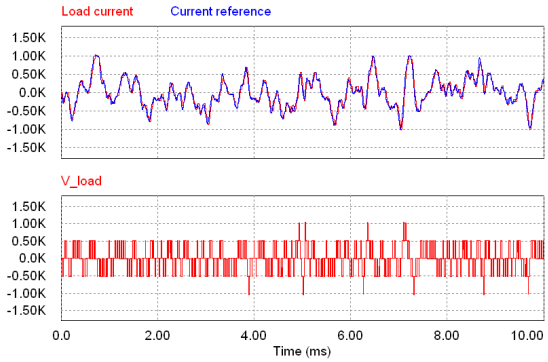

Figure 4.30: A-Coils PS. Load Current with pinkish noise current reference

voltage ripple is quite limited (around 2%) while the profiles are characterized by non-periodic shapes due to the randomness of the output current profiles.

4.6.2 B_U-coils power supply simulations

The Model

The B_U and B_L Coils power supply are based on the same PSIM model (showed in figure 4.32), the components of the power supply module, the control and the modulation subsystems are identical to the ones used for the A-Coils (see 4.6.1)..

DC Scenario

The B-Coils PSIM model has been used to verify the operation of the system when reproducing a step request of 1kA. As for the A-Coils simulation, since we were not interested in thermal analyses (the IGBTs juction temperature evaluation is reported on 4.6.5), the next simulations do not reproduce the entire length of the AUG pulse. The load current and voltage profiles are reported in figure 4.33.
Total ripple of the load current (respect its average value) is higher respect the A-Coils PS system due to the halved virtual frequency in the load and to smaller load inductance. With the PI controller and the selected rectifier section used in this simulation the total ripple is $\pm 1,3\%$.

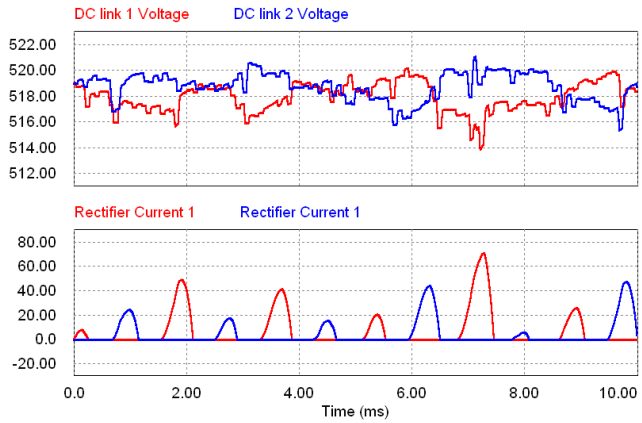

Figure 4.31: Dc link Voltages and rectifiers current for the A-Coils (RWM scenario)

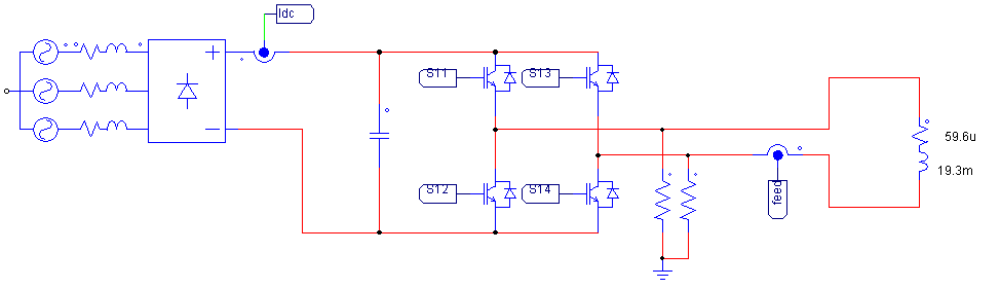

Figure 4.32: B_U and B_L-Coils Power supply PSIM Model (power section)

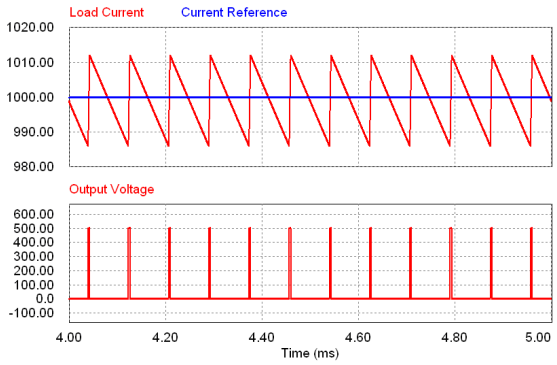

Figure 4.33: B_U-Coils PS output profiles for the dc current scenario

AC Scenario

Figure 4.34 shows the current and voltage profiles of the BL-Coils PS when a sinusoidal waveform (440A @ 500 Hz) is requested, in the same figure is reported the FFT of the current waveform used to evaluate the harmonic distorsion introduced by the switching power supply: the rms value of the output current 304,84 A and the rms value of the fundamentals harmonic: 303,7A, the resulting THD is 0,75%.

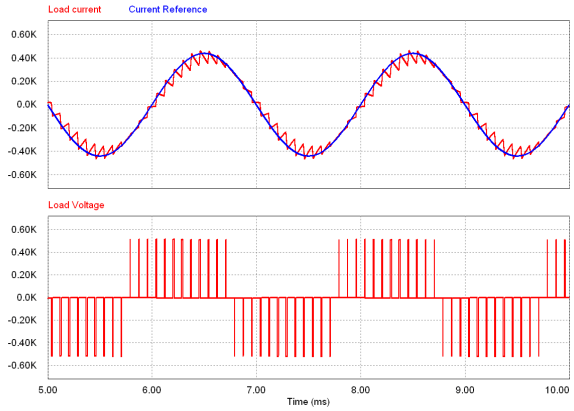

(a) Time domain

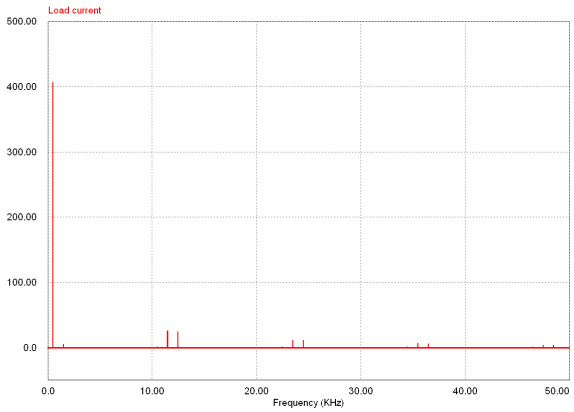

(b) FFT of output current signal

Figure 4.34: B_U-Coils PS output profiles for the ac current scenario

Ramp-up Scenario

Figure 4.35 shows the current waveform in case of slow ramp up request, the system is able to reproduce with good accuracy the current reference, the ripple during the flat top is the same of dc current request (Figure 4.33).

RWM Scenario

The current reference of this scenario is pink-noise with a 500 Hz bandwidth. The model adopted to generate this type of current waveform is the same used in the

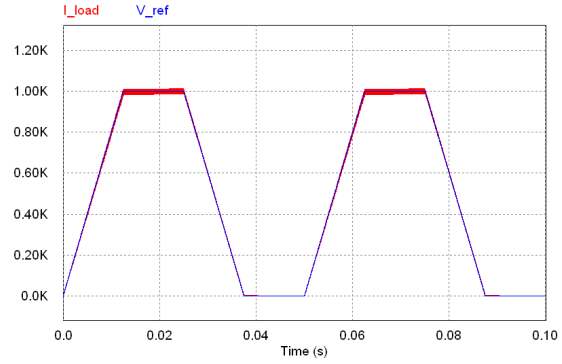

Figure 4.35: B_U-Coils PS output profiles for the ramp-up scenario

A-Coils PS simulation (see Figure 4.29 for details).

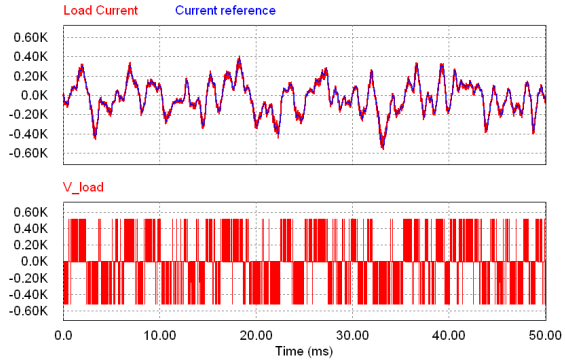

Figure 4.36: B_U-Coils PS output profiles for the RWM scenario

4.6.3 B_L-coils power supply simulations

In this section are reported the simulations of B_L power supply over the different operational scenarios foreseen for this power supply system. The results are close to the simulation of B_U-coils power supply model; the small differences are due to the slight different of load parameters.

DC Scenario

In figure 4.37 are showed the power supply output profiles for the dc current scenario. The results are similiar to the B_U-coils simulation but it can be noted that the current ripple is higher ($\pm 1.7\%$) due to the smaller DC inductance of B_L coils.

AC Scenario

In figure 4.38 are showed the power supply output profiles for the ac current scenario ($440\,A_{peak}/500$ Hz). From the PSIM simulation data has been derived the rms value

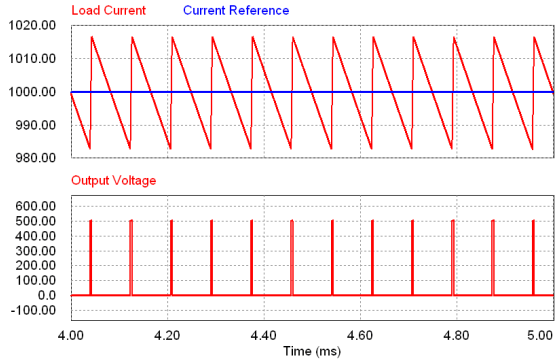

Figure 4.37: B_L-Coils PS output profiles for the dc current scenario

of the output current (289,58 A) and the rms value of the fundamentals harmonic (288,09 A), the THD is equal to $1,03\%$ within the requirements.

Ramp-up Scenario

In figure 4.39 are showed the power supply output profiles for the slow ramp up current scenario (amplitude 1 kA, frequency 20 Hz). The current ripple during the flat top is the same of dc scenario.

RWM Scenario

The current reference of this scenario is pink-noise with a 500 Hz bandwidth, the same used for the B_U-coils PS simulation. The output current follows the reference without particular problems. In figure 4.40 is reported the simulation result for this scenario, it could be noted that the Dc-link voltage ripple is quite small (lower than 1%).

4.6.4 Summary of power supply performance

In Table 4.9 are reported the results of the simulations respect the requirements given on paragraph 4.9.

4.6.5 IGBT Temperature profile simulation

In order to verify the maximum junction temperature og IGBT the current and voltage profiles of the IGBT composing the power modules of A-Coils and B-Coils power supply have been used to calculate the avarage power dissipation of the switches (the results are reported in Table 4.3) with a dedicated Simulink Model.
Being the time scale of the power supply simulations much shorter with respect to the pulse lenght of the AUG operation (600 s with a duty cycle of $\delta = 1.67 \cdot 10^{-2}$) the calculated wasted power in the semiconductor has been used as a constant imput of the IGBT-heatsink-ambient thermal model. The temperature profiles of IGBT junction are then evaluated considering two types of heatsink: one based on

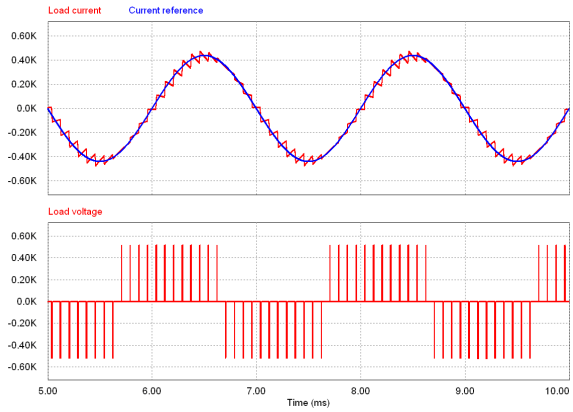

(a) Time domain

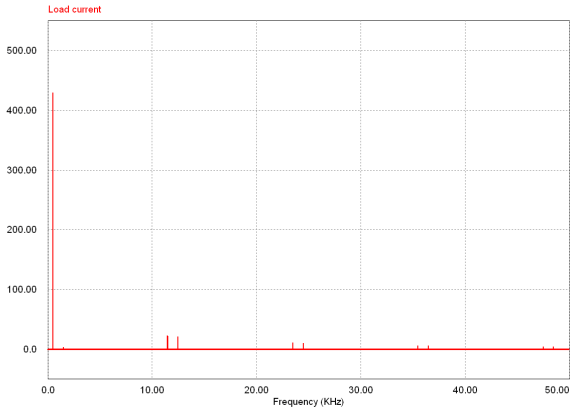

(b) Output Current signals FFT

Figure 4.38: B_L-Coils PS ac current scenario

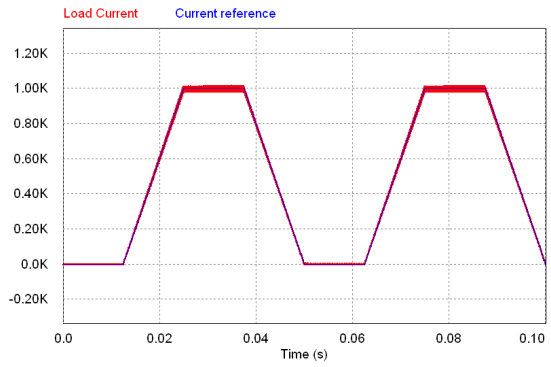

Figure 4.39: B_L-Coils PS output profiles for the ramp-up scenario

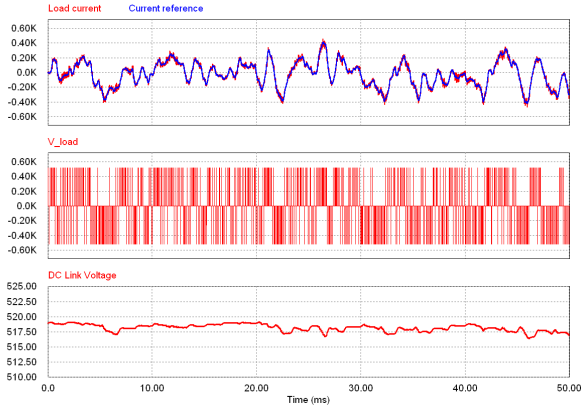

Figure 4.40: B_L-Coils PS output profiles for the RWM scenario

		Simulation results	Requirements
A-Coils PS	Current Ripple	$\pm 0.75\%$	$< \pm 1\%$
	Rise Time	$70\mu s$	$< 100\mu s$
	THD	$\pm 1.56\%$	$< \pm 2\%$
B_U-Coils PS	Current Ripple	$\pm 1.7\%$	$< \pm 2\%$
	Rise Time	$120\mu s$	$< 200\mu s$
	THD	$\pm 0.78\%$	$< \pm 2\%$
B_L-Coils PS	Current Ripple	$\pm 1.3\%$	$< \pm 2\%$
	Rise Time	$120\mu s$	$< 200\mu s$
	THD	$\pm 1.1\%$	$< \pm 2\%$

Table 4.9: Summary of power supply performance

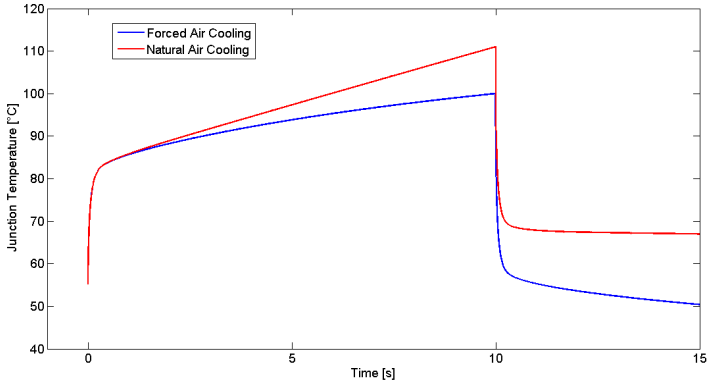

(a) AUG pulse phase: 0-15s

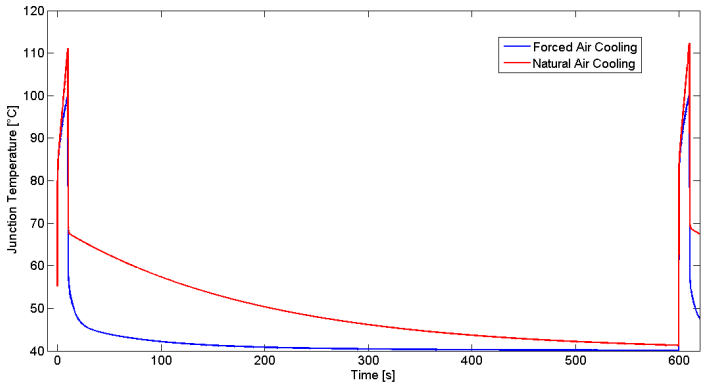

(b) Total AUG period: 0-600s

Figure 4.41: Simulation results for Inverter IGBTs junction temperature profile in the worst case scenario.

forced-air commercial component: Semikron, 2-fold SKiiPPACK (Forced Air Cooling $V_{air}/t = 310m^3/h$) the other is based on natural air cooling. Both simulations consider the scenario with the maximum power losses on IGBT (1 kA dc in the load, see Table 4.3), the results are reported in figure 4.41.
The maximum temperature reached by the inverter IGBT junction is 111 °C and 100°C for the natural and forced air type of cooling. The small differences with respet to the calculation made on section 4.2.4 are due to the power losses derived by system simulations with is slight higher respect the one used in thermal calculation and the non-adiabatic temperature rise of the two heatsink which are able to transfer heat to the ambient during the operational phase.
In conclusion natural air cooling could represent a good solution for the power supply system, obvioulsy the forced air cooling is prefereable in case of more stressful AUG machine duty cycle (longer pulse duration or lower period between pulses).

4.7 Protection system and analysis of fault conditions

4.7.1 Introduction

In this section three types of fault will be investigated: coils short circuit, effect of plasma disruption and internal fault of H-bridge inverter. Goal of the design is to define the more appropriate protection strategy for the power supply and the coils system.

4.7.2 A-Coil short circuit

The analysis of coils short circuit fault is presented in the following section. For the analyses it has been considered the worst case scenario: full short circuit between the coil poles and maximum current fed by the power supply.
The model used to simulate the fault condition of A-Coils PS is showed in figure 4.42, the control system and the protection system are depicted separately in figure 4.43.

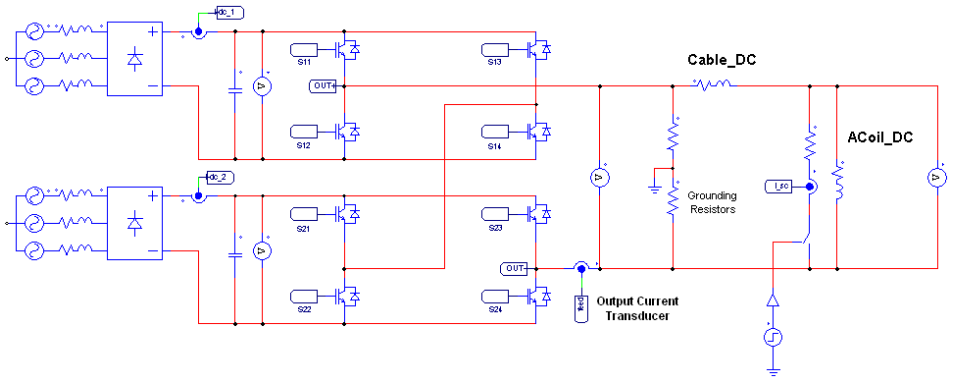

Figure 4.42: A-Coils PS PSIM model used to simulate a load short circuit - power section

The simplest protection strategy can be the based on the control of the output current of the power supply, if the module of the feedback signal exceeds a certain threshold the protection system stops the firing signals to the inverters. Using the load parameters of the dc scenario the a first tentative choice is fixing to 1200 A the current threshold for the protection intervention, the voltage and current profiles in case of full load short circuit are showed in figure 4.44.
The short circuit of the load is triggered at 2 ms, it can be noted the unstable behaviour of the current profiles (due to the changed parameters of the power supply load) which carry to the protection triggering at 2.21 ms, after the stop of the inverters all the remaining coil current flows into the short circuit. The limited magnetic energy stored into the coil leads to a total I^2t of $721A^2s$ into the short circuit (the I^2t depends mostly on the current present in the coil when the inverter are switched off: $I^2t = 1/2 \cdot I_0^2 \cdot \tau$).
Due to the low inductance and resistance of the A-coils the detection of the load short circuit by the power supply could be problematic: the major risk is the undetection of the load fault, in this scenario the power supply continues to feed the

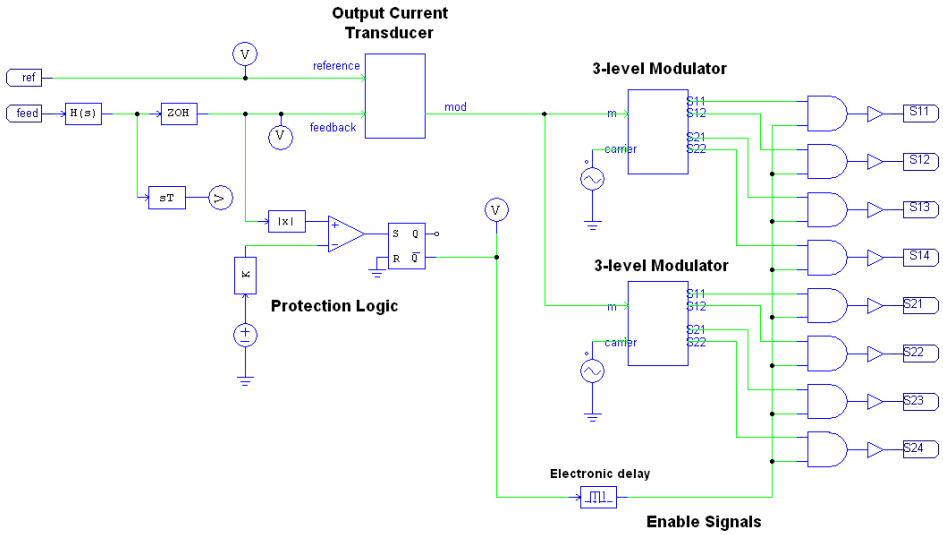

Figure 4.43: A-Coils PS PSIM model used to simulate a load short circuit - control and protection subsystem

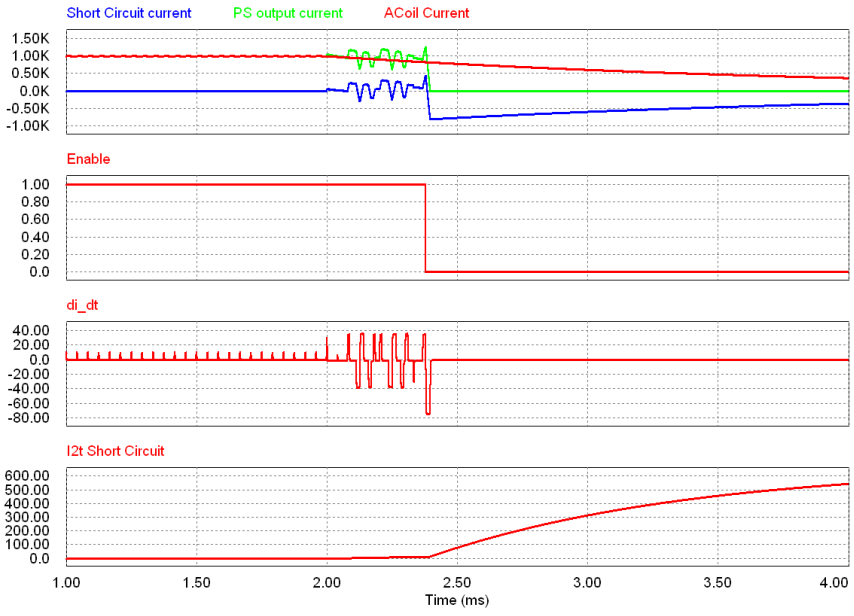

Figure 4.44: Current profiles on A-Coils PS in case of short circuit

requested current into the short circuit with an unacceptable I^2t. Respect the fault detection it is necessary to point out that the simple detection strategy described above could be ineffective in many operational scenarios: the unstable behaviour of current profiles doesn't assure fast short circuit detection, moreover in case of partial short circuit of the coils it is possible that the current threshold is not reached. While the power supply could be work properly on a partial short circuit of the load to preserve the coils functionality short circuit detection based on different approach is mandatory to assure the overall system reliability. Different strategies are hereafter described:

- Magnetic Measurements: is possible to use the magnetic field measurements of the A-Coils and compare it with the coils current signals, in case of mismatch (the currents flows into the short circuit) the protection will be triggered. This solution needs to consider the mutual coupling of different coils, as drawback a short circuit upstream the current measurement can't be detected.

- Coil Voltage Measurement: a voltage transducer could be placed nearby the coil feedthrough, in case of short circuit the voltage amplitude drops and the protection will be triggered.

- Current Measurements: in case of short circuit the load parameters change with an impact in the current profiles dynamic. The simple control of current amplitude could be ineffective for the reasons described above. A possible approach is the control of error current ($I_{ref} - I_{PS}$) or checking the output current derivative dI_{PS}/dt.

In this conceptual design the approach selected to detect a short circuit is based on the latter option described above. The maximum expected derivative of the output current occurs in the ac scenario when the load (coils and cable) inductance decreases its value to 39.1 μH:

$$Max\ \frac{dI_{ps}}{dt} = \frac{V_{out\,max}}{L_{min}} = \frac{1000\ V \cdot 0.97}{39.1\ \mu H} = 26.4\ A/\mu s \tag{4.38}$$

The protection logic circuit is depicted in figure 4.45 while in figure 4.46 are showed the output voltage and current profiles in case of fault during ac operation (the short circuit has been synchronized with the peak current in the load). The threshold of current derivative has been fixed to 1.5 times the values gives by Eq.4.38.

4.7.3 B-Coil short circuit

The same consideration made above for the A-Coils Power supply remains valid for the design of the B-Coils Power supply protection. Logic based on current amplitude and derivative could be applied to this set of power supplies changing the various thresholds. Respect the A-Coils PS the I^2t through the short circuit is higher due to the higher time constant of the B-coils (the B_U coils has $\tau = 8.9ms$ with respect to the A-Coils PS which has $\tau = 2ms$). In figure 4.47 is reported the simulation result for the B-Coil short circuit fault.

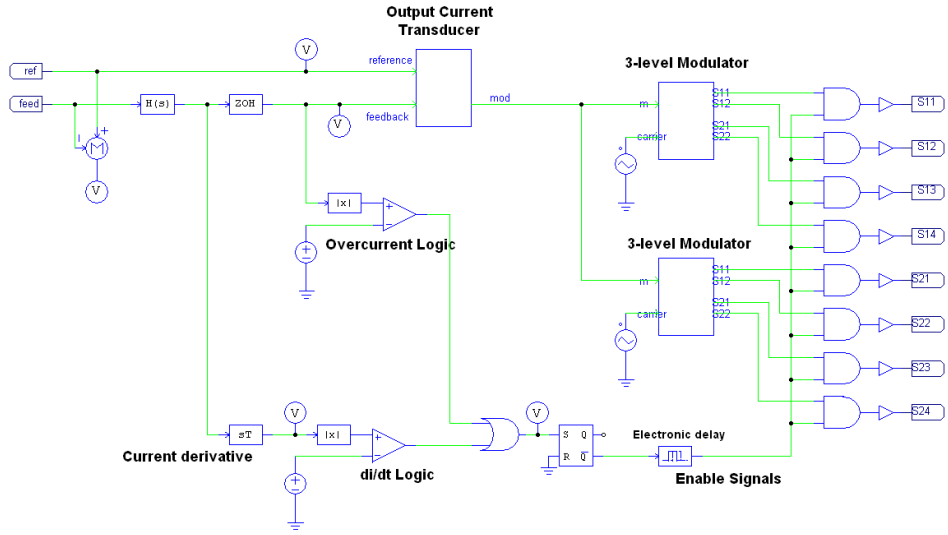

Figure 4.45: A-Coils PS PSIM model used to simulate a load short circuit - control and protection subsystem (modified)

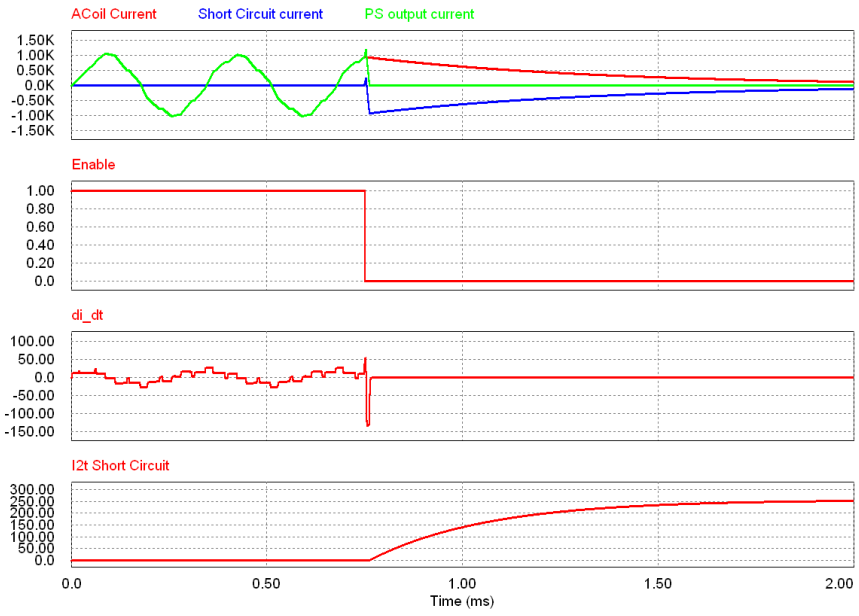

Figure 4.46: Current profiles on A-Coils PS in case of short circuit

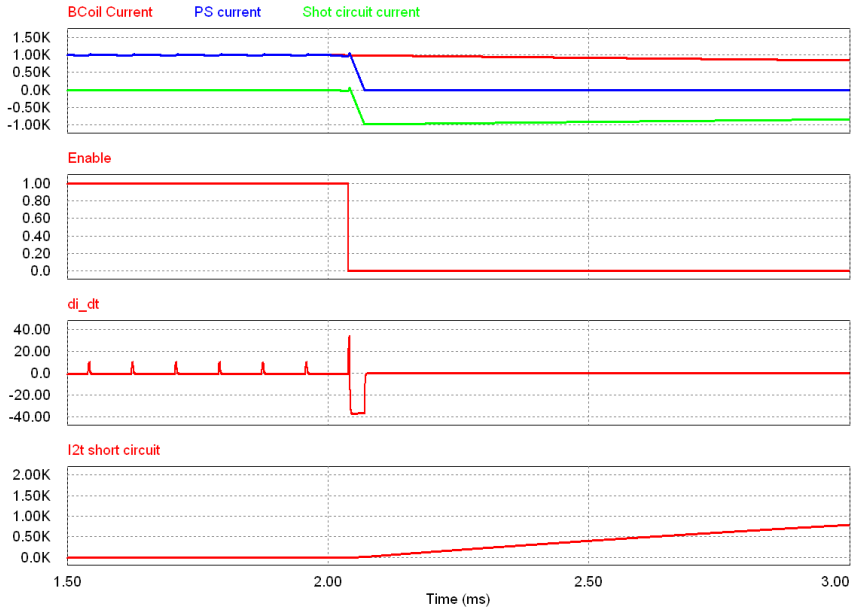

Figure 4.47: Current profiles on B-Coils PS in case of short circuit

4.7.4 Plasma Disruption

The most severe system fault during the Asdex Upgrade operation is represented by the plasma disruption. Plasma disruption is caused by plasma instabilities which in same case cause a sudden termination of experimentally confined plasma, as result all the stored energy in the plasma is rapidly dumped into vacuum vessel walls, magnetic coils, etc.
The ASDEX Upgrade team has made several analyses to understand the effect of plasma disruption in the A and B-Coils. Starting from the geometry of the coils and their placement inside the vacuum vessel the analyses were focused on the flux changes evaluation due to disrupting plasma which induce voltage on both A and B-Coils. Due to the particular placement of the coils (which lay on the surface of the vacuum vessel and therefore are not affected, in principle, by a fast change of a plasma toroidal current) the maximum induced voltage in the coils is relative low: the induced voltage on A-Coils is 45 V and 240 V for the B-Coils.
From the power supply point of view the inducted voltage in the coils due to the disruption could be seen as a forced emf applied in series to the coil. For both power supply the induced voltage is lower than the dc-link voltage, no current can flow from the load to the dc-link capacitor because the freewheeling diodes of the inverters are always reverse polarized and the power supply system represents a potential barrier (1kV for the A-Coils PS and 500 V for the B-Coils PS) for the forced emf.
In figure 4.48 is reported the simplified circuit used to evaluate the effect of disruption on B-Coils. It is clear that no current flows from the load to the dc-link capacitor (the freewheeling diodes of inverter act as a full bridge rectifier), while a possible path for the current is through the grounding resistors placed at the output

side of the power supply.

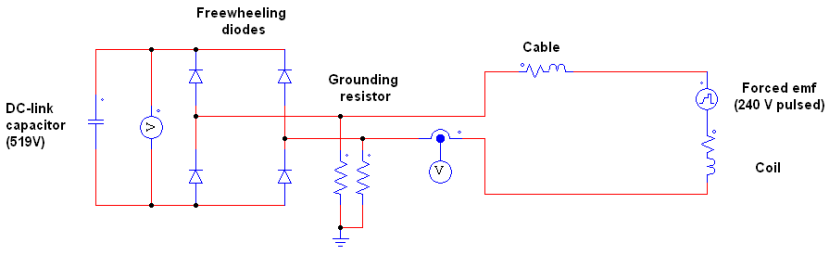

Figure 4.48: Simplified circuit for the Disruption effect evaluation on B-coils PS

4.7.5 Internal faults

In this paraghraph a short description of possible internal fault of power supply and the protection strategy will be described. Among all the possible finternal fault the most dangerous are:

- Short circuit on IGBT component inside the bridge.
- Short circuit at the output of the inverter bridge upstream the power cables.

The most severe internal fault for the power supply system is the short-circuit of an IGBT of the inverter bridges, resulting in a short-circuit of the dc-link: high current peaks are expected in this case, limited only by the stray inductance of busbar connection and the stray inductance of the inverter legs. Since the energy stored on single dc-link module is quite limited: 3 kJ, no active crowbar are required, a simple protection based on dc-link fuses could be used to limit the effect of this fault. Usually the IGBT gate drivers include a short circuit detection (based on saturation voltage measurements) which turn off the switches in case of overcurrent. Considering a time intervention of gate driver protection of 2.2 μs (voltage transducer: 0.5 μs, protection circuit delay 0.5 μs, IGBT turn off delay 1.2 μs,) and a total stray inductance of 1 μH between dc-link and the fault switch the maximum current reach in the inverter leg will be within the capability of the selected component:

$$I_{max} = I_{DC} + \frac{V_{dc\,link}}{L_{stray}} \cdot \Delta T = 2141.8A \tag{4.39}$$

The short circuit at the output of the inverter bridge could be treated with the same procedure assumed above. Respect the previous fault the worst case is represented by a short circuit at the output side of the A-Coils power supply, in this scenario the dc-link voltage is double respect the short circuit inside a single power module, the peak current remain within the maximum value accepted by the selected components (3600 A):

$$I_{max} = I_{DC} + \frac{2 \cdot V_{dclink}}{L_{stray}} \cdot \Delta T = 3285.8A \tag{4.40}$$

The little margin suggests the insertion of a filter inductance (in the range of 1 μH

at the output poles of the power supply (nearby the active switches) which limits the peak current in case of fault.

Chapter 5

EMI issues due to switching power supplies on AUG

5.1 Introduction

Power electronic devices based on switching converter are source of Electromagnetic Interference (EMI). This type of electric noise is transmitted in two forms: radiated and conducted [56]. This chapter will be focused on the conducted noise.
Switching converters due to the fast voltage slopes generate noises with significant power levels at harmonic frequencies several order above the fundamental frequency of the power supply. The conducted noise can be divided in two main categories: differential-mode and common-mode (Figure 5.1).

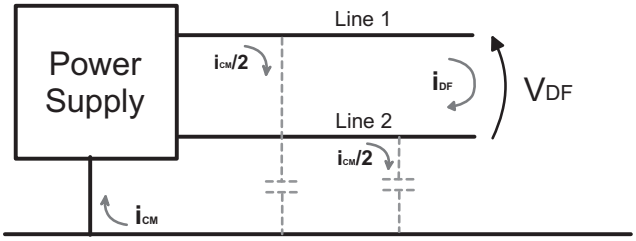

Figure 5.1: Conducted Interference. Two type of noise are generated by the power supply: differential noise i_{DF} and common-mode noise i_{CM}.

While the transmission of differential-mode noise is present mainly through the power lines, the common-mode noise is transmitted through stray capacitance to ground of the circuit; the current path of common-mode noise is closed by the ground conductor. With respect to Figure 5.1 the common-mode voltage to ground present on the output side of the power supply is defined as the average of the two floating potential:

$$V_{CM} = \frac{V_{Line\,1} + V_{Line\,2}}{2} \tag{5.1}$$

In the fusion devices equipped with a large number of diagnostics and electronic devices, usually characterized by high EMI susceptibility, the presence of a switching converter can represent an unacceptable source of noise (on [57] is described the problem of EMI on the RFX-mod machine where a large number of switching power

supplies to control the MHD instabilities of plasma have been installed).
This chapter deals with the common-mode noises on AUG Tokamak generated by the new switching power supply systems.

5.2 Generation of CM-noise in H-Bridge inverter

Power converter based on H-bridge topology can be source of common mode voltage. The H-bridge inverter can be divided in two categories depending on the number of output states that can be generated: bipolar or unipolar voltage switching. The former type of modulation can generate two output states: $+V_{DC}$ and $-V_{DC}$, where V_{DC} is the dc-link voltage. The latter type of modulation can produce also 0 V on its output poles.
Most single-phase H-bridge inverters use Unipolar switching technique in order to improve the virtual frequency on the load and therefore the quality of the current injected into the circuit. The main drawback of this technique is the generation of common mode voltage. On the following it is showed, depending on the grounding point of the H-bridge, how this common mode voltage is generated.
In case the grounding point is placed at the input side of the inverter (for example in the middle point of the dc-link capacitor bank) the common-mode voltage on the output poles of the power supply (which are floating) is non-null when the inverter applies 0 V to the load (using the S_1-S_3 or the S_2-S_4 pair). In figure 5.2 are showed the two switches configurations that generate non-null common-mode voltage.

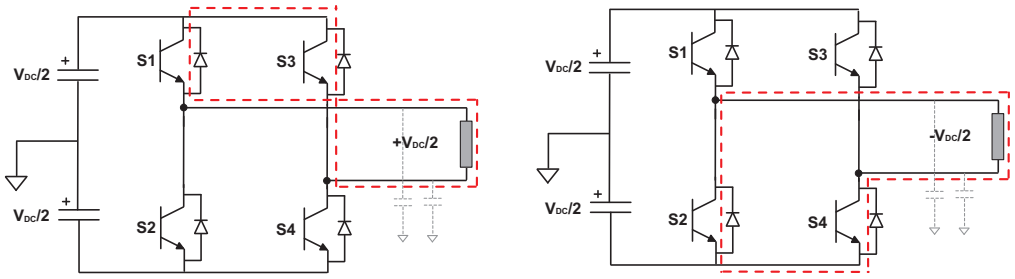

(a) Zero vector applied to the load using S_1-S_3 switches

(b) Zero vector applied to the load using S_2-S_4 switches

Figure 5.2: Input grounded H-bridge common-mode generation.

Another way of grounding a H-bridge is at the output side of the system. The grounding reference are usually given connecting the output poles of the H-bridge to ground through a pair of resistor as showed in Figure 5.3, as result the floating potentials are on the input side of the inverter and the common-mode noise pass through the stray capacitance to ground of the power supply.
In figure 5.4 is showed the differential and common-mode voltage profiles for an Unipolar H-bridge based on PWM modulation.
If the power supply system is composed of multiple H-bridges, the possibility of grounding it at the output side of the converters is possible only if the dc sources can be kept floating with respect to ground. When multiple H-bridges share the same dc-link section (to contain the system cost and size) the only solution is to ground the system at the input side. This is the case of RFX powers supply for the

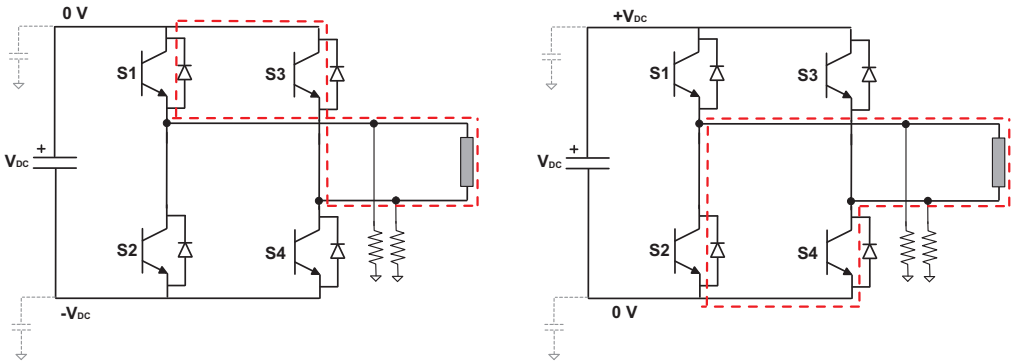

(a) Zero vector applied to the load using S_1-S_3 switches

(b) Zero vector applied to the load using S_2-S_4 switches

Figure 5.3: Output grounded H-bridge common-mode generation.

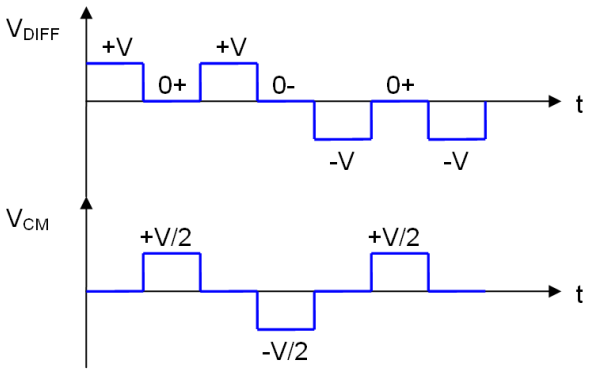

Figure 5.4: Differential and Common-Mode profiles for an Unipolar PWM H-bridge.

MHD control where each coil is isolated with respect to vessel and ground and the dc-link buses are grounded through a pair of resistors [59].

5.3 EMI reduction techniques

The issues related with common mode noise in switching power supply have been widely investigated, in literature a large number of papers are dedicated to industrial applications as inverters feeding induction motors or, more recently, electric power generation by means of photovoltaic panels [1].
Different approaches are possible for mitigating the conducted noise effects; the various techniques can be divided in two categories: active and passive techniques. Active techniques for 3-phase applications can be based both on the modification of modulation techniques [60] or in quite complex modification of the inverter topology [61]. For single phase applications, where only bipolar modulation can avoid common-mode issues, the standard approach is the modification of the inverter topology (some interesting topologies have been reported on [62], the main idea of these solutions is give an alternative path through active devices for the current on zero-state of the inverter). Another active techniques can be based on filters where proper circuit injects current having an opposite phase of leakage current [63] or the so called *active common noise canceller* where the an external circuit superimposes a voltage from the control voltage source that is opposite the common-mode voltage V_{CM} [64].
A wide range of passive methods are described in the literature, the strategy adopted to reduce the leakage current is to insert passive filter in the common-mode current path [65][66][67]. In many applications inductive filters (chokes) are used, figure 5.5 illustrates one implementation: the common mode currents, which flow in the same direction, produce a large magnetic flux on the choke's core, as a result the choke represents an high impedance for them. On the contrary, differential currents produce ideally zero flux on the core and the total inductance is therefore negligible. Design of passive EMI filter presents non-negligible difficulty due to the uncertainty of the frequency behaviour of the EMI interference, state-of-the-art techniques are mainly based on worst-case methodologies or on empirical assumptions [68].
Among the passive techniques for EMI reduction; inverter snubber can be quite effective since it reduces both *dv/dt* and *di/dt* of the circuit but make more complex the bridge topology.

5.4 Provisions to limit Electro Magnetic Interferences on AUG

5.4.1 Introduction

The new AUG MHD control power supply system represents a noise source since the type of modulations adopted (3-levels PWM and 5-levels PWM for B and A-coils

[1] The large surface of photovoltaic panels implies a large stray capacitance to ground. Transformerless converters, which are less expensive with respect to other solutions, can introduce in the grid a large amount of common-mode current unacceptable in some cases for the tight EMI standards [58]

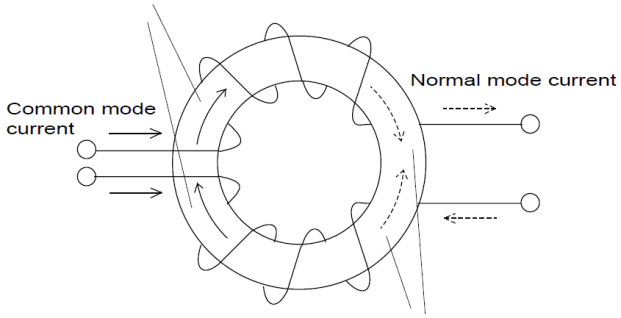

Figure 5.5: Common Mode Choke

PS) implies the generation of common-mode voltage and therefore the circulation of common-mode current.
The new set of AUG control coils presents a non negligible stray capacitance to ground (the mechanical structure of the coils screen face the metallic vessel of AUG which is grounded). In presence of common-mode voltage with a derivative in the order of $1\,kV/\mu s$, typical of these application, this stray capacitance becomes a low impedance path for common-mode current.
Common mode currents can be a problem for electronic devices operating on AUG and for the control system of the power supply itself. With regards to diagnostic systems, stray currents can perturb the equipotential of the reference grid of the AUG machine, as a result different equipments can present different reference potential with a heavy effect on the measurements.
The possible consequence of noise due to the new MHD control system has been taken into account during the design of the power supplies. The objective of the design from the point of view of EMI reduction is to minimize the common-mode current at the load side of the new AUG power supply system.

5.4.2 Selection of power supply systems grounding point

A suitable design of the grounding system can contribute to reduce the negative effects of the common-mode voltages above described; the location of the ground connections and value of the relevant impedances have to be carefully selected, within the constraints stated by the overall design.
Since the dc sources of the new AUG power supply system are independent it is possible to ground the system on both sides of power supply inverter. The selection of the optimal grounding strategy has been carried out by means of computer simulations. The simulations results show that the output grounding strategy (where the output side of the PS inverter is connected to ground through a couple of resistors) presents a smaller amplitude of stray currents on the load side with respect the other solution. In figure 5.6 is sketched the current paths for the common-mode current considering the proposed grounding strategy.
Preliminary evaluation on the magnitude of stray capacitance of the circuit has been carried out to perform the numerical simulation. Considering the mechanical design of the A and B-Coil and the measured capacitance of the feedthrough (done during the experimental campaign described in 5.5) the expected stray capacitance

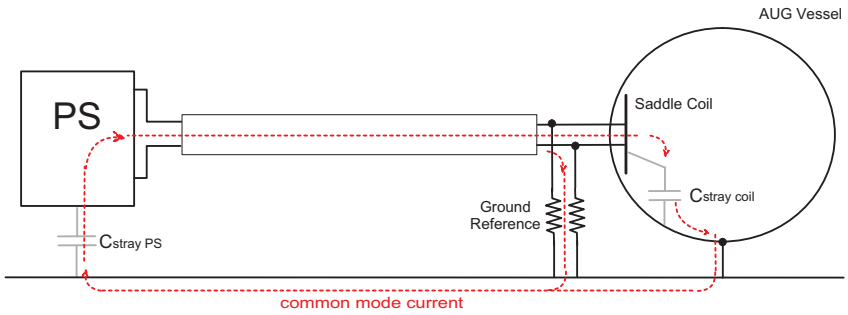

Figure 5.6: Current paths for common mode noise on AUG due to the new switching power supply systems.

of the load to vessel (i.e. to ground) is in the range of 1 nF. An evaluation of the stray capacitance of the PS module is difficult being its geomentry and size not yet defined, therefore it has been decided to use the known value of an operating power module with similar power rating: 200 pF distributed among the two dc-link buses of the power module.
The output grounding of the PS is as more effective as smaller is the ground resistance. The minimum value of ground resistance is limited by two constraints: one is related to the impedance of the load, the other depends on its power dissipation. The impedance of A-Coils at 3 kHz is 0.565 Ω ($Z_{A\,coil} = 2 \cdot \pi \cdot f_{max} \cdot L_{A\,coil}$), a simple approach is to keep the total impedance of the grounding resistor ($2 \cdot R_{ground}$) 100 times the previous value: $R_{ground} > 28.3\,\Omega$.
The second constraint is given by the power dissipation of the grounding resistors. The worst case scenario is represented by the AC operation (on DC operation a small duty cycle is sufficient to assure the continuous dc current on the load). The power dissipation in grounding resistances is therefore:

$$P_{R\,ground} = \frac{V_{dc\,link}^2}{4 \cdot R} \tag{5.2}$$

The maximum power dissipation could be fixed at 500 W (1/100 of the rated power of B-Coils PS module) this gives a minimum value of ground resistance of 125 Ω which has been selected.
On Figure 5.7 has been reported the PSIM models and simulation voltage profiles for B-Coils PS systems with ground reference at the inverter output side (AC). The parameters used on the simulation were: grounding resistors: 125 Ω, power supply stray capacitance to ground: $2 \times 100\ pF$, stray capacitance of B-Coils to ground: 1 nF. In the simulation have been reported, for comparison, also the results related to the simulation of a DC grounded system (the blue profiles on simulation results). It could be noted that the common-mode noise on the load stray capacitance is lower for the AC grounded system (the noise current peaks are 518 mA with respect to the 3.42 A of DC grounded system) while a large peak of noise current flows through the power supply stray capacitance.
The model and the simulation profiles showed in figure 5.7 are related to the B-Coil PS schematic which is composed by a single H-Bridge. The A-Coils PS has a more complex topology since its output section is composed of two H-Bridges in series.

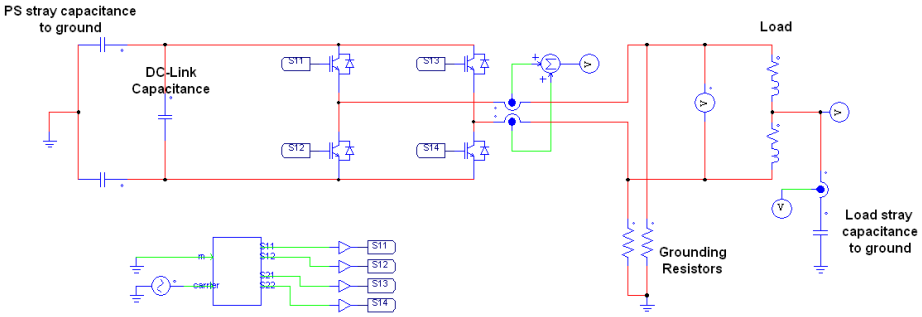

(a) PSIM model of B-Coils PS showing the stray capacitances to ground of the system and the grounding resistances.

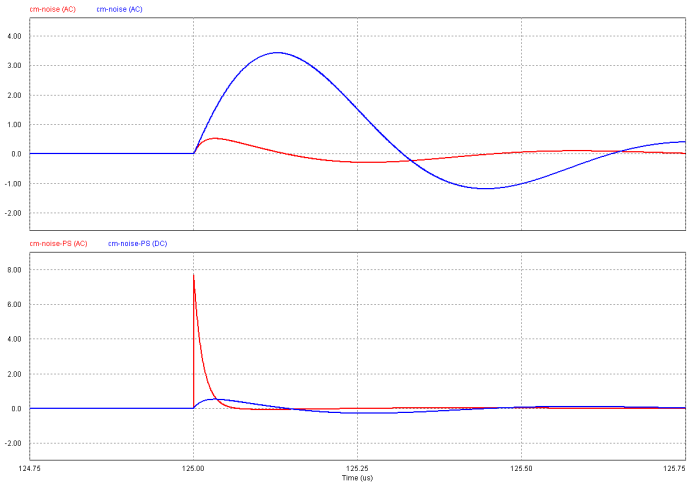

(b) Simulation results: common-mode current profiles on the load side (upper plot) and on the power supply side (lower plot). Red profiles: AC grounding; Blue profiles: DC grounding.

Figure 5.7: PSIM Simulation for evaluation of common-mode currents on B-Coils PS.

The simulation results show that the output grounding is suitable also for this type of power supply.

5.4.3 Design of passive filter for EMI mitigation

Even if the selected grounding point permits a better EMI mitigation with respect to other grounding strategies the limitation of the minimum value for the grounding resistors implies a non null common mode current through load stray capacitance. Among the variuos EMI mitigation techniques reported in section 5.3 it is here proposed to use a passive filter to further reduce the magnitude of common-mode current. The filter will be inserted between the power supply and the power cables. The major constraint for the design of this component is the large dc current (1 kA for 10 s) that can flow through the filter conductors which can produce thermal and mechanical stress of the component. Another important aspect is related to chokes parasitic capacitance. Chokes composed of multiple windings can exhibit a not negligible stray capacitance among windings which can represent a bypass path for the high frequency components of common-mode noise. As a result the effectiveness of the common-mode filter depends on also the component geometrical structure.
In this paragraph a simple and reliable common-mode filter with a different geometry with respect to the choke outlined in figure 5.5 is proposed. It is based on a set of toroidal rings made of high magnetic permeability material that surrounds the two output cables of the power supply as depicted in Figure 5.8.

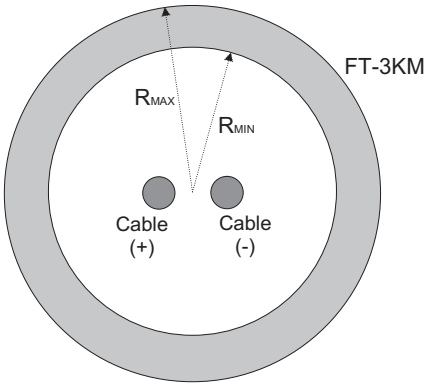

Figure 5.8: Common Mode Filter structure proposal.

To design the common mode filter it is important to maintain the B-field inside the magnetic core lower than its saturation limit, to assure a sufficient cross section to obtain significant common mode inductance and to minimize the capacitance between two conductors.
The selected material for the filter's core is FINEMET FT-3KM[69]which present good magnetic properties ($\mu_{r\,100\,kHz} = 18 \cdot 10^3$) and high saturation limit ($B_{sat} = 1.23\,T$). The needed common mode inductance to reduce the peak current of conducted noise to 1/10 is $100\,\mu H$ (value derived by computer simulations).
The common-mode inductance per meter of the proposed filter depends, negleting

the magnetic flux in the air, is given by the following equation:

$$L_{cm} = \frac{\mu_0\,\mu_r}{2\pi}\int_{R_{min}}^{R_{max}}\frac{1}{r}dr \;=\; \frac{\mu_0\,\mu_r}{2\pi}\cdot log\,\frac{R_{max}}{R_{min}} \tag{5.3}$$

The radial dimensions of the common mode filter depends on the required space for the power cables: fixed the maximum current density on power cables ($4\,A/mm^2$) and therefore its size the dimension of ferromagnetic core has been derived (core with inner radial dimension equal to 76 mm can hose easily the two power cables). A 2-D FEM[2] analysis of the filter has been carried out to evaluate both the common-mode and the differential-mode inductance of the component (on figure 5.9 is showed the magnitude of the magnetic fields considering a common mode current of 1 A).

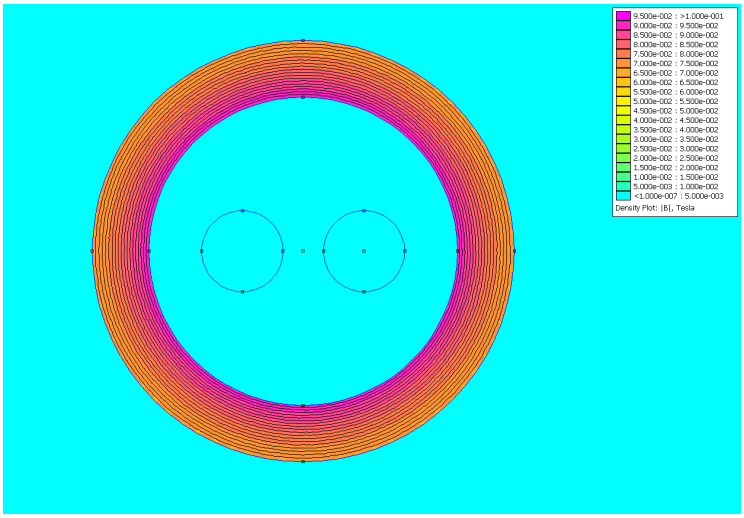

Figure 5.9: 2-D FEMM analisys of the Common Mode Filter proposal.

The results of 2-D analysis is compatible with the result of equation 5.3. Being the common-mode inductance of each commercial toroidal ring (which deep is 2.5 mm) $L_{cm\,ring} = 28.2\,\mu H$ it is necessary to use four rings in order to obtain the requested common-mode inductance ($100\,\mu H$). A PSIM simulation B-Coils PS with common-mode filter has been carried out considering that the choke total inducatance is $112.8\,\mu H$.
The result of simulation, showing the common mode current measured on the output poles of PS and on the load stray inductance is reported on figure 5.10. It could be noted that the peak of stray current descrease to 46.9 mA with respect to the 518 mA of the circuit without the common-mode filter. On other hand the perturbation due to the common-mode voltage swing persists for a longer period.
The proposed filter presents also a negligible capacitance among the input and output ports. The bypass effect presents in other kind of devices is therefore avoided.

[2]Finite Element Method, the program used is FEMM 4.2[70]

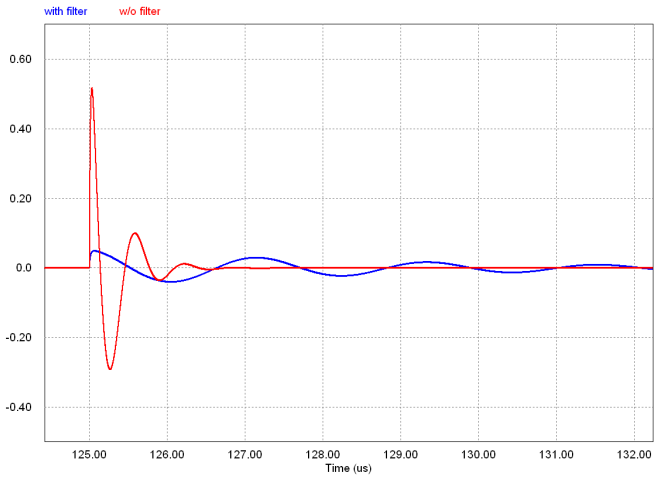

Figure 5.10: Current through the stray capacitance of B-Coils. The blue line represents the scenario with the proposed CM-filter, the red one the scenario without the CM-filter.

5.5 Experimental campaign on AUG feedthrough

In the framework of the RFX-AUG Team collaboration on power supplies design an experimental campaign has been carried out in late 2009. The research activity has been focused on the characterization of conducted noise due to switched power supply used for testing in-vessel saddle coils feedthroughs prototype. The research activity was performed during AUG experimental campaigns, with all the plasma diagnostic equipments in operation.
The power supply used for the tests was a 4-quadrant IGBT switching inverter, a power unit given to AUG Team in loan by the Consorzio RFX (the device is the back-up unit for the power supply system used to MHD control on RFX-mod), on figure 5.11 is showed the power supply cubicle placed inside the AUG torus hall and the termination poles of the feedthrough prototype.
The simplified schematics of the tests arrengment is depicted in figure 5.12. The circuit was composed of:

- Ac/dc rectifier and dc-link capacitances with the middle point connected to ground.
- H-bridge with 3-levels modulation
- Inductor used as output filter for the power amplifier (the feedthrough acts as a short circuit).
- Common-mode inductance
- Cables with a screen conductors available
- Feedthrough
- Stray electrical path (dashed red line) for the common mode current injected through the stray capacitance to AUG vessel of the feedthrough.

A series of measurements was carried out in order to characterize the circuit parameters; the results of this preliminary activity are reported in the following:

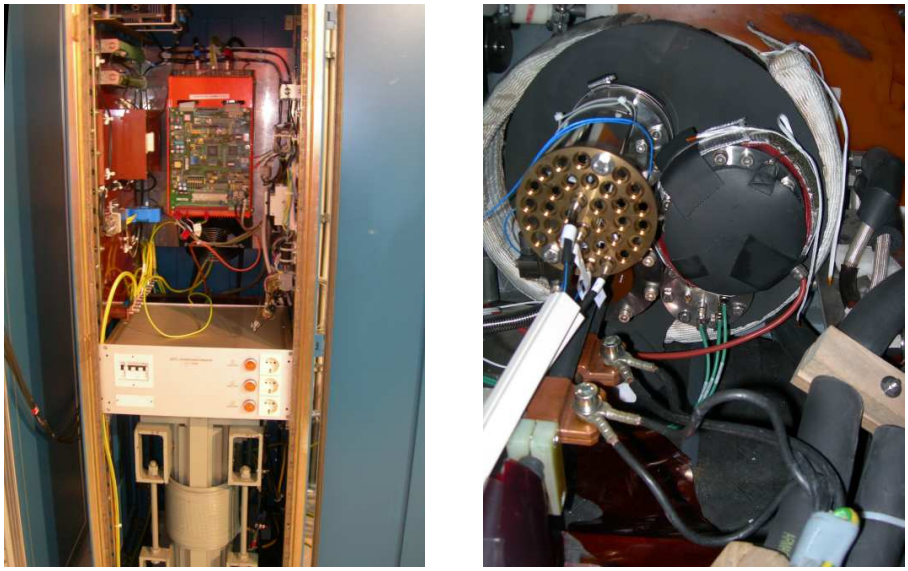

(a) Power supply cubicle

(b) Termination poles of the feedthrough prototype

Figure 5.11: Experimental campaign on AUG feedthrough.

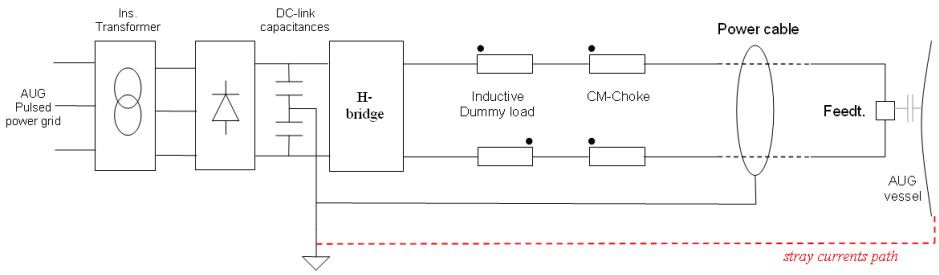

Figure 5.12: Electrical scheme of the test circuit for the AUG feedthrough.

Common-mode choke the filter used in this experimental campaign was a big iron-core inductance (rated for 500 A and 1 mH). The DC resistance of the windings is 7.8 $m\Omega$ which increases with the frequency because of the skin effect. The self inductance of windings is 250 μH while the coupling coefficient is 0.6.

Power Cable with the ending poles of the cable short-circuited the measured resistance and inductance at the start of the cable (downstream the common-mode choke) was 15.5 μH and 75 $m\Omega$ evaluated both at 1 kHz. The cable is composed of four conductors pair connected: capacitance between one pair to screen is 37.1 nF, capacitance between pairs is 20.7 nF.

Feedthrough The feedthrough can be considered as a short circuit (FT resistance $< 1 m\Omega$), the stray capacitance to vessel is equal to 650 pF. The water cooling system represents a resistive path to ground, the measured resistance is 300 $k\Omega$.

The main scope of the feedthrough tests was to analyze mechanical stress on the components caused by the electromagnetic forces due to the cross product of AUG toroidal field and ac current on the test device. Considering this scenario it was taken the opportunity to study the effect of the operation of switching device on the diagnostics placed nearby the feedthrough prototype.
The first series of test was carried out connecting directly the ac/dc rectifier to the ASDEX power grid, the results of the operations of the switching power amplifier was dramatic for the entire set of AUG diagnostics. The main source of noise was the pulsed power grid of AUG which powered the thyristor converters that fed the TF coils of the machine. The solution adopted was the inserction of an insulation transformer (with line filters) to feed the diode rectifier. This component decoupled the switching power supply from the AUG pulsed power grid, as a result the problems with many diagnostics was solved. After the circuit modification, see figure 5.12, the research activity was focused on the analysis of the signals from a pressure probe placed near the feedthrough which was subjected to noise caused by switching converter.
In Figure 5.13 is showed the pressure probe signal and its spectrogram[3]. At the start of the inverter operation (1.4 s to 7.4 s) can be noted that noise appears; its main harmonic is centered at 10 kHz, the frequency of the common mode voltage swing.
A series of circuit modification has been carried out. It was verified that the noise level diagnostic (see 5.13) was independent of the presence or absence of the common-mode filter; this is in contrast with the theory and the results of PSIM simulation used to verify the measurements. The reason of this is probably due to the stray capacitances among windings of the common-mode filter (the device proposed by the AUG team was a big inductance used for current ripple reduction in an old power supply operating on Asdex) Its windings stray capacitances act like a bypass for the high frequency harmonics of the common mode current: the effect of the high impedance of the cm-inductance is then neutralized.

[3]a Matlab routine using short-time Fourier transform has been used, the result image show shows how the spectral density of a signal varies with time

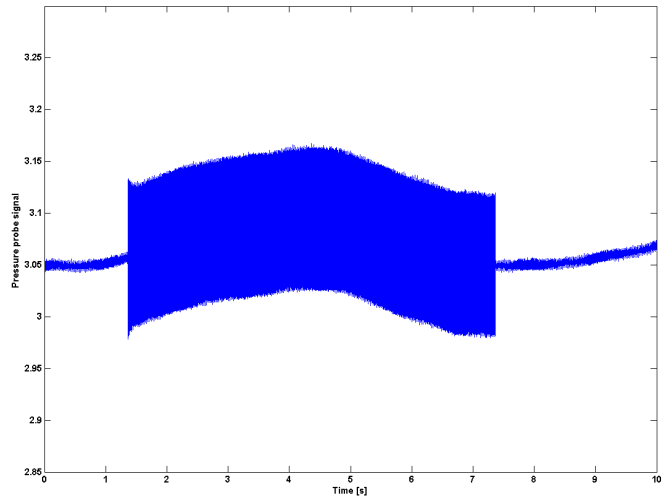

(a) Pressure signal profile

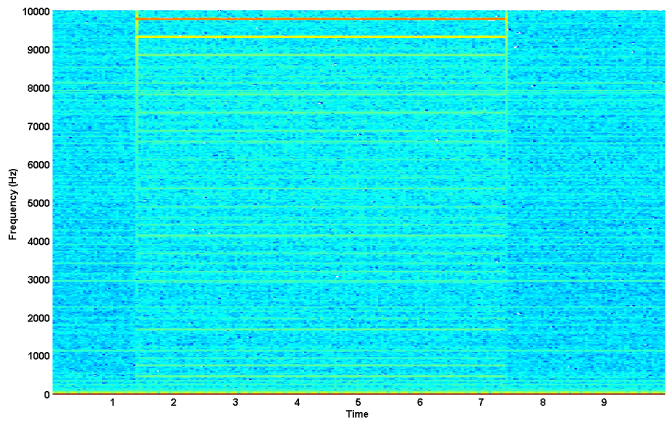

(b) Spectrogram

Figure 5.13: Pressure scan signal affected by the operation of power amplifier.

It is here remarked that the design of the new filter for common-mode noise (see section 5.4.3) implies a negligible stray capacitances between input and output ports of the filter. As a result the bypass effect presents on the filter used during the 2009 campaign will be avoided, this, obviously, permits an improvement of the filter performance.
A new series of experiment will be carried out in the future: nowadays the B-Coils have been installed inside the machine (on the stage 1 and 2 of the enhancement the saddle coil are supplied by an existing DC power supply which was dismissed after the shut-down of Wendelstein 7-AS stellaretor at Garching). The next step will be the test of the new common mode filter proposed in section 5.4.3 directly on one B-Coils circuit.
In the next experimental campaign, due to the presence of the new magnet system, it will be possible a more precise evaluation of the noise injection in the ground conductors of AUG. Therefore it will be possible the evaluation of the effectiveness of the common mode filter designed with the new approach proposed on this thesis.

Conclusions

This doctoral thesis, whose related activity is inserted in the framework of the research for the enhancement of ASDEX Upgrade (AUG) Tokamak, is focused on the design of the power supply system of the new set of coils (dubbed A and B) used to control the plasma MHD instabilities.
The design of power supply operating in the scenario of large fusion devices such Tokamaks is subjected to a series of constraints and presents some peculiarities with respect to the standard design of an industrial power supply. One of the major problems is the difficult characterization of the load and the presence of many uncertainties on the requirements since the future plasma scenarios are usually unpredictable.
The new power supply system that will be installed in AUG requires both high dc current and high bandwidth for ac operations. The design studies carried out during the PhD have been focused on the selection of the more suitable electrical scheme. The solution presented on this work is customized for the different requirements relevant to the specified controls for A and B coils but, at the same time, it has a sufficient modularity degree, adopts components widely used in the market and presents a very good ratio between performance and cost/size limitation.
In addition to computer simulation used to evaluate the performance of the proposed solution a series of relevant fault simulations have been carried out. Scope of these studies was to evaluate the effect of faults on power supply operation. A proposal for the protection logic against load short circuit has been given.
A series of analyses have been carried out to analyze the impact of the new switching power supply in terms of electrical noise which can has a dramatic impact on the diagnostics operation. The phenomena responsible for the generation of EMI have been identified. Taking advantage of the input section topology of the scheme proposed, the references to ground have been placed on the output side of power supplies. This grounding strategy shows better performance in terms of noise reduction with respect to other solutions.
During the PhD an experimental campaign has been carried at IPP laboratory of Garching. Scope of the research activity, performed during the normal operation of AUG Tokamak, was to analyze the impact of noise generated by switching power supplies on the machine diagnostics.
A new approach for the design of common mode filter has been proposed to mitigate the effects of EMI; it will be implemented and tested in a future experimental campaign.

Bibliography

[1] Ongena J and Van Oost G 1998 Energy for future centuries Trans. Fusion Technol. 30 9

[2] Peter M. Cox et alt. Acceleration of global warming due to carbon-cycle feedbacks in a coupled climate model Nature 408, 184-187 (9 November 2000)

[3] R. A. Kerr, Do We Have the Energy for the Next Transition? Science, 13 August 2010, Vol 329, 780-781.

[4] K.S.Deffeyes, Hubbert's peak : The impending World Oil Shortage, Princeton University Press (2001).

[5] D. Clery, Sending African Sunlight to Europe, Special Delivery, Science, 13 August 2010, Vol 329, 782-783.

[6] J. D. Lawson, Some criteria for a power producing thermonuclear reactor, Proc. Phys. Soc. B 70, 6 (1957).

[7] J. A. Wesson, Tokamaks, Oxford University Press, Oxford, UK, 1987.

[8] H. Vernickel, et alt, ASDEX upgrade: A poloidal divertor tokamak adapted to reactor requirements, Journal of Nuclear Materials, Volumes 128-129, December 1984, Pages 71-77.

[9] ASDEX Upgrade Team 2003 Fusion Sci. Technol. 44 1

[10] Home page of ITER organization *http://www.iter.org*.

[11] Holtkamp N. and the ITER project team, An overview of the ITER project, Fusion Engineering and Design, Vol. 82, no. 5-14, 2007, pp. 427-434.

[12] ITER Technical Basis, ITER EDA Documentation Series No. 24, IAEA, Vienna, 2002.

[13] S. Konishi, S. Nishio, K. Tobita, The DEMO design team, DEMO plant design beyond ITER, Fusion Engineering and Design, Volumes 63-64, December 2002, Pages 11-17,

[14] R. J. La Haye, Neoclassical tearing modes and their control, Phys. Plasmas 13, 055501 (2006)

[15] G. Rostagni, RFX: an expected step in RFP research, Fusion Engineering and Design, Volume 25, Issue 4, 2 January 1995, Pages 301-313

[16] H Zohm, Edge localized modes (ELMs), Plasma Phys. Control. Fusion 38 (1996) 105-128

[17] http://www.jet.efda.org/focus-on/edge-localised-modes/elm-classification/

[18] T. Evans, et al., Suppression of large edge localized modes with edge resonant magnetic fields in high confinement DIII-D plasmas, Nucl. Fusion 45 (2005) 595-607.

[19] P. R. Brunsell, K. E. J. Olofsson, L. Frassinetti, and J. R. Drake, Resistive wall mode feedback control in EXTRAP T2R with improved steady-state error and transient response Phys. Plasmas 14, 102505 (2007)

[20] G. Holmes and T. Lipo, Pulse Width Modulation for Power Converters, Principles and Practice, ser. IEEE Press Series on Power Engineering. New York: Wiley-Interscience, 2003.

[21] V. Toigo et. al, Conceptual design of the enhanced radial field amplifier for plasma vertical stabilisation in JET, Fusion Eng. Design, Volume 82, Issues 5-14,

[22] W Suttrop et al, Design of in-vessel saddle coils for MHD control in ASDEX Upgrade 35th EPS Conference on Plasma Phys. Hersonissos, 9 - 13 June 2008 ECA Vol.32D, P-4.075 (2008)

[23] A.W. Leonard et al. , The impact of ELMs on the ITER divertor Journal of Nuclear Materials 266-269 (1999) 109-117

[24] T H Osborne et al, Edge stability of stationary ELM-suppressed regimes on DIII-D, J. Phys.: Conf. Ser. 123 012014

[25] H. Zohm et al Control of MHD instabilities by ECCD: ASDEX Upgrade results and implications for ITER, 2007 Nucl. Fusion 47 228

[26] M. Rott et al, Electro-magnetic modeling of the planned active in-vessel coils at ASDEX Upgrade Fusion Eng. Design 84 (2009) 1653

[27] Irene Zammuto et. alt. Conceptual design of in vessel mid-plane saddle coils for fast ac operation in ASDEX upgrade 26th Symposium on Fusion Technology - Porto, September 27, 2010 - October 1, 2010

[28] Thomas Vierle et. alt PEEK-insulated conductors of fast in-vessel saddle coils for ASDEX Upgrade 26th Symposium on Fusion Technology - Porto, September 27, 2010 - October 1, 2010

[29] M. Cavinato, D. Gregoratto, G. Marchiori, R. Paccagnella, R. Brunsell, D. Yadikin, Comparison of strategies and regulator design for active control of MHD modes, Fusion Eng. Des. 74 (2005) 549-553.

[30] W Suttrop et al, Physical description of external circuitry for ResistiveWall Mode control in ASDEX Upgrade, 36th EPS Conference on Plasma Phys. Sofia, June 29 - July 3, 2009 ECA Vol.33E, P-1.165 (2009)

[31] Malesani, L.; Tenti, P.; , A novel hysteresis control method for current-controlled voltage-source PWM inverters with constant modulation frequency, Industry Applications, IEEE Transactions on , vol.26, no.1, pp.88-92, Jan/Feb 1990

[32] Bose, B.K.; An adaptive hysteresis-band current control technique of a voltage-fed PWM inverter for machine drive system, Industrial Electronics, IEEE Transactions on , vol.37, no.5, pp.402-408, Oct 1990

[33] G. H. Bode, D. N. Zmood, P. C. Loh, and D. G. Holmes, A novel hysteresis current controller for multilevel single phase voltage source inverters, in Proc. IEEE PESC'01, 2001, pp. 1845-1850.

[34] S. Klaka, M. Frecker, H. Grüning, The Integrated Gate-Commutated Thyristor: A New High-Efficiency, High-Power Switch for Series or Snubberless Operation, PCIM, Nürnberg, Germany, 1997.

[35] Rahimo, M.; Schlapbach, U.; Kopta, A.; Linder, S.; , An assessment of modern IGBT and anti-parallel diode behaviour in hard-switching applications, Power Electronics and Applications, 2005 European Conference on , vol., no., pp.10 pp.-P.10, 0-0 0

[36] J. Vobecky, Future trends in high power devices, Microelectronics Proceedings (MIEL), 2010 27th International Conference on , vol., no., pp.67-72, 16-19 May 2010

[37] Q. Jinrong, A. Khan, I. Batarseh, Turn-off switching loss model and analysis of IGBT under different switching operation modes, Industrial Electronics, Control, and Instrumentation, 1995., Proceedings of the 1995 IEEE IECON 21st International Conference on , vol.1, no., pp.240-245 vol.1, 6-10 Nov 1995

[38] S. Eio, N.Y.A. Shammas, IGBT tail current reduction by current injection technique, Universities Power Engineering Conference, 2008. UPEC 2008. 43rd International , vol., no., pp.1-4, 1-4 Sept. 2008

[39] Jih-Sheng Lai; Fang Zheng Peng; , Multilevel converters-a new breed of power converters, Industry Applications Conference, 1995. Thirtieth IAS Annual Meeting, IAS '95., Conference Record of the 1995 IEEE , vol.3, no., pp.2348-2356 vol.3, 8-12 Oct 1995

[40] J. Rodriguez, J.-S. Lai, and F. Z. Peng, Multilevel inverters: A survey of topologies, controls, and applications, IEEE Trans. Ind. Electron., vol. 49, no. 4, pp. 724-738, Aug. 2002.

[41] Franquelo, L.G.; Rodriguez, J.; Leon, J.I.; Kouro, S.; Portillo, R.; Prats, M.A.M.; , The age of multilevel converters arrives, Industrial Electronics Magazine, IEEE , vol.2, no.2, pp.28-39, June 2008

[42] A. Nabae, I. Takahashi, and H. Akagi, A new neutral-point clamped PWM inverter, IEEE Trans. Ind. Applicat., vol. IA-17, pp. 518.

[43] Wu, Lau, Chung, A five-level neutral-point-clamped H-bridge PWM inverter with superior harmonics suppression: a theoretical analysis, Circuits and Systems, 1999. ISCAS '99. Proceedings of the 1999 IEEE International Symposium on , vol.5, no., pp.198-201 vol.5, 1999

[44] Lau, W.H. Zhou, B.; Lee, C.K.; Chung, H.; , Realization of a five-level NPC inverter using carrier phase-shift technique, ENCON '02. Proceedings. 2002 IEEE Region 10 Conference on Computers, Communications, Control and Power Engineering , vol.3, no., pp. 1978- 1981 vol.3, 28-31 Oct. 2002

[45] C. R. Baier, J. I. Guzman, J. R. Espinoza, M. A. Perez, and J. R. Rodriguez, Performance evaluation of a multicell topology implemented with single-phase nonregenerative cells under unbalanced supply voltages, IEEE Trans. IEEE Trans. Ind. Electron., vol. 54, no. 6, pp. 2969-2978, Dec. 2007.

[46] P. Flores, J. Dixon, M. Ortuzar, R. Carmi, P. Barriuso, and L. Moran, Static Var compensator and active power filter with power injection capability, using 27-level inverters and photovoltaic cells,IEEE Trans.Ind. Electron., vol. 56, no. 1, pp. 130-138, Jan. 2009.

[47] S. Mariethoz and A. Rufer, Multisource DC-DC converter for the supply of hybrid multilevel converter, in Conf. Rec. 41st IEEE IAS Annu. Meeting, Oct. 2006, vol. 2, pp. 982-987.

[48] M. F. Escalante and J. J. Arellano, Harmonics and reactive power compensation using a cascaded H-bridge multilevel inverter, in Proc. IEEE Int. Symp. Ind. Electron., Jul. 2006, vol. 3, pp. 1966-1971.

[49] S. Kouro, P. Lezana, M. Angulo, and J. Rodriguez, Multicarrier PWM with DC-link ripple feedforward compensation for multilevel inverters, IEEE Trans. Power Electron., vol. 23, no. 1, pp. 52-59, Jan. 2008.

[50] U. Scheuermann, U. Hecht, Power Cycling Lifetime of Advanced Power Modulesfor Different Temperature Swings, Proc. PCIM, PE4.5, 59-64, Nürnberg 2002

[51] M.Held, P.Jacob, G.Nicoletti, P.Scacco, M.H.Poech, Fast Power Cycling Test for IGBT Modules in Traction Application, Proc. Power Electronics and Drive Systems 1997, 425-430.

[52] W. Förster, J. Alex, High-voltage, high-power, pulse-step modulators for the accurate supply of gyrotron and other heating devices, 25th International Power Modulator Symposium, 30 June - 3 July 2002.

[53] V. Tripathi et. al, Development of cast resin multisecondary 1600kVA transformer for Regulated High Voltage Power Supply- A prototype 2010 J. Phys.: Conf. Ser. 208 012005

[54] C Sihler, P Fu, M Huart, B Streibl, W Treutterer, Paralleling of two large flywheel generators for the optimisation of the ASDEX Upgrade power supply, Fusion Engineering and Design, Volumes 58-59, November 2001, Pages 41-45.

[55] Home page of PSIM Software by Powersim Inc www.powersimtech.com

[56] N. Mohan, T.M. Undeland and W.P. Robbins, Power Electronics, J. Wiley and Sons, Inc. Ed. (1995).

[57] E. Gaio, R. Piovan, V. Toigo, EMI on diagnostics and control circuits due to switching power supplies, Fusion Engineering and Design, Volumes 75-79, Proceedings of the 23rd Symposium of Fusion Technology - SOFT 23, November 2005, Pages 61-66

[58] R. Gonzalez, J. Lopez, P. Sanchis, and L. Marroyo, Transformerless inverter for single-phase photovoltaic systems, IEEE Trans. Power Electron., vol. 22, no. 2, pp. 693-697, Mar. 2007.

[59] V. Toigo, E. Gaio, N. Balbo, A. Tescari, The power supply system for the active control of MHD modes in RFX, Fusion Engineering and Design, Volumes 66-68, 22nd Symposium on Fusion Technology, September 2003, Pages 1143-1147.

[60] Haoran Zhang; Von Jouanne, A.; Shaoan Dai; Wallace, A.K.; Fei Wang; Multilevel inverter modulation schemes to eliminate common-mode voltages, Industry Applications, IEEE Transactions on , vol.36, no.6, pp. 1645-1653, Nov/Dec 2000

[61] H. Zhang, A. von Jouanne, Suppressing common-mode conducted EMI generated by PWM drive systems using a dual-bridge inverter, Applied Power Electronics Conference and Exposition, 1998. APEC '98. Conference Proceedings 1998., Thirteenth Annual , vol.2, no., pp.1017-1020 vol.2, 15-19 Feb 1998

[62] T. Kerekes, R. Teodorescu, P. Rodriguez, G. Vazquez, E. Aldabas, E. , A New High-Efficiency Single-Phase Transformerless PV Inverter Topology, Industrial Electronics, IEEE Transactions on , vol.58, no.1, pp.184-191, Jan. 2011

[63] Takahashi, I.; Ogata, A.; Kanazawa, H.; Hiruma, A.; , Active EMI filter for switching noise of high frequency inverters , Power Conversion Conference - Nagaoka 1997., Proceedings of the , vol.1, no., pp.331-334 vol.1, 3-6 Aug 1997

[64] S. Ogasawara, H. Ayano, and H. Akagi, An active circuit for cancellation of common-mode voltage generated by a PWM inverter, Proc. IEEE PESC'97, vol. 2, pp. 1547 - 1553, 1997.

[65] Y. Murai, T. Kubota, Y. Kawase, Leakage current reduction for a high-frequency carrier inverter feeding an induction motor IEEE Transactions on Industry Applications. Vol. 28, no. 4, pp. 858-863. July-Aug. 1992

[66] Akagi, H.; Hasegawa, H.; Doumoto, T.; , Design and performance of a passive EMI filter for use with a voltage-source PWM inverter having sinusoidal output voltage and zero common-mode voltage, Power Electronics, IEEE Transactions on , vol.19, no.4, pp. 1069-1076, July 2004

[67] Cochrane, D.; Chen, D.Y.; Boroyevic, D.; , Passive cancellation of common-mode noise in power electronic circuits, Power Electronics, IEEE Transactions on , vol.18, no.3, pp. 756-763, May 2003

[68] Tihanyi, L. Electromagnetic Compatibility in power electronics (IEEE Press, Piscataway, NJ, USA, 1995)

[69] Hitachi Metglas®, www.metglas.com.

[70] www.femm.info